ANALYSIS AND IDENTIFICATION OF DYNAMIC TRANSMISSION ERROR PARAMETERS IN A GEARED ROTOR USING FULL SPECTRUM

A Thesis Submitted in Partial Fulfilment of the Requirements for the Degree of

DOCTOR OF PHILOSOPHY

by

BHYRI RAJESWARA RAO

DEPARTMENT OF MECHANICAL ENGINEERING

INDIAN INSTITUTE OF TECHNOLOGY GUWAHATI

GUWAHATI 781039, INDIA

January 2023

ANALYSIS AND IDENTIFICATION OF DYNAMIC TRANSMISSION ERROR PARAMETERS IN A GEARED ROTOR USING FULL SPECTRUM

A Thesis Submitted in Partial Fulfilment of the Requirements for the Degree of

DOCTOR OF PHILOSOPHY

by

BHYRI RAJESWARA RAO

DEPARTMENT OF MECHANICAL ENGINEERING

INDIAN INSTITUTE OF TECHNOLOGY GUWAHATI

GUWAHATI 781039, INDIA

January 2023

Department of Mechanical Engineering

Indian Institute of Technology Guwahati

GUWAHATI - 781039, INDIA.

CERTIFICATE

It is certified that the research contained in this Thesis titled "**Analysis and Identification of Dynamic Transmission Error Parameters in a Geared Rotor Using Full Spectrum**" submitted by Mr. Bhyri Rajeswara Rao (Roll no. 156103029) to the Indian Institute of Technology Guwahati for the award of the degree of Doctor of Philosophy has been carried out under our supervision in the Department of Mechanical Engineering, Indian Institute of Technology Guwahati. This research work has not been submitted elsewhere for the award of any other degree or diploma.

January 2023

Dr. Rajiv Tiwari

Professor

Department of Mechanical Engineering

Indian Institute of Technology Guwahati, Guwahati, 781 039, INDIA.

Dr. Maruthi Rao D

Program Manager

Engineering analysis

TCS, Creator Building, ITPL, Bangalore

560066, INDIA.

Dedicated to My Parents

Bhyri Latchanna & Rajyalakshmi and Family

ACKNOWLEDGEMENTS

The journey towards the accomplishment of this thesis has been ideal because of the presence of the people around me. First, I would like to express my sincerest regards and gratitude to my supervisor, Dr. Rajiv Tiwari for his persistent guidance and suggestions during my PhD (during M. Tech. during year 2003 to 2005) and serving as my thesis supervisor. I would like to thank my organisation General Motors Technical Centre India (GMTCI) Private Limited, Bangalore for giving me the opportunity to pursue my Ph. D research at IIT Guwahati. I would like to thank for the motivation and guidance I got from Dr. Maruthi Rao D who is internal supervisor in my organisation after the parent company GMTCI is taken over by TCS, Bangalore in 2019. I also thank my current project manager at TCS Bangalore, Mr. Vadamaduri Arulanandam Muruganandam and long-time collages of GMTCI and current TCS Bangalore Mr. S P Ganesan, Mr. Datla Ramakrishna Raju, Mr. Manish Bisht and Mr. Bhaskara Kishore Ch and for their continued support until the completion of my research activity at IITG.

I also extend my deep sense of respect and thanks to my doctoral committee members, namely, Dr. S K Dwivedy, Dr. A. Banerjee and Dr. Arbind Kumar Singh for the valuable suggestions provided during my progress seminars. I thank the IIT Guwahati administration for whatever amenities I have utilised during my stay at the campus. I thank the past and present heads of Department of Mechanical Engineering Dr. A. K. Dass, Dr. S. K. Dwivedy, Dr S. Senthilvelan and Dr. K. S. R. K. Murthy for availing various departmental facilities. My stay during IIT Guwahati was made pleasant by many friends and seniors of the research fraternity. Dr. D. J. Bordoloi of Vibration and Acoustics Lab, IIT Guwahati for helping me to conduct the experiments smoothly. I thank Dr. Dipendra Kumar Roy, Dr. Purushottam Gangsar, Dr. Rapur Janani Shruti, Dr. Nilakshi Sarmah, Dr. Siva Srinivas, Dr. Gargi Majumder, Dr. Prabhat Kumar, Mr. Gyan Ranjan, Mr Pantha P Das, Mr. Atul Kumar Gautam and other students, for making my stay in the institute a memorable one. I will cherish the memories I have spent with all of my friends here at Guwahati and elsewhere.

I pay my foremost respect to my parents, Bhyri Latchanna and Rajyalakshmi, they are not alive to see this accomplishment today, banking on whose advice and well-wishes I have been able to

successfully carry out my Ph.D. I would like to thank the Almighty God for having blessed me with all the happiness in life to keep me motivated towards the goal.

January 2023

Bhyri Rajeswara Rao
IIT Guwahati.

ABSTRACT

Geared rotor bearing systems are widely used torque carrying components in most of the mechanical and electrical equipment in the automotive, aerospace and ship building industries. A dominant source of vibration in geared rotor systems are the gear mesh dynamic transmission error (TE) parameters. These include the static TE, the mesh stiffness and damping, and the gear runout. One needs to know additionally these dynamic parameters along with the gear macro-geometry (for examples, the number of teeth, pitch circle diameter, pressure angle, and tooth geometries), load and rotating speed, for the vibration-based diagnosis of geared rotor power transmission units.

A novel transverse excitation due to asymmetric transmission error is considered in this research work during torque transfer in a geared rotor system at an oblique orientation of a gear-pair. However, the conventional approach uses the transmission error excitation force direction (i.e., the pressure line) aligned along the vertical direction, which eliminates the excitation in the horizontal direction. In this research, an effort has been made to analyse and estimate these multiple dynamic TE parameters through an identification methodology using the system responses obtained from a numerical simulation and experimental rig. During formulation, the torsion and transverse vibration coupling is ignored for low torque applications.

A mathematical model of geared rotor has been developed. It has the input and output flexible shafts mounted on rigid supports with the asymmetric transmission error as a transverse excitation force along with gear runouts. The time-varying gear mesh stiffness is approximated as time-invariant using a constant gear mesh stiffness and asymmetric transmission error. Equations of motion of the geared rotor system model are derived using Lagrangian dynamics. These are linear differential equations of motion of a geared rotor with chosen gear mesh parameters based on the physical consideration. Numerically obtained responses in time domain are plotted and analysed using orbit response plots to detect the dominant source of vibration.

As the frequency spectrum gives insights into sources of vibration through its order content in responses, the time domain response is converted into frequency domain. The response is plotted using full spectrum, which unwraps the traditional fast Fourier transform (FFT) spectrum into the forward

and backward whirl frequencies. The full-spectrum is suitable for analysing response of geared rotor system as it is an augmented version of the Campbell diagram. The full spectrum response is analysed to detect the asymmetric transmission error, which is dominant source of vibration in a geared rotor.

The time domain equations of motion are then transformed into frequency domain in a complex form. Equations of motion in frequency domain are written for various excitation frequencies of the considered dynamic TE. These linear equations are written in a matrix form by separating the unknown dynamic TE parameters from those of full spectrum response terms. A novel effort is made in this research to develop a three-step identification algorithm based on least-squares fit using frequency domain transformation to identify all the dynamic TE parameters of gear mesh. It has been tested using numerically calculated full spectrum responses for chosen geared rotor parameters. The robustness of the algorithm is checked by introducing the white Gaussian noise in the simulated responses.

An experimental geared rotor system was designed and fabricated for the gear vibration measurement to validate the system model. The experimental rig resembles the system model configuration. Also, it accommodates switching of gear sets having varied shaft centre distance, which is fabricated with known lead and profile crown. During measurement, the gear mesh was loaded with a low torque by a magnetic brake to avoid separation of gears. The horizontal and vertical shaft displacements at gears were captured using eddy current type proximity probes, which were mounted on the rigid base plate. The reference signal was also measured on the input shaft close to coupling using another proximity probe for obtaining the phase of the rotor displacement. This reference signal was used for the output shaft also by expanding the time scale using a gear ratio of the gear set.

The measured responses from the test setup in time domain are analysed using orbit response plots. The time domain signal is converted into frequency domain and the responses are analysed in full spectrum form. A phase compensation of the measured signal is done by subtracting the phase of input and output shaft responses with the reference phase of the input and output shafts, respectively. The full-spectrum plot of measured response shows distinct peaks up to five gear mesh forward and backward whirl frequencies. Relatively smaller amplitude peaks are reflected in the full spectrum at higher harmonics due to relatively small TE in test gears so in the higher harmonics of gear mesh

frequency. Also, there is a relative difference in the peak amplitudes at all five harmonics of gear meshing frequencies in the forward and backward whirls, which demonstrates the asymmetric TE.

Using the same numerically tested identification algorithm, the gear mesh dynamic TE parameters of geared rotor experimental rig are estimated using the test measured full spectrum responses. These identified dynamic TE parameters of experimental rig are supplied to generate the full spectrum plot numerically. This numerically generated full spectrum plot with experimental rig gear mesh dynamic parameters is compared with original test measured spectrum responses to validate the system model and proposed identification algorithm. The matching of full spectrum responses is excellent to confirm the novel asymmetric model of the variable components of static TE in this research work.

Contents

List of Figures

List of Tables

Nomenclature

Parameters in Roman letters

c_m	Gear mesh damping (Ns/m)
c_{s1}	Input shaft mesh damping (Ns/m)
c_{s2}	Output shaft damping (Ns/m)
e_p	Pinion runout (m)
e_g	Gear runout (m)
$e(t)$	Transmission error (m)
e_m	Mean transmission error (m)
e_{rx}	Variable transmission error in x direction (m)
e_{ry}	Variable transmission error in y direction (m)
f_e	Gear meshing frequency (Hz)
F_c	Force at the gear contact along line of action (N)
F_x	Force at the gear contact in *x* direction (N)
F_y	Force at the gear contact in *y* direction (N)
g	Acceleration due to gravity (m/s^2)

I_p, I_g	Mass moment of input and output shafts (kgm^2)
k_{s1}	Stiffness of input shaft (N/m)
k_{s2}	Stiffness of output shaft (N/m)
L	Length of input and output shafts (m)
m_2	Mass of gear (kg)
m_{avg}	Average gearing mass (Kg)
N_p	Spin speed of Pinion (rpm)
N_g	Spin speed of Gear (rpm)
P	Response function frequency domain (m)
R	Force function in frequency domain (N)
r_p	Base radius of pinion (m)
r_g	Base radius of gear (m)
r_{b1} r_{b2}	Base radius of gear (m)
t_p	Number of teeth on pinion
t_g	Number of teeth on gear
T_d	Drive torque (Nm)
T_l	Load side torque (Nm)

x	Lateral vibration in x direction (m)
Y	Lateral vibration in y direction (m)

Matrices

A	Stiffness matrix in frequency domain (N/m)
C	Damping matrix (Ns/m)
K	Stiffness matrix (N/m)
P	Response vector in frequency domain (m)
M	Mass matrix (kg)
S	Force vector in frequency domain (N)

Parameters in Greek Letters

α	Angle of obliquity of gear mesh with respect to vertical axis (deg)
δ	Dynamic transmission error along line of action
δ_x	Dynamic transmission error in x direction (m)
δ_y	Dynamic transmission error in y direction (m)
$\varphi(t)$	Angular motion
ϕ_p	Phase of pinion runout (rad)

ϕ_g	Phase of gear runout (rad)
ϕ_{ex}	Phase of variable transmission error in x direction (rad)
ϕ_{ey}	Phase of variable transmission error in y direction (rad)
ω_e	Gear meshing frequency (rad/s)
ω_p	Angular velocity of Pinion (rad/s)
ω_g	Angular velocity of Gear (rad/s)
ζ_m	Gear mesh damping ratio

Abbreviations

AI	Artificial Intelligence
ANNs	Artificial Neural Networks
CNN	Conventional Neural Networks
DL	Deep Learning
DTE	Dynamic Transmission Error
EV	Electric Vehicles
FEM	Finite Element Method
FFT	Fast Fourier Transform

GA	Genetic Algorithms
IC	Internal Combustion
IA	Identification Algorithm
LOA	Line of Action
MBD	Multi Body Dynamics
ML	Machine Learning
NVH	Noise Vibration & Harshness
PHM	Prognostic and Health Management
RMS	Root Mean Square
SDOF	Single Degree of Freedom
SMVs	Support Vector Machines
STE	Static Transmission Error
TE	Transmission Error
HGRBS	Helical Gear-Rotor-Bearing System

CHAPTER 1

INTRODUCTION AND LITERATURE REVIEW

1.1 Introduction

Complex nature of rotating machinery fascinated many researchers to study their dynamic behaviour. These studies resulted in the design of lighter, high-speed and highly reliable automotive, aerospace and other industrial machinery. Rotating machinery vibration and its associated noise issues due to inherent faults have attracted many researchers and vast amount literature is available in this domain (Rao, 1996; Genta, 2007; Friswell et al., 2010; Tiwari, 2017). Advances in high-speed computing has given impetus to the advancement of ongoing research by quenching thirst of many researchers and practitioners. Automotive and aerospace industry are in the forefront of research in this domain by developing new methodologies and techniques to have competitive edge in market. Vibration and associated noise issues have become key quality issue for the customers while choosing the right product from market. Especially in automotive industry engineers have real challenge in drawing a line between weight savings for fuel economy and optimum structural stiffness in designing quieter vehicles. Noise from heavy trucks, passenger vehicles and other machines is an important environmental issue. The human ear has a remarkable way of detecting pure tones of which the noise from loaded gears are annoying. The noise in decibel (dB) levels of breathing is around 10 dB which is barely audible; whisper rustling levels are at 20 dB; quiet rural area is at 30 dB levels whereas bird calls are at 40 dB; and normal conversation happens at 60 dB. Exposure to noise levels beyond 70 dB for more than 24 hours causes loss of hearing in human ears. Noise from transportation has been the major contributor, and consequently, governments are under increasing pressure to introduce legislation, like mandatory pass-by noise test, to restrict noise emissions from vehicles and other machines, and thus steadily reduce the permissible noise levels (Harris, 1991; Challen, 1999; Guo, 2019). These noise levels are described to give an understanding about its severity, however, the noise and its measurement or simulation is out of the scope of the present thesis.

Several sources contribute to the total vibration level of a vehicle, such as the engine, gearbox, tires, etc. Much of the vibration and associated noise reduction research carried out in the past focused on the structure and radiating surfaces of the internal combustion (IC) engines. Combustion in the engine has received substantial attention over the last two decades, with other systems given slightly less priority. However, as most forcing functions are engine performance related and thus impossible to change dramatically without making serious compromises in engine performance, emissions, and fuel economy, this leaves the workable aspects of the forcing functions, such as the timing gear systems, comprising of the injection timing gear, fuel pump gear, camshaft gear and transmission systems to be examined more closely.

With advances in vehicle technology, usage either fully electric vehicles (EV) or hybrids have gained prominence in propulsion markets. With the advent of Tesla model S, Nissan LEAF and GM Volt has given impetus to EV segment of vehicles. Where AC permanent-magnet synchronous electric motor is as a source of power. Due to lack of engine masking noise in the EV, even the low-level tonal noise from gearbox clearly visible in the noise spectrum and is annoying for the occupants (Qin et al., 2020; He et al., 2020). The noise engineer has real challenge in dealing with this kind of noise problems, which needs attention from researchers by developing new methodologies to detect and identify dominant gear vibration sources up front to deal with associated noise issues from the electric and hybrid drive units (DU).

Gear transmissions are an integral part of automotive and other industrial machinery. Gears are transmitting power through shorter distances by supporting them on shaft bearing assembly. In keeping with the current trend towards high mechanical efficiency, the pursuit of compact and lightweight transmission systems, to achieve higher fuel economy, cause an increasing amount of elastic deformation of the gears. The study and understanding of gear dynamics is fundamentally important for the monitoring, control and design of better gear transmission systems.

Theoretically, a pair of meshing gears with perfectly involute teeth profile should transmit uniform angular motion. "The law of gearing states that the angular velocity ratio of all gears of a meshed gear system must remain constant also the common normal at the point of contact must pass

through the pitch point for all positions of mating gear." This law forms the basis for the gear profile design in rigid gears. This is a usually the condition for the two gears to perform properly. But in reality, elastic deformations cause most gear systems fail to transmit uniform angular motion. This difference between the theoretical and actual angular velocity is the transmission error (TE) of the pair of gears in mesh (Harris, 1958).

Impacts between gears have long been identified as one of the main contributors of vibration emission within the transmission systems and this is often referred to as the gear rattle. Most of these gear train impacts are caused by alternating torque fluctuations produced by combustion in internal combustion engines or torque ripple in case of electric drive transmissions of hybrids/battery electric vehicles, and inertia forces acting on the main running gear. The alternating torque accelerates and decelerates individual gears, mainly the unloaded gears of the transmission, which results in the excitation of gears. The similar vibration behaviour occurs suddenly during short span of time when releasing clutch during change of gear and this is called declutch “clunk” or “de clutch clunk”. The clunking may also occur when the load state of the vehicle changes from drive to coast during sudden acceleration and deceleration of the vehicle and this event is called “load reversal clunk”. The other important vibration from transmission loaded gear meshes caused by excitation at the pitch point due to gear profile errors, which is often referred to as transmission error, is called “gear whine”.

Unlike other power transmission mechanisms, gears generate tonal noise at their meshing frequency due to vibration originated at the pitch point of the gear mesh due to transmission error (TE) excitation, which is called gear whine (Morgan, 2007; Rao, 2018). TE is caused by variation of mesh stiffness due to number of teeth in contact during gear mesh during torque transfer and due to either designed or manufacturing deviation from perfect involute profile. Gear whine can be very disturbing for the vehicle occupants, even if the noise level from the gearbox is lower than the total noise level.

In simple terms, the TE is defined as the difference between the actual position of driven gear and the ideal position the gear would have occupied if the driving and driven gears are of perfect conjugate profile, which sets gear mesh in continuous contact without any deformation of gear mesh. It is almost impossible with existing manufacturing technology to achieve the ideal gear tooth profile,

which has zero TE. In addition to manufacturing errors, gear designers introduce known profile modifications based on empirical rules, or they are selected based on similar best practices. The empirical relations related profile modifications to reduce the gear noise and vibration was first published by Walker (1940) to avoid stress concentration at contact zones. These gear profile modifications are usually represented as gear micro geometry. At low speeds (quasi-static) conditions, the difference between the actual and theoretical positions of the output gear is called TE. This form of transmission error is called the static transmission error (STE). Harris (1958) presented the STE amplitude of the gear mesh for different torque increments and are later called as Harris maps.

When the STE is applied in linear models as the main displacement excitation at the gear mesh, it becomes linearly proportional to its counterpart under dynamic conditions. In other words, the amount of reduction in the transmission error under dynamic conditions, called the dynamic transmission error (DTE), would be proportional to the amount of reduction in STE (Benatar, 2019). Fig. 1.1 shows typical gear geometry with line of action and pitch point, where the transmission error creates excitation from the start of engagement of each tooth to the end of its engagement, which constitutes a mesh cycle (Harris, 1958; Benatar, 2019). TE is considered to be the main source of excitation in loaded gears. This thesis is focused on source level analysis for upfront identification by modelling the source of vibration as fault parameters and to avoid excessive vibration of supporting structure to prevent failure of machinery.

The literature review is organised in the following four sections: Transmission error-based gear dynamic models, fault identification in machine elements, and vibration signal processing techniques. Based on the research gaps in dynamics of geared rotor from the literature review the objectives of the present research are derived.

1.2 Transmission Error based Gear Dynamic Models

Plenty of researchers studied geared rotor vibration through numerous mathematical models. Most of the researchers considered TE as excitation source for the gear vibration problem. TE is specified at pitch point of the gear mesh and it is mathematically expressed as change in driven gear position with

respect to the position of a perfect gear drive. Figure 1.2 shown some of the gear tooth terminology discussed in the literature.

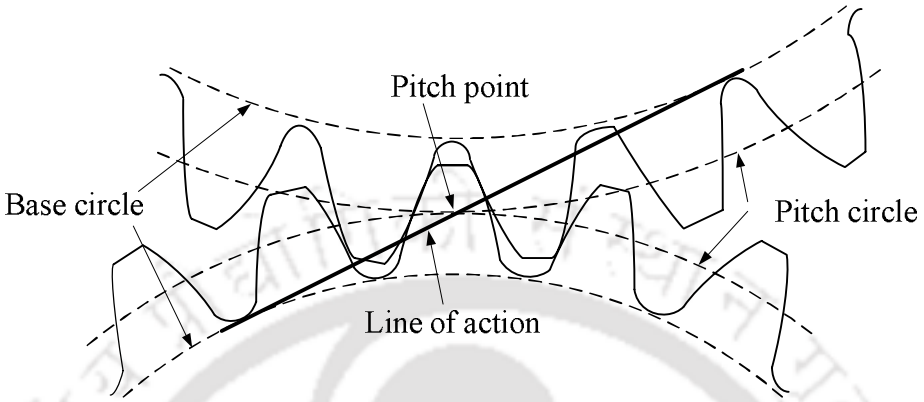

Figure 1.1: Gear pair showing the base and pitch circles and the line of action and pitch point

Özgüven and Houser (1988) reviewed numerous works on mathematical models used in gear dynamics three decades prior to publishing their research article. In this publication, authors review vast amount literature into five categories as given below.

a. *Dynamic Factor Models*: Models used to calculate gear root stress formulae through empirical, semi-empirical methods and dynamic models for determination of the dynamic factor, which is applied to the static load to determine the strength and life of gears under actual operating loads.

b. *Flexible Teeth Models*: The models where flexibility of gear body, shafts, bearings are neglected and the tooth stiffness is considered as the only energy store are called flexible teeth model, which usually reduces to a Single Degree of Freedom (SDOF) mass-spring model. These models can be further developed to determine the dynamic factor.

c. *Gear Dynamic models*: These models include stiffness of shafts and bearings. The torsional flexibility of shafts is found to be important along with the transverse flexibility of the bearings. Traditionally tooth compliance contribution is introduced through the time varying mesh stiffness.

d. *Geared Rotor Dynamic models*: These models specify transverse shaft vibrations in two perpendicular directions, which allows the shaft to whirl. The torsional vibration is usually considered with gear dynamic models, which include vibrations due to teeth flexibility through time varying mesh stiffness

e. *Torsional vibration models*: Those models where the flexibility of the gear teeth is neglected, and the torsional model is obtained with the use of flexible shafts connected to rigid gears are categorised into this bucket.

The authors also discussed about the experimental correlation of widely varied models reviewed in this research article. About these correlations, the authors concluded that the choice of particular experiment based on assumptions made in the model facilitated the correlation. Therefore, the selected models in these research works are specific to the experimental situation and the required outcome.

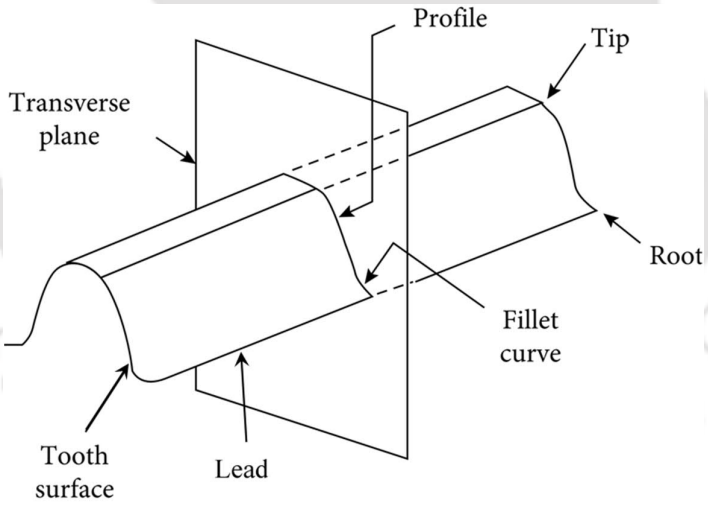

Figure 1.2: Spur gear tooth terminology

Munro (1990) summarized research works on the fundamental concepts of the TE and its measurement techniques. He gave the original definition of TE as the difference between theoretical and actual position of gear. The TE is expressed as a linear deviation measured at the pitch point and calculated at successive positions of the pinion as it goes through the meshing cycle. If a pinion and gear have ideal

involute profiles running with no loading torque they should theoretically run with zero transmission error. However, when these same gears transmit torque, the combined torsional mesh stiffness of each gear changes throughout the mesh cycle as the teeth deflect, causing variations in the angular rotation of the gear body. The author gave insights into sources of the mesh excitation and its contribution to the system excitation, pertaining to the gear noise.

Although a lot of research has been carried out in the field of gear dynamics, there is still scope to investigate thoroughly certain areas that were not well developed before. In the past, the computational limitations were a barrier to certain methods of investigation, and as a result theoretical and numerical methods were prevalent in trying to understand the dynamic behaviour of gears.

Kahraman et al. (1992) presented a finite element model of a geared rotor system on flexible bearings. The model includes the rotary inertia of shaft elements, the axial loading on shafts, flexibility and damping of bearings, material damping of shafts and the stiffness and the damping of gear mesh. The coupling between the torsional and transverse vibration of gears were considered in the model. With the constant mesh stiffness and STE combination, they demonstrated to simulate time varying mesh stiffness approximately. The analysis procedure can be used for the forced vibration analysis of geared rotors by calculating the critical speeds and determining the response of any point on the shafts to mass unbalances, geometric eccentricities of gears, and displacement transmission error excitation at the mesh point. The dynamic mesh forces due to these excitations can also be calculated. The model has been applied to several systems for the demonstration of its accuracy and for studying the effect of bearing compliances on system dynamics. Kahraman (1993) extended his research work on spur gears to helical gear to study the effect of axial vibration on gear dynamics. Subsequently, Blankenship (1996) reviewed research works on gear-pair dynamic characterization based on gear dynamic experiments.

Kahraman (1999a) studied effect of involute tip relief on spur gear dynamics. Fig. 1.3 shows involute tip relief. The influence of gear tooth flank modifications in the form of linear involute tip relief on the torsional vibration behaviour of a spur gear pair is investigated by using an experimental test stand. Measured dynamic transmission error (DTE) values are compared and a family of forced response curves is presented. Guidelines for the design of quiet spur gear sets are also given. Kahraman

(1999b) studied the influence of involute contact ratio on the torsional vibration behaviour of a spur gear pair is investigated experimentally by measuring the dynamic transmission error of several gear pairs using a specially designed gear experimental rig. Measured forced response curves are presented, and harmonic amplitudes of the dynamic transmission error are compared above and below gear mesh resonances for both unmodified and modified gears having various involute contact ratio values. The influence of involute contact ratio on the dynamic transmission error is quantified and a set of generalized, experimentally validated design guidelines for the proper selection of involute contact ratio to achieve quite gear systems is presented. The authors also proposed a simplified analytical model, which accurately describes the effects of involute contact ratio on the dynamic transmission error.

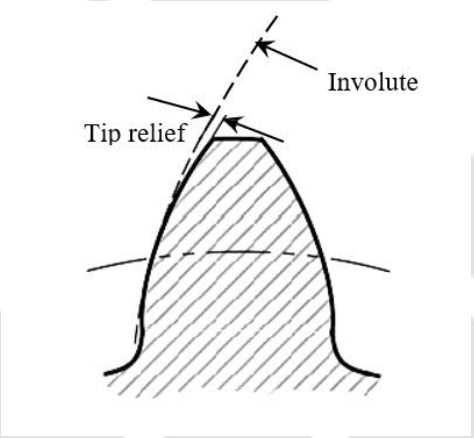

Figure 1.3: Involute tip relief

Choi (2001) presented an analytical study of the dynamic characteristics of a geared rotor-bearing system by the transfer matrix method. Rotating shafts of the system are modelled as Timoshenko beams with effects of shear deformation and gyroscopic moment considered. The gear mesh is modelled as a pair of rigid disks connected by a spring-damper set along the pressure line and the transmission error is simulated by a displacement excitation at the mesh. The transfer matrix of a gear mesh is developed. The coupled lateral-torsional vibration of a geared rotor-bearing system is studied. Natural frequencies and corresponding mode shapes, and whirl frequencies under different spin speeds are determined. Howard et al. (2001) presented a simplified gear dynamic model aimed at exploring the effect of friction on the resultant gear case vibration. The model incorporates the effect of

variations in gear tooth torsional mesh stiffness, developed using finite element analysis, as the gears mesh together. The method of introducing the frictional force between teeth into the dynamic equations is given. The comparison between the results with friction and without friction was investigated using the Matlab and Simulink models developed from the differential equations. The effects the single tooth crack on the frequency spectrum and on the common diagnostic functions of the resulting gearbox component vibrations were also shown.

Lee et al. (2003) presented a study to examine the coupled vibration characteristics of a turbo-chiller rotor-bearing system having a bull-pinion speed increasing gear. They used a coupled lateral and torsional vibration finite element model of a gear pair and provided the mechanism of the characteristic changes. The investigations were systematically carried out by comparing the uncoupled and coupled natural frequencies and their mode shapes with varying gear mesh stiffness, considering rotating speeds, and by comparing the strain energies of the lateral and torsional vibration modes. The results showed that some modes may yield coupled lateral and torsional characteristics when the gear mesh stiffness increases over a certain value. In addition, that their associated dominant modes may be different from their initial modes, i.e. a given dominant mode may change from an initial torsional one to a lateral one or vice versa.

Kubur et al. (2004) presented a dynamic model of a multi-shaft helical gear reduction unit formed by flexible shafts. The model consists of a finite element model of shaft structures combined with a three-dimensional discrete model of helical gear pairs. The bearing and housing flexibilities are included in the model. Eigenvalue solution and the modal summation technique are used to predict the free and forced vibrations of the system. Results of experimental study on a helical gear-shaft-bearing system are also presented for validation of the model. It is demonstrated that the predictions match well with the experimental data in terms of excited modes and the forced response given in the form of the dynamic transmission error. Forced vibrations of an example system formed by three shafts were also studied to demonstrate the influence of some of the key system parameters. Maliha et al. (2004) presented a nonlinear dynamic model for a gear-shaft-disk-bearing system. A nonlinear dynamic model of a spur gear pair is coupled with linear finite element models of shafts carrying them, and with discrete

models of bearings and disks. The nonlinear elasticity term resulting from backlash is expressed by a describing function, and multi harmonic responses are determined of nonlinear multi-degree-of-freedom systems.

Lee (2005) presented a general method for obtaining the unbalance response orbit of a gear-coupled two-shaft rotor-bearing system, based on the finite element approach. Specifically, analytical solutions of the maximum and minimum radii of the orbit were proposed. The method was applied to the unbalance response analysis of a 600 kW turbo-chiller rotor-bearing system, having a bull-pinion speed increasing gear. Bumps in the unbalance responses were observed at the first torsional natural frequency because of the coupling between the lateral and torsional dynamics due to gear meshing. In addition, the analytical solutions were validated with results obtained by a full numerical approach. The proposed method can be generally applied to an analysis of the unbalance response orbits of dual-shaft rotor-bearing systems coupled by bearings as well, which are often found in aerospace gas turbine engines.

In the last two decades, the general trend has been to reduce TE by optimised profile modification for specific operating conditions. Sato et al. (1983) studied analytically and experimentally the influence of profile modifications on gear vibration. In this paper gear performance on vibration is discussed in a wide range of contact ratios from 1.26 to 2.46 using a developed simulator. And tooth profile correction is investigated in relation to pressure angle error. The simulation results are verified with results of dynamic meshing tests. From this investigation the effects of contact ratio and profile correction are clarified.

Tavakoli and Houser (1986) employed an optimisation algorithm based on the modified complex method to a particular objective function based on the mean value of harmonics of the transmission error. They suggested different combinations of tip and root relief to be used to achieve optimization, like varying the starting point of relief and varying the magnitude of relief and selecting the gear and/or the pinion teeth to be tip and/or root-relieved. In addition to the presentation of optimal profile modifications, the effects of off-design loads, non-optimum modifications, and random spacing errors are presented in this research work.

Simon (1989) developed a method for the simultaneous calculation of optimal tooth tip relief and tooth crowning for spur and helical gears. The representation of tip relief and crowning are shown in Fig. 1.3 and Fig. 1.4. The authors described tooth profile modification by a linear function. They introduced linear and parabolic crowning in this research work. The authors set the following two conditions for the optimization of the tooth modifications: (a) the teeth are entering in mesh smoothly, without interference and (ii) the load distribution factor is minimized. A computer program was developed for the calculation of the optimal tooth tip relief and crowning for the spur and helical gears. By using this program, the influence of type and length of optimal crowning and length of tooth tip relief on load distribution factor was investigated. Also, the influence of gear parameters on optimal tooth profile modification was discussed. On the basis of the obtained results, by regression analysis an equation was derived for the calculation of the optimal tooth tip relief.

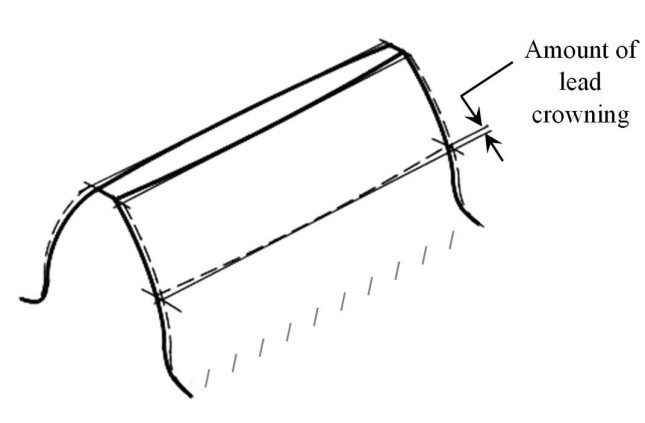

Figure 1.4: Crowned spur gear tooth

Wang et al. (2003) surveyed research works on non-linear gear dynamics modelling. In this paper, the progress in nonlinear dynamics of gear driven systems in the past twenty years was reviewed, especially the gear dynamic behaviour, by considering the backlash and time-varying mesh stiffness of teeth. The authors then reviewed the basic concepts, the mathematical models and the solving methods for the non-linear dynamics of geared systems. The authors also discussed critical issues for further research on the nonlinear vibration in gear transmission systems. Parker (2003) presented problems in gear vibration and noise. He demonstrated the importance of comprehensive experimental

investigations to reveal the complexities involved in it. Fonseca et al. (2005) optimized the harmonics of the static transmission error using the same static model of Tavakoli and Houser (1986) by means of a genetic optimization algorithm. This paper describes the development of a genetic algorithm (GA) model to minimize the weighted sum of the magnitudes of gear mesh frequency components. The GA algorithm was designed based on a mathematical formulation for computing static transmission error and load sharing for low-contact-ratio external spur gears. The constructed GA was able to overcome the local optima and achieve global optimal/near-optimal solutions.

Kayama (2005) and Beghini (2004) carried out many theoretical and numerical studies on the gear contact, the main assumptions in both these cases was the constant torque acting on the gears and also the exclusion of time varying mesh stiffness in the case of the research carried out by Kamaya (2005). Although, the results of most of these investigations carried out are widely accepted as quantitatively correct, one wonders if the assumptions could have made a difference to the outcome. Generally speaking, taking a gear system and modelling it without any simplifying assumptions would create a great deal of complication in solving the equations of motion and extracting a meaningful result. Velex and Ajmi (2006) introduced theoretical approach for the modelling of pinion–gear excitations valid for three-dimensional models of single-stage geared transmissions. Shape deviations and errors on gears are considered and the associated equations of motion account for the time-varying mesh stiffness, and also the torsional, flexural and axial couplings. Starting from the instantaneous contact conditions between the teeth, the equations of motion are re-formulated in terms of quasi-static transmission errors under load and no-load transmission errors. The range of application of transmission error-based formulations is analysed and equations are derived, which make it possible to introduce rigorously meshing excitations via transmission errors. Using an extended finite element model of a spur and helical gear experimental rig, the dynamic results from the formulations based on transmission errors were correlated with reference solution.

Rao and Tiwari (2007) developed a constraint non-linear optimization procedure based on Genetic Algorithms (GA) for designing rolling element bearings based on maximum fatigue life as objective function and associated kinematic constrains. The design parameters include the bearing pitch

diameter, the rolling element diameter, number of rolling elements and inner and outer-race groove curvature radii. The constraints contain unknown constants, which have been given ranges based of parametric studies through initial optimization runs. In the final run of the optimization, these constraint constants are also included as design parameters. The optimized design parameters have found to be yielded better fatigue life as compared to those listed in standard catalogues. The authors performed a convergence study to ensure that the optimized design variables do not suffer from local extremes.

Inalpolat (2010) presented a nonlinear time-varying dynamic model to predict modulation sidebands of planetary gear sets. This discrete dynamic model includes periodically time-varying gear mesh stiffnesses and the nonlinearities associated with tooth separations. The model uses forms of gear mesh interface excitations that are amplitude and frequency modulated due to a class of gear manufacturing errors to predict dynamic forces at all sun-planet and ring-planet gear meshes. The predicted gear mesh force spectra are shown to exhibit well-defined modulation sidebands at frequencies associated with the rotational speeds of gears relative to the planet carrier. This model is further combined with a previously developed model that accounts for amplitude modulations due to rotation of the carrier to predict acceleration spectra at a fixed position in the planetary transmission housing. Individual contributions of each gear error in the form of amplitude and frequency modulations are illustrated through an example analysis. Comparisons are made to measured spectra to demonstrate the capability of the model in predicting the sidebands of a planetary gear set with gear manufacturing errors and a rotating carrier. Wadkar and Kajale (2011) studied geared rotor natural frequencies and mode shapes. Also, the reliability of geared rotor using the time-varying mesh stiffness was investigated.

Chen (2012) Presented a dynamic lumped-parameter gear model by incorporating the effects of a time-varying and asymmetric mesh stiffness and a backlash nonlinearity is formulated to analyze the spur gear rattle response under the idling condition. He assumed a rectangular time-varying mesh stiffness function. The phase shift between the mesh stiffness for the forward and backward contacts was examined. Numerical studies are employed to examine the effects of engine torque fluctuations and tooth surface friction on the gear rattle response and the corresponding tooth impact behaviour.

Comparisons between the results from the time-invariant mesh stiffness model and the proposed time-varying mesh stiffness model reveal differences in the gear responses, especially when the mean rotational speed of the fluctuating gear pair is non-zero. The analysis revealed significant effects on the high frequency response components. However, the author examined the idling gear dynamics are relatively insensitive to the tooth surface friction. Li et al. (2014) studied coupled lateral-torsional-axial vibration problem of a helical gears mounted on flexible bearings using system model approach. Considering the axial and radial loads, a mathematical model of angular contact ball bearing was derived with Hertz contact theory. With the coupling effects of lateral, torsional and axial vibrations considered, a lumped-parameter nonlinear dynamic model of helical gear-rotor-bearing system (HGRBS) is established to obtain the transmission system dynamic response to the changes of different parameters. The vibration differential equations of the drive system were derived through the Lagrange equation, which considers the kinetic and potential energies, the dissipative function and the internal/external excitation. Based on the Runge-Kutta numerical method, the dynamics of the HGRBS is investigated, which describes vibration properties of HGRBS more comprehensively. The results showed the obvious fluctuation in the vibration amplitudes, the frequency multiplication and random frequency components become increasingly obvious with changing rotational speed and eccentricity at gear and bearing positions. Axial vibration of the HGRBS also had some fluctuations.

Zhou et al. (2015) presented a 16-DOF lumped parameter dynamic model considering the gravity, eccentricity, bearing clearance, transmission error, and coupled lateral-torsional vibration. Based on the dynamical equation, the dynamic behaviours of the spur gear rotor bearing system are investigated by using Runge-Kutta method. Their research focused on the effect of rotational speed, eccentricity, and bearing clearance on the nonlinear response of the coupled multibody dynamics and presented in the form of the vibration waveform, spectrum, and 3D frequency spectrum. The results showed that the rotational frequency of the driven gear appears in the driving gear, and the dynamic characteristics of gears have obvious differences due to the effects of the gear assembly and the coupled lateral-torsional vibration. The bearing had its own resonance frequency, and the effect of the variable stiffness frequency of the bearings should be avoided during the system design. The results presented

in this paper showed an analysis of the coupled lateral-torsional vibration of the spur gear system. Temis et al. (2015) compared two different methodologies to simulate the dynamic behaviour of geared systems. The nonlinear torsion vibrations of the geared systems are studied at resonance frequency with the contact loss of the meshing teeth. The authors modelled a time-varying mesh stiffness of tooth pairs by considering viscous damping proportional to the meshing stiffness. Gear errors of each meshing tooth pair are also included. The dynamic motion of the spur gear pair over wide range of excitation frequency using the finite element method was simulated. Results of bending stress distribution during overall operation speeds were obtained by the finite element analysis. The authors suggested it to be used as a tool for aiding the gear fault diagnosis.

Zhang (2017) presented empirical gear profile micro-modifications to study the accuracy of gear transmission. The authors modelled a helical gear pair analyzed in RomaxDesigner software to investigate the utility of these modification methods to select some of them for experimental proposals for gear pairs. Rao and Ganti (2018) presented a multibody dynamics (MBD) analysis approach for analysing gear whine noise of a 6-speed automotive transmission with static transmission error (STE) based gear contact modelling. The transmission error is calculated using Load Distribution Program (LDP) incorporating gear micro geometry variation as excitation. Dynamic bearing loads were calculated at the interface of transmission housing for given loading and speed sweep. The calculated loads were applied on the finite element (FE) system level transmission model. The FE model includes lumped mass and inertia of non-structural components of transmission along with its housing. This model was used to identify critical noise paths by considering calculated acceleration on housing as a noise metric. The authors calculated pseudo-sound power with mass compensated FE model using ABAQUS with the calculated dynamic bearing load excitations from the MBD model are applied to it. These results are validated with transmission noise test measured sound power in dyno. Stiffening/softening the critical noise paths and hot spot regions on the housing are used to minimize noise by avoiding the resonance. A unique process flow is proposed to mitigate gear noise issues at the early stage of design.

Benatar et al. (2019) presented a set of motion transmission error data for a family of helical gears having different profile and lead modifications operated under both low-speed (quasi-static) and dynamic conditions. The authors used power circulatory test machine along with encoder and accelerometer-based transmission error measurement systems to quantify motion transmission behaviour within wide ranges of torque and speed. Results of these experiments indicate that the tooth modifications impact the resultant static and dynamic transmission error amplitudes significantly. In their study, a design load was shown to exist for each gear pair of different modifications, where the static transmission error amplitude is minimum. Forced response curves and waterfall plots were also presented to demonstrate that the helical gear pairs act linearly with no signs of nonlinear behaviour, such as the tooth contact separation. Furthermore, the static and dynamic transmission error amplitudes are observed to be nearly proportional, suggesting that the static transmission error can be employed in helical gear dynamic models as the main gear mesh excitation.

Celikay (2021) studied a subharmonic resonance observed in spur gear pairs as a parametrically excited system. The stiffness at the gear contact interface that couples the gear bodies is a periodically time-varying due the fluctuation of number of tooth pairs in contact. In presence of such stiffness fluctuation as part of the excitations, various published studies predicted subharmonic resonances near speeds that are integer multiples of the speed at which the primary resonance occurs, with little or no validation. This study presents an extensive experimental investigation to show such subharmonic resonances and various associated period-n motions ($n \geq 2$) under both transient and steady-state conditions. A test set-up and a pair of test gears developed for this purpose are described along with solutions to various measurement and data processing challenges. Two different models of the gear pair, a purely torsional discrete model and a deformable-body model, are employed, and their predictions are compared to the measured period-1 and period-n motions to assess their accuracy.

Flek et al. (2021) presented time-varying stiffness of spur gears in the dynamic model of transmission systems as an internal excitation of the dynamic system. The authors introduced ways to approach the modelling of gear stiffness using analytical calculations, which allow to model the course of mesh stiffness depending on its rotation. For the verification an analytical model were created of five

different gearings, and based on their geometry, the respective stiffness curves were analytically determined. Subsequently, a finite element simulation was performed in the Abaqus CAE software to identify and objectively compare the stiffness curves and further determine the suitability of using the analytical model to determine the mesh stiffness of gearing.

There are many software packages available to calculate TE, like Windows LDP 4.9.0 (Load Distribution Program) from the Gear Dynamics and Gear Noise Research Laboratory of the Ohio State University. The LDP 4.9.0 calculations do not consider system deflections while calculating TE. MASTA 11 is a gear transmission specific system model software, it considers system deflections while calculating TE. As the speed of gears increases the TE changes from being purely geometric and load dependent property to include system level dynamics, which gives rise to dynamic transmission error (DTE). While the DTE is the transmission error, which is most closely related to gear noise, it is of course the most difficult to obtain, either by analysis or measurement. There are hardly any efforts in the modelling gear vibration considering DTE using practical considerations of the gear mesh whirling behaviour. This has motivated the authors to consider a novel system model approach, which can be used for the identification of DTE at a later stage.

It is found from the surveyed literature that all the gear contact models are excited with STE as a source of disturbance at the pitch point of gear, which is modelled along the line of action. For analysing, the response in time and frequency domain, signal processing techniques are discussed in the next sections

1.3 Fault Identification in Machine Elements

Gears are considered as dominant source of vibration due to deviation from perfect conjugate profile caused by the dynamic nature of gear contact between flanks of mating gears. These dominant sources, such as the transmission error, gear mesh stiffness and gear runout errors, individually or in combination caused peak amplitudes in the response. In addition to these inherent manufacturing errors, geared rotors may experience other faults, like the missing tooth, cracks in ger tooth or shafts, misalignments, unbalance, shaft bow, motor faults, nearing faults, etc. These dynamic effects may sometimes cause

catastrophic failure of mechanical systems and subassemblies attached to the supporting structure. Estimation of these gear parameters by modelling them as fault parameters is having paramount importance (Mitchell, 1993; Edwards et al., 1998).

A brief literature review is presented below on fault detection and identification in rotating machinery.

Lee (1994) presented a comprehensive identification method for rotary asymmetry in rotating machines based on the complex modal testing method. In this research authors showed that the reverse directional frequency response function (dFRF), which indicates the degree of asymmetry, can be identified with a simple testing method requiring only a single vibration sensor and a single exciter. To clarify physical realization associated with estimation of the reverse dFRF, its relation to the conventional frequency response functions, which are defined by the real input (excitation) and output (vibration measurement), are discussed extensively.

Sekhar (2004) presented the study a model-based method for the on-line identification of two cracks in a rotor. The fault-induced change of the rotor system is considered by equivalent loads in the mathematical model. The equivalent loads are virtual forces and moments acting on the linear undamaged system to generate a dynamic behaviour identical to the measured one of the damaged systems. The rotor is modelled using finite element method, while the cracks are considered through local flexibility changes. The cracks are identified for their depths and locations on the shaft. The nature and symptoms of the fault, that is crack, are ascertained using the FFT. Darpe (2007) presented a fatigue shaft crack detection methodology for its diagnosis. The coupling of bending and torsional vibrations is the basis for the proposed methodology in general and the presence/absence of such cross-coupling terms at various orientation of crack in a rotor due to its opening and closure under the influence of gravity, in particular. A transient torsional excitation is applied for a very short duration at specific angular orientation of the rotor and its effect in the lateral vibrations is investigated. Wavelet transforms is used in revealing the transient features of the resonant bending vibrations, which are set up for a short duration of time due to transient torsional excitation.

Chaari et al. (2009) studied faults incurred by gears, the authors found the change in stiffness and consequently vibration characteristics of the damaged tooth. In this research, an analytical formulation of the time-varying gear mesh stiffness was derived. An original analytical modelling of tooth cracks is presented and the gear mesh stiffness reduction due to this fault was quantified. A comparison with the finite element model is presented in order to validate the analytical formulation. Mohammed et al. (2013) presented vibration-based condition monitoring of geared rotors and to prevent occurrence of catastrophic gear failures. It is important to improve the simulated dynamic response of the studied gear model. The authors considered reduction in the gear mesh stiffness to assess the status of tooth damage and, therefore, by increasing the accuracy of the calculated mesh stiffness, dynamic simulations of a gear can be improved. In this paper a method is presented for calculating the gear mesh stiffness for a propagating crack in the tooth root. The influence of gear mesh stiffness on the vibration-based fault detection indicators, the RMS, kurtosis and the crest factor are investigated. The authors proposed an improved mesh stiffness calculation for the purpose of fault detection in geared rotors using vibration signals.

Shravankumar and Tiwari (2013) studied a Laval rotor with the transverse crack and disc unbalance, and identified different rotor system parameters, such as the viscous damping, disc eccentricity along with the stiffness and crack excitation force in the switching crack model, using a regression matrix approach. Singh and Tiwari (2016) extended the identification of crack using a Jeffcott rotor incorporating active magnetic bearing (AMB) with and without considering the gyroscopic effect. The AMB was used to suppress the vibration, and the controller current of AMB along with the displacement of disc in the form of full spectrum data were used to identify the crack. Singh and Tiwari (2017) further extended the research based on the FEM modelling including the gyroscopic effect incorporating with an AMB onto the rotor system. Srinivas and Tiwari (2019) studied model-based analysis and identification of multiple fault parameters in coupled rotor systems with offset discs by integrating with an active magnetic bearing in the presence of angular misalignment using least-squares fit.

Mark et al. (2019) presented models of missing working-surface material caused by damage and are used to show where transmission-error rotational-harmonic spectrum changes will take place. Bending fatigue damage is shown to initially cause maximum changes in rotational harmonic amplitudes well below the tooth-meshing fundamental harmonic, whereas small pits are shown to cause changes in higher-frequency rotational-harmonic amplitudes. Good agreement is shown between an experimentally obtained rotational-harmonic spectrum caused by tooth-surface damage and that predicted from damage measured on the failing teeth. Substantial increases in high-frequency rotational-harmonic amplitudes are shown to be expected from gear teeth undergoing significant plastic deformation in later stages of bending-fatigue failure. Accurate assessment of damage contributions using before-damage non-negligible rotational-harmonic amplitudes (sideband harmonics, etc.) are shown to suggest use of complex rotational-harmonic amplitudes. Huangfu et al. (2020) presented a dynamic model for spalled gear pairs by considering the realistic spalling morphology obtained from the fatigue experiment. The authors used loaded tooth contact analysis method to evaluate the meshing characteristics of spalled gear pairs. In order to verify the proposed method, the mesh stiffness and contact stress obtained from the proposed method are compared with those obtained from the finite element method and the method in published literature. The mesh stiffness and the non-loaded static transmission error are imported into the geared rotor dynamic model to acquire the dynamic responses. The spectrum characteristics and statistical indicators under different spalling patterns are acquired by the proposed model. The authors validated the simulated fault features with experimental data.

Yu (2021) presented research paper on gearbox fault diagnosis based on bearing dynamic force identification. In these attempts, authors used the analytical, transfer matrix and finite element methods. Wherein, the model of faults with unknown parameter are considered. Through least-squares or other fitting technique the unknown fault parameters are estimated with the help of system responses.

Nowadays, deep learning is the most attractive research trend in the area of machine learning for fault diagnosis with the ability of learning features from raw data by deep architectures with many layers of non-linear data processing units. A brief of artificial intelligence and machine learning techniques in fault detection and identification are reviewed in the next section.

1.3.1 Artificial Intelligence and Machine Learning Based Fault Detection

Samanta (2004) presented a study to compare the performance of gear fault detection using artificial neural networks (ANNs) and support vector machines (SMVs). The time-domain vibration signals of a rotating machine with normal and defective gears are processed for feature extraction. The extracted features from the original and pre-processed signals are used as inputs to both classifiers based on ANNs and SVMs for two-class (normal or fault) recognition. The number of nodes in the hidden layer, in case of ANNs, and the radial basis function kernel parameter, in case of SVMs, along with the selection of input features are optimised using genetic algorithms (GAs). For each trial, the ANNs and SVMs are trained with a subset of the experimental data for known machine conditions. The trained ANNs and SVMs are tested using the remaining set of data. The procedure is illustrated using the experimental vibration data of a gearbox. Widodo (2007) presented the use of machine learning based support vector machine in machine condition monitoring and fault diagnosis. These works give lot of insights into fault identification techniques required for gear fault identification.

Chen (2015) presented an implementation of deep learning algorithm convolutional neural network (CNN) for the fault identification and classification in gearboxes based on vibration signals. Different combinations of condition patterns based on basic fault conditions are considered. Twenty test cases with different combinations of condition patterns are used, where each test case includes 12 combinations of different basic condition patterns. Vibration signals are pre-processed using statistical measures from the time domain signal, such as the standard deviation, skewness, and kurtosis. In the frequency domain, the spectrum obtained with FFT is divided into multiple bands, and the root mean square (RMS) value is calculated for each one so the energy maintains its shape at the spectrum peaks. Lu (2017) proposed intelligent fault diagnosis technique of rolling bearing using hierarchical convolutional network-based health state classification. Due to the strong non-linear and non-stationary characteristics, an effective and reliable deep learning method based on a convolutional neural network (CNN) is investigated in this paper by making use of cognitive computing theory, which introduces the advantages of image recognition and visual perception to bearing fault diagnosis by simulating the cognition process of the cerebral cortex. The novel feature representation method for bearing data is

first discussed using supervised deep learning with the goal of identifying more robust and salient feature representations to reduce information loss. Next, the deep hierarchical structure is trained in a robust manner that is established using a transmitting rule of greedy training layer-by-layer. Convolution computation, rectified linear units, and sub-sampling are applied for weight replication and reducing the number of parameters that need to be learned to improve the general feedforward back propagation training. The CNN model could thus reduce learning computation requirements in the temporal dimension, and an invariance level of working condition fluctuation and ambient noise is provided by identifying the elementary features of bearings. A top classifier followed by a back-propagation process is used for fault classification. Contrast experiments and analyses were undertaken to delineate the effectiveness of the CNN model for fault classification of rolling bearings.

Hoang (2019) surveyed on the deep learning-based bearing fault diagnosis. The authors proposed three popular deep learning algorithms for bearing fault diagnosis including Autoencoder, restricted Boltzmann machine, and convolutional neural network are briefly introduced. And their applications are reviewed through publications and research works on the area of bearing fault diagnosis. Further applications and challenges in this research area are also discussed.

Rezaeianjouybari and Shang (2020) presented the state-of-the-art deep learning-based prognostics and health management frameworks for efficient and effective system health monitoring methods, including processing and analysing massive machinery data to detect anomalies and performing diagnosis and prognosis. It emphasizes on the most recent trends within the field and presents the benefits and potentials of state-of-the-art deep neural networks for system health management. In addition, limitations and challenges of the existing technologies are also discussed, which leads to opportunities for future research. Khan et. al. (2021) presented a framework for testing the robustness of AI-based prognostic and systems health management (PHM). It reviews some key milestones achieved in the AI research community to deal with three particular issues relevant for AI-based PHM in safety-critical applications: robustness to model errors, robustness to unknown phenomena and empirical evaluation of robustness during deployment. To deal with model errors, many techniques from probabilistic inference and robust optimisation are often used to provide some

robustness guarantee metric. In the case of unknown phenomena, techniques include anomaly detection methods, using causal models, the construction of ensembles and reinforcement learning. It elicits from the authors' research on fault diagnostics and robust optimisation via machine learning techniques to offer guidelines to the PHM research community. Finally, challenges and future directions are also examined; on how to better cope with any uncertainties as they appear during the operating life of an asset.

Gai et al. (2021) presented a parameter-optimized deep belief network (DBN) based on sparrow search algorithm (SSA) for gear fault severity detection. Firstly, the initial DBN is trained by the labelled gear fault signals in different severities. Secondly, SSA is introduced to optimize the learning rate and the batch size of the initial DBN, so as to avoid the interference caused by selecting network parameters by subjective experience. Finally, the detection method of gear fault severity based on the improved DBN with the optimal parameter combination is constructed. The performance of the proposed method is evaluated by analysing the gear datasets under five degrees of tooth-breaking fault, the results show that the average detection accuracy reaches over 96% with a standard deviation of 1.46%. Compared with other methods, it is proven that the proposed method has better feature extraction ability, stability, and accuracy for gear fault severity detection. Xingxin et al. (2022) presented Artificial Intelligence based unsupervised learning for fault detection to shift the attention from supervised learning algorithms for fault detection and classification which is well-studied in. Additionally, research on substation fault detection has emphasized the use of unsupervised learning in conjunction with neural network modelling to detect and diagnose unknown fault states. The authors combined an incremental one-class method for detecting anomalies and a dynamic shallow neural network for the fault state to accomplish it. Moreover, the proposed research was used to data samples to detect faults, and the results were superior to those obtained in prior research work. Additionally, experimental research is performed on online process-based substation equipment to determine the validity of the technique. The findings indicate that the suggested framework is an effective tool for detecting and categorizing known and unknown process problems.

Chen et al. (2022) proposed an AI based identification algorithm to identify the state variables of physical phenomenon without feeding any existing mathematical relationships. All physical laws are described as mathematical relationships between state variables. These variables give a complete and non-redundant description of the relevant system. However, despite the prevalence of computing power and artificial intelligence, the process of identifying the hidden state variables themselves has resisted automation. Most data-driven methods for modelling physical phenomena still rely on the assumption that the relevant state variables are already known. A longstanding question is whether it is possible to identify state variables from only high-dimensional observational data. In this research work, the authors proposed a principle for determining how many state variables an observed system is likely to have, and what these variables might be. The authors demonstrated the effectiveness of this approach using video recordings of a variety of physical dynamical systems, ranging from elastic double pendulums to fire flames. Without any prior knowledge of the underlying physics, the proposed AI based algorithm discovers the intrinsic dimension of the observed dynamics and identifies candidate sets of state variables.

This section is not directly related to the present research but for completeness briefly literatures based on Artificial Intelligence (AI) and Machine Learning (ML) of geared-fault detection and classification has been done. Signal processing techniques for rotating systems are disused in the next chapter.

1.4 Vibration Signal Processing Techniques

To analyse the geared rotor response in frequency domain, the signal processing techniques is very important. It separates response due to different fault frequencies and helps in the identification of TE and other gear mesh faults. Southwick (1993) presented the full-spectrum analysis, which unwraps the traditional fast Fourier transform (FFT) spectrum into the forward and backward whirl frequencies. The full-spectrum is suitable for analysing response of geared rotor system as it is an augmented version of the Campbell diagram. Qu et al. (1993) studied vibration measurement of large machinery by short period Fourier Transform and Wigner distribution to nullify the shortfalls in conventional FFT methods.

Southwick (1994) studied response of a rotor using full-spectrum for obtaining the asynchronous and synchronous vibrations. He investigated the ellipticity of whirling orbits under various conditions that paved motivation for the progress to the full-spectrum. Goldman and Muszynska (1999) presented a method for the detection of various rotating machinery faults with the full-spectrum. They also presented phase correlation of rotor orbits in the horizontal and vertical spectrum components.

Bachschmid et al. (2004) analysed rotating machinery vibrations using full-spectrum with shape and directivity index method for analysing the ellipticity of filtered orbit. Tuma and Bilos (2007) studied rotor mounted on fluid film bearings to identify fluid-induced instability and whirl frequency components with full-spectrum response plots. Patel and Darpe (2011) investigated cracked rotors using full-spectrum response for identification of the crack rub with directional nature of higher harmonics. Shravankumar and Tiwari (2013) studied the model-based crack identification in cracked rotors with full-spectrum response plots. Hong and Dhupia (2014) demonstrated time domain approach to identify the gearbox faults using measured response from an experimental rig. Sawalhi and Randall (2014) presented a method on the identification of teeth count of two parallel stages of gears without speed reference signal under variable speed condition. Feng et al. (2016) proposed an order spectrum analysis method based on the iterative generalized demodulation for the characteristic frequency identification in a faulty planetary gearbox.

Sarmah and Tiwari (2019) proposed a model-based approach for identifying rotodynamic parameters using full spectrum using a mathematical model of a cracked shaft system with an offset-disc integrated with an active magnetic bearing (AMB). Subsequently, an identification algorithm is developed based on the proposed mathematical model to estimate the multiple critical parameters of the model with the help of displacements and AMB currents obtained from full spectrum analysis. Roy (2020) studied internal damping due to rub between transverse fatigue crack faces. In experimental setup, a hairline fatigue crack was artificially developed by three-point bending procedure in a shaft at a notch location. The opening and closure behaviour of crack faces during rotation of the shaft leads to the forward and backward whirls of the rotor at multiple frequencies, which are apparent in the full spectrum. Amplitudes of full spectrum are used for qualitative indication of crack.

The research gaps of the literature reviewed in the above sections are discussed in the following section.

1.5 Research Gaps in Dynamics of Geared rotor from Literature Review

Traditionally the transmission error (TE) is considered to be the source of gear vibration and associated noise. Modelling of the TE and its quantitative prediction of TE in a pair of gears transferring power is a challenge to the researchers. A lot of research has been done on geared rotor with the TE as a major source of excitation. Apart from the TE, some of the researchers also studied other system level excitations, like the variation in gear mesh stiffness, gear eccentricities and geared rotor unbalances. Still, lot of research efforts are required in accurately modelling and qualitatively predicting these excitations in a geared rotor assembly. Some of the important research gaps in model based geared rotor system analysis and identification are as follows:

(a) Modelling of TE: Often it is found in the literature that the static TE is assumed to be oriented along line of action, which in turn assumed to be oriented in vertical direction to make it one directional symmetric excitation. This approach lacks excitations caused in mutually orthogonal directions during power transmission in a practical gear drive. These excitations at the gear mesh may not be symmetric due to geometric imperfections in the gear profile and unbalance in the geared rotor assembly. Also, there is lack of fundamental studies in the literatures on modelling of TE and its contribution to overall vibration spectrum.

(b) Geared rotor DTE parameters: Apart from the static TE, there are many other geared rotor parameters, which may excite or affect the system responses, like the dynamic transmission error, gear mesh time variant stiffness, unbalances, gear runouts, and gear mesh damping. Modelling of geared rotor considering all these parameters, which may influence the gear vibration and noise is lacking in the literature.

(c) Identification of dominant gear mesh parameter: Out of many system level excitations, which influence geared rotor response, the identification of dominant source of excitation using appropriate

signal processing technique in conjunction with system modelling is hardly attempted in the literature. Identification of critical source is useful to mitigate dominant noise source in the geared rotor system.

(d) Identification of transmission error: Validation of transmission error by quantitatively identifying it using the geared rotor response is hardly attempted in the literature. Validation of the TE requires a geared rotor test kit to measure the geared rotor response and appropriate signal processing techniques.

(e) Identification and validation of multiple gear mesh DTE parameters: Identification of multiple gear mesh parameters including the TE, gear mesh stiffness, gear mesh damping, and gear eccentricities as fault parameters due to dynamic TE using appropriate signal processing technique in conjunction with system model is lacking in the literature. The accurate estimation of these DTE gear mesh parameter are still a challenge. Validation of identified multiple gear mesh parameters using geared rotor test kit measured response and appropriate signal processing technique is hardly attempted in the literature.

1.6 Objectives of the Present Research

The objective of this research is to analyse and identify geared rotor DTE parameters, which includes the TE, gear mesh stiffness, gear mesh damping, and gear eccentricities. The analysis is to be carried out using system model approach. So, a system model of the geared rotor needs to be developed. Responses of the system model is to be generated using the mathematical model. The response is to be analysed both in time and frequency domain. The time domain equations of motion are to be transformed into frequency domain. A geared rotor experimental kit is to be developed to validate the system model by correlating test measured response with numerical simulations. An attempt is to be made in this research to develop an identification algorithm in frequency domain to estimate various faults and uncertain system parameters. Also, the identified parameters are to be validated by comparing frequency domain response of identified parameters with test measured response. The following are main objectives of the present research:

(1) Geared rotor system modelling with asymmetric transmission error excitation

A geared rotor system model is to be developed with asymmetric TE excitation in mutually orthogonal transverse directions at the gear mesh. The equations of motion of the geared rotor system model is to be derived for transverse vibration using Lagrangian dynamics by considering shafts as torsionally rigid. Linear differential equations of motion of the geared rotor with asymmetric TE excitation is to be analysed in time domain.

(2) Analysis of geared rotor response in frequency domain

Geared rotor response is to be analysed both in time and frequency domain to study the effect of asymmetric transmission error and other DTE gear mesh parameters. Time domain analysis is to be performed by plotting the responses of both the shafts in mutually orthogonal directions in the form of an orbit plot. To identify the variation in fault frequencies in the response, frequency domain analysis is to be made after converting time domain response into frequency domain using the fast Fourier transform (FFT). For analysing geared rotor responses on both gears, which rotate in opposite directions, full spectrum response plots that unwraps frequency spectrum into forward and backward whirl frequencies are to be chosen for the analysis. The time domain equations of motion are to be transformed into frequency domain in complex domain. The asymmetric TE, which excites the geared rotor to be modelled with multiple harmonics of the meshing frequency.

(3) Identification of dominant source of vibration in the geared rotor

A numerical simulation is be carried out by changing the DTE gear mesh parameters and the response is to be analysed using both orbit and full spectrum response plots. Variation of responses with variation geared rotor DTE parameters are to be studied in both time and frequency domain to identify the dominant source of vibration.

(4) Identification of multiple gear mesh DTE parameters

An identification algorithm is to be developed with an objective to identify all the DTE gear mesh parameters, including the asymmetric TE. Developed equations of motion need to be transformed into

frequency domain and rearranged in a regression form to estimate the asymmetric transmission error and the associated gear meshing DTE fault parameters. Gaussian white noise is to be introduced into the mathematically calculated response to check the robustness of the identification algorithm.

(5) Geared rotor experimental rig design, development and validation of system model response

A geared rotor experimental rig is to be designed and developed to validate mathematical model developed for this purpose. Geared rotor experimental rig is to be loaded with nominal torque to avoid separation of gears during torque transfer and response is to be captured using displacement probes at the gears. Measured response is to be analysed in time domain using orbits plots. Time domain response is to be converted into frequency domain using FFT and the response is analysed in full spectrum plots. The system model response is to be compared with test measured response in an effort to validate it.

(6) Identification of multiple gear mesh parameters using measured responses and its validation

Geared rotor experimental rig DTE parameters, like the asymmetric TE and their phases of test gear mesh, gear mesh stiffness, gear mesh damping and gear runouts and their phases are to be identified using test measured vibration signal with the proposed identification algorithm. With the identified experimental rig DTE parameters, orbit and full spectrum plots are to be generated. These plots are compared with original test measured orbit and full spectrum plots for validation.

1.7 Thesis Outline

The thesis comprises of a total seven chapters and brief description of them are now given.

- Chapter 1: Introduction and Literature Review: This chapter gives overview of the problem and the motivation of the current research. It identifies gaps in the literature in the chosen research field based on literature survey, and the objectives of the present research are derived based on that.
- Chapter 2: Modelling of Geared rotor System: This chapter describes system model approach used for mathematically modelling the asymmetric TE and other DTE fault parameters. The

equations of motion of 4-DOF gear vibration problem is derived in this chapter using Lagrangian dynamics.

- Chapter 3: Transformation of Equations of Motion of Geared Rotor into Frequency Domain: This chapter describes the transformation of time domain equations of motion into frequency domain using Euler's equations by separating steady state response based on excitation frequency.
- Chapter 4: Detection and Identification of Gear mesh Dynamic Transmission Error Parameters using full spectrum analysis: This chapter describes the numerical solution to the equations of motion in time domain and converting it frequency domain to analyse the response with the help of orbit and full spectrum plot for detection of dominant source of vibration in geared rotors. Also, it presents identification algorithm developed for estimating gear mesh DTE parameters with numerical test using full spectrum response.
- Chapter 5: Experimental rig Design and Development for Validation of Geared rotor System Model: This chapter describes geared rotor experimental rig design and development. It gives experimental rig's gear vibration measurement procedure using displacement probes. It also describes the estimation of experimental rig gear mesh DTE parameter identification using the algorithm discussed in Chapter 4 and its validation using test measurements.
- Chapter 6: Conclusions and Future Recommendations: This chapter gives conclusion derived from the current research work and lists the future recommendation.

CHAPTER 2

MODELLING OF GEARED ROTOR SYSTEM WITH TRANSMISSION ERROR

Equation Chapter (Next) Section 2

2.1 Introduction

A geared rotor system model is developed with gear mesh mounted on the input and output shafts and supported on rigid bearings. The input shaft is driven with a motor drive and resisting torque is applied on the output shaft through a magnetic brake. The gear mesh is modelled with two discs connected with spring and damper elements along the line of action with the gear mesh stiffness and gear mesh damping, respectively. At the pitch point of the gear mesh a static transmission error (STE) excitation is modelled. The variation of the static transmission error during the torque transfer due to system level effect, like the shaft stiffness, gear runouts and their phases is considered by combining them into dynamic transmission error (DTE) excitation at the pitch point of the gear mesh. Equations of motion of the proposed system model are derived using Lagrangian dynamics.

Apart from having many gear dynamic models available in the literature to solve the gear vibration problem, there are many commercially available software for modelling and analysing gear vibration problem. However, the system model approach provides opportunity to use innovative modelling approaches, which are not tried before to understand more about the dynamic behaviour of the gear mesh and its response. So, in the present section equations of motion of a geared rotor with the asymmetric transmission error has been derived.

2.2 Geared Rotor System Model

Gears are known for its non-linear torsional and bending couple during high torque transfers. However, often gears are operated at low torques even though they are designed for higher torques. For example, automotive transmission gears are designed for high torque transfers but may time those gears are operated at low torques in top gears. Similarly, there are many industrial equipment, which are operated with gears at low torques during part load operations even though they are designed for higher torques

to sustain during peak operating conditions. Under part load operations the gears and supporting shafts exhibit negligible torsional twist and supporting bearings also exhibit similar behaviour with negligible flexibility. Under these operating conditions lateral vibration is predominant in the geared rotors. As torsional vibrations in gears are studied with many advanced modelling techniques as discussed in the literature. In this research work attempt is made to model lateral vibration based geared rotor system by ignoring its coupling with the torsional vibration. This situation is possible in geared rotors during torque transfer when the gears tooth takes entire loading at the contact zone due to torque transfer and tooth deformations at the contact zone happen due to TE, which excites lateral vibration of supporting shafts.

The proposed research will be helpful to understand the impact of asymmetric STE on geared rotors and fills the gaps in the literature lateral vibration of shafts and their whirling aspects. This has motivated to come up with geared rotor system model by neglecting the torsional vibration and its coupling with transverse vibration. This assumption also eliminated the non-linearities associated with resulting geared rotor equations of motion. This approach provides the opportunity to study more about gear transmission dynamics problem with matured linear mathematical techniques. Also, this novel approach makes use of existing simple measurement techniques available to for lateral vibration in rotor dynamic systems to validate the system model and identification of asymmetric TE instead of going for expensive torsional vibration measuring equipment if not available in hand. Also, it is practically easy to access gear transmission shafts with displacements probes for lateral vibration measurements rather than mounting high quality encoders to measure the TE of gear mesh by phase demodulation of the pulse signals of encoders as followed in transitional approach Munro (1990).

A geared rotor system model is developed to calculate lateral vibrations of the gear mesh due to the TE excitation at the pitch point. To reduce the complexity of equations of motion, the bearings are considered to be rigid, and shafts and body of the gears are also considered to be rigid in torsional mode of vibration as discussed in the above paragraph. Gear deformation at pitch point is considered to study the effect of TE in transverse vibration only. The dynamic aspects considered in this model are gear runouts and TE. These runouts generated unbalance force at the centre of gravity of the gears. The

peak-to-peak loaded TE is assumed to be acting the pitch point as a sum of mean component and variable components with respective initial phases. In this model the tooth-to-tooth variation of the peak-to-peak TE is neglected for simplicity. One of the novel approaches in this model is that the line of action is oriented in the oblique plane by considering realistic aspects of gear mesh unlike the approach of orienting the line of action along *y*-axis, which makes zero mesh forces along *x*-axis. This approach gives a better understanding on gear mesh behaviour by giving excitation in both transverse directions, which is helpful for studying the transverse forward and backward whirl aspects of the gear mesh. This approach has necessitated the consideration of TE excitation components to be acting in both *x* and *y* directions with asymmetry at the surface contact zone created at the pitch point due to profile variations in the gear mesh during complete mesh cycle.

The main innovative aspect of present modelling is asymmetric STE and its initial phase-in both pressure line (*y* direction) and line perpendicular to it (*x* direction) at the pitch point of the gear mesh. Choice of this asymmetric TE excitation at the gear mesh came from realistic gear mesh operating conditions where excitation from mutually perpendicular transverse directions are not ruled out. These novel modelling approaches in the system model presented in this research work has facilitated the study of the forward and backward whirl aspects of geared rotor with asymmetric excitations caused by modelled TE.

The proposed geared rotor system model is shown in Fig. 2.1. It has a simple spur gear pair mounted on flexible shafts with rigid end bearings. The geared rotor system consists of a motor connected to input shaft through a rigid coupling. Input shaft carries a pinion at the mid-span, which is meshed with a gear mounted on the mid-span of output shaft, which carries a load (e.g., magnetic brake) at one end through a rigid coupling. Both shafts are supported by rigid bushings. Since motor and load are connected through flexible couple from the geared shaft, and the motor and load shafts are short so their effects on transverse vibration of gears is ignored.

At the gear-pair contact the mesh stiffness and damping are considered apart from the transmission error (TE) at the pitch point, which gives excitation during tooth engagements during mesh cycles. The model consists of two uniform flexible shafts of lengths l_1 and l_2. The gear pair, which

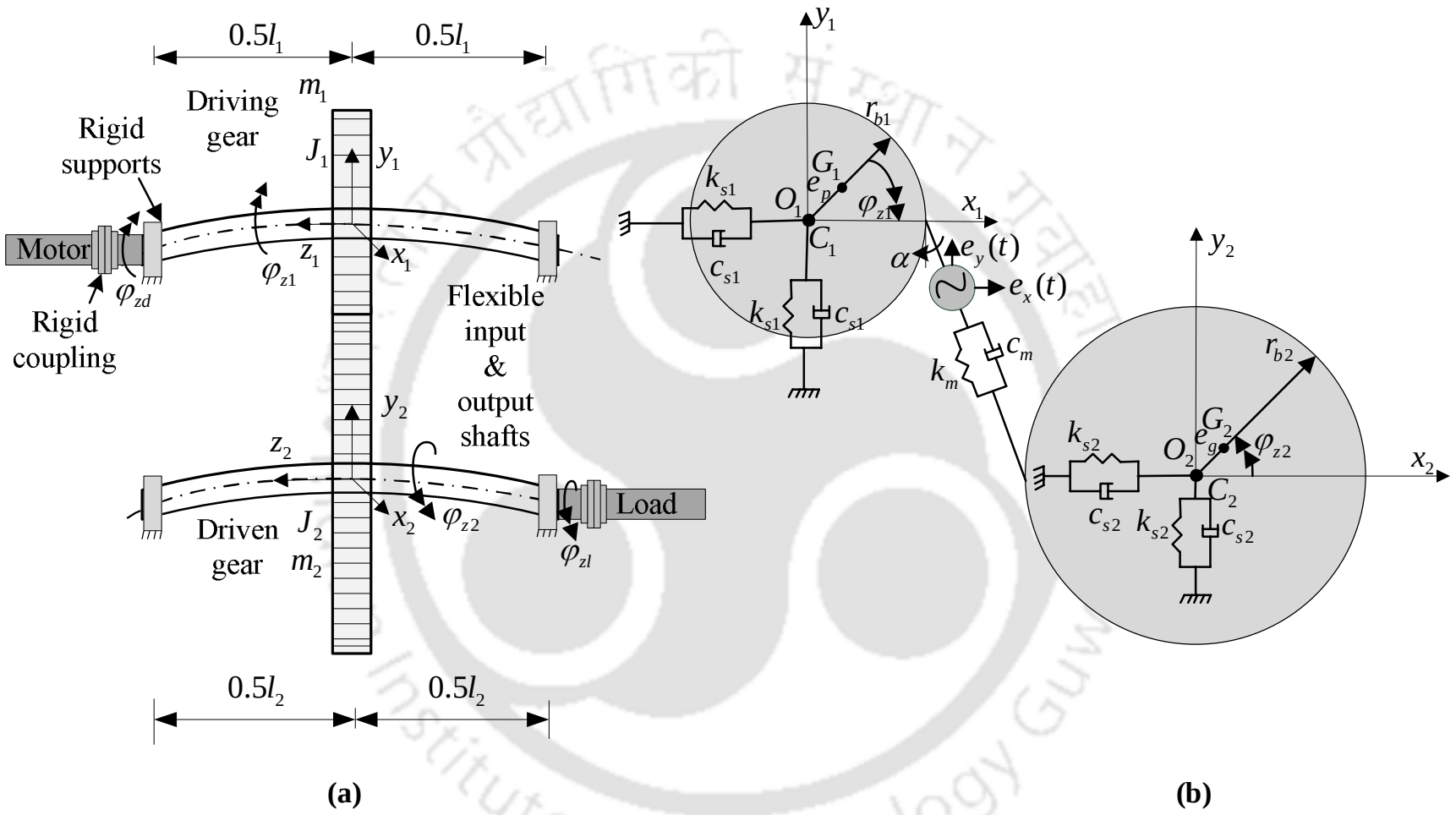

Figure 2.1: (a) Geared rotor system model; (b) Dynamic parameters of gear mesh

is modeled as two discs connected by a spring (k_m , mesh stiffness) and a damper (c_m , mesh damping) along the pressure line, which is tangent to the base circles of gears as shown in Fig. 2.2. From here the TE as per definition given in Chapter 1 can be written as $r_{bp}\varphi_p - r_{bg}\varphi_g$, which is responsible for excitation at the gear mesh due to geometric imperfections in the gear profile.

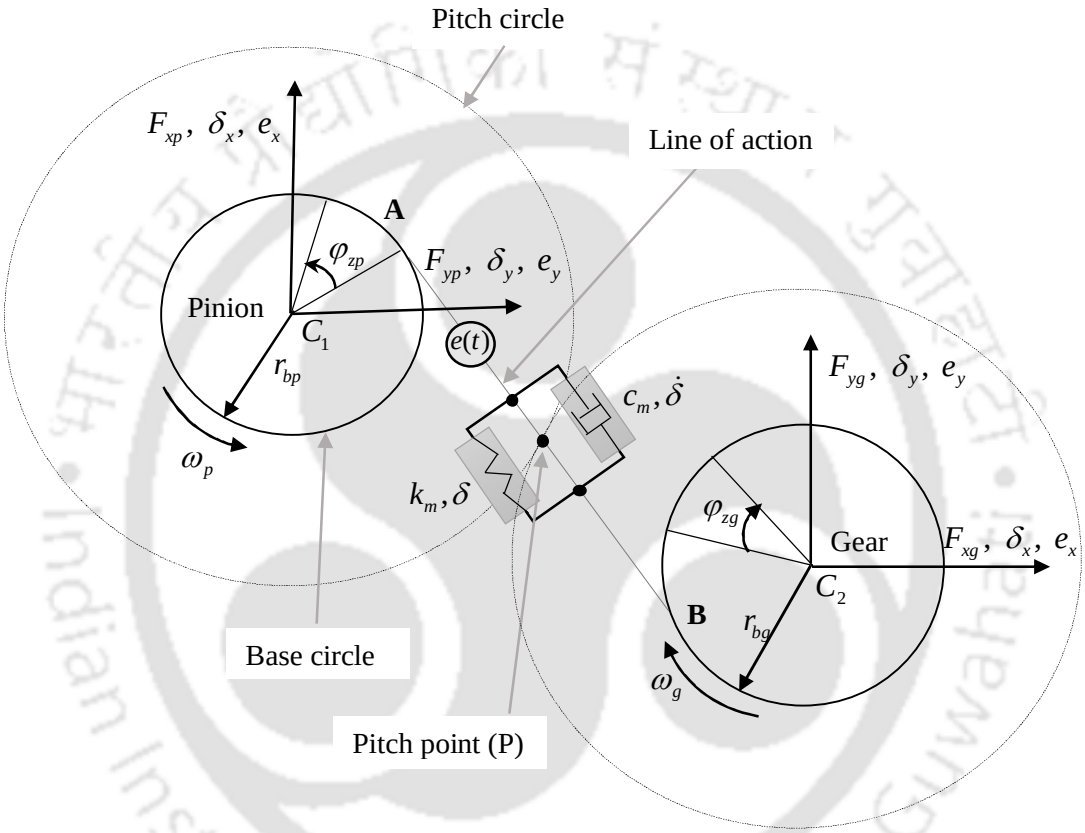

Figure 2.2: Gear contact modelling

In order to consider the gear engagement during the power transmission between two shafts, it is assumed that the meshing line is making angle α with *y*-axis as shown in Fig. 2.1. Components of gear mesh deformations and resulting gear contact forces are generated in the *x* and *y* directions as shown in Fig. 2.2. As the torsional vibration of the geared rotor system is neglected, so fluctuations in the angular motion

of shafts are ignored. Therefore, the angular motions $\varphi_{z1}(t)$, $\varphi_{z2}(t)$, $\varphi_{zd}(t)$ and $\varphi_{zl}(t)$ of the pinion (driver gear), gear (driven gear), drive and load, respectively, are expressed as

$$\varphi_{zd}(t) = \omega_p t + \phi_d; \qquad \varphi_{z1}(t) = \omega_p t + \phi_p; \qquad \varphi_{z2}(t) = \omega_g t + \phi_g; \qquad \varphi_{zl}(t) = \omega_g t + \phi_l \tag{2.1}$$

where ω_p and ω_g are constant angular velocities of the driving (pinion or drive) and driven (loaded gear) gears, ϕ is the initial phase of respective subscripts with subscripts: *d* indicates the drive, *p* indicates the pinion, *g* indicates the gear and *l* indicates the load. Also, the gyroscopic effect is not significant in this formulation as the pinion and the gear are fixed at mid-span of the shafts and speeds of operation are much below the critical speeds. The relationship between gear centers G_1 and G_2; rigid bearing centers O_1 and O_2 with gear eccentricities e_p and e_g due to runout error can be written as

$$x_p = x_1 + e_p \cos(-\varphi_{z1}); \quad y_p = y_1 + e_p \sin(-\varphi_{z1}); \quad x_g = x_2 + e_g \cos\varphi_{z2}; \quad y_g = y_2 + e_g \sin\varphi_{z2} \tag{2.2}$$

On substituting equation (2.1) into equation (2.2), we get

$$\begin{aligned} &x_p = x_1 + e_p \cos(-\omega_p t - \phi_p); \qquad y_p = y_1 + e_p \sin(-\omega_p t - \phi_p) \\ &x_g = x_2 + e_g \cos(\omega_g t + \phi_g); \qquad y_g = y_2 + e_g \sin(\omega_g t + \phi_g) \end{aligned} \tag{2.3}$$

The mass unbalances of the pinion and the gear due to gear runout eccentricities can be given as

$$U_p = m_1 e_p; \quad U_g = m_2 e_g \tag{2.4}$$

where m_1 and m_2 are equivalent masses of the pinion and gear, respectively

2.3 Dynamic Transmission Error (DTE)

The displacement $e(t)$, which is considered to be STE excitation along line of action, which is aligned in the vertical direction (y) which is seen in literature from Ozguven (1988b), Kahraman (1992), Kahraman (1993), Li et al. (2014) and Zhou et al. (2015). In the present research, the components of this STE excitation in the x and y directions are taken as $e_x(t)$ and $e_y(t)$, respectively, which are applied at the pitch point as asymmetric STE excitation. These displacements are taken to be sinusoidal only along the pressure line at the gear mesh frequency by Kahraman (1992) and Zhou (2015) with zero initial phase. As a novel approach, in the present formulation an initial phase is considered to include the sine and cosine variations and also higher harmonics of gear mesh frequency are included in the modelling. It has been demonstrated by Ozguven and Houser (1988b) that a variable mesh stiffness is approximately simulated by using a constant mesh stiffness with a displacement excitation representing the static transmission error excitation. Thus, the variable mesh stiffness is approximated in this work with variable asymmetric STE model along with constant mesh stiffness.

In order to ensure the contact of the teeth surface during the power transmission, it is assumed that the relative deformation of gears is completely changed into the elastic deformation on teeth surface along the gear mesh line direction. In this work, the meshing gears are assumed to be connected through the spring and damper. Therefore, the total deformation (δ) between the driving and driven gears is along the line of action (LOA). The gear runouts generate unbalance force in the pinion and the gear, in addition, they give rise to relative deformation of shafts during the torque transfer. The STE along with the runout errors, which alone contributes to no load static transmission error constitute the dynamic transmission error (DTE). The DTE is defined along the LOA, and it is expressed as,

$$\delta = r_{l1} - r_{l2} - e_{lp} - e_{lg} + r_p\varphi_p - r_g\varphi_g - e(t) \tag{2.5}$$

where r_{l1} and r_{l2} are elastic deformations of the input and output shafts; e_{lp} and e_{lg} are gear runouts of pinion and gear along line of action; $e(t)$ is STE, which is modelled along the LOA; φ_p and φ_g are the angle of rotations of the pinion and the gear, for a constant gear ratio, the fifth and sixth terms of above equation remains the same and together they become zero. Along the LOA, the dynamic meshing force is given as

$$F_m = c_m\dot{\delta} + k_m\delta \tag{2.6}$$

where k_m and c_m denotes the average meshing stiffness and damping along the LOA. The DTE excites the gear mesh in the *x* and *y* directions depicts a practical state of power transmission as shown in Fig. 2.1. For the system model described in Fig 2.1, the counter parts of δ from the existing literature in the *x* and *y* directions of the current system model, can be written from Eqn. 2.5 by considering the displacements of gear and pinion along the *x* and *y* directions from Eqn. 2.3, and are given as

$$\begin{aligned}\delta_x &= x_1 - x_2 + e_p\cos(-\omega_p t + \phi_p) - e_g\cos(\omega_g t + \phi_g) - e_x(t);\\ \delta_y &= y_1 - y_2 + e_p\sin(-\omega_p t + \phi_p) - e_g\sin(\omega_g t + \phi_g) - e_y(t)\end{aligned} \tag{2.7}$$

The dynamic mesh force given in Eqn. (2.6) is resolved in the *x* and *y* components. The elastic deformation in the contact region at the pitch point as given by Eqns. (2.7). The STE components of DTE $e_x(t)$ and $e_y(t)$ in the *x* and *y* directions are modelled as a mean value and a fluctuating part, and can be given as

$$e_x(t) = e_m + e_{fx}(t); \qquad e_y(t) = e_m + e_{fy}(t) \tag{2.8}$$

with

$$e_{fx}(t) = \sum_{i=1}^{n} e_{fxi} \sin(i\omega_e t + \phi_{exi}); \quad e_{fy}(t) = \sum_{i=1}^{n} e_{fyi} \sin(i\omega_e t + \phi_{eyi}) \tag{2.9}$$

where, e_m and $e_f(t)$ refer to the mean and fluctuation of transmission error, respectively; $e_{fxi}(t)$ and $e_{fyi}(t)$ are coefficients of various harmonics of the fluctuating part of the TE in the *x* and *y* directions, respectively; i = 1, 2, …, n is the harmonic index; ω_e is the gear meshing frequency with $\omega_e = t_p\omega_p = t_g\omega_g$; ω_p and ω_g are rotational speed of the pinion and gear, respectively; t_p and t_g are number of teeth of the pinon and gear, respectively; $\omega_e = 2\pi N_p t_p / 60 = 2\pi N_g t_g / 60$ where N_p and N_g are rotational speeds of pinion and gear; ϕ_{exi} and ϕ_{eyi} are phases of various harmonics of fluctuating part of the STE in *x* and *y* directions, respectively, with respect to the body fixed coordinate system.

2.4 Equations of Motion of a Geared Rotor

The generalized displacement vector of shaft centers at gear mesh can be expressed as follows:

$$\mathbf{X} = \begin{bmatrix} x_1 & y_1 & x_2 & y_2 \end{bmatrix}^T \tag{2.10}$$

Using Lagrangian dynamics, the equations of motion are to be established for the system. Considering the STE, gear runouts and mass unbalances, the kinetic energy *T*, the potential energy *U*, the dissipation function *D* and the external force vector *P* are derived as,

$$T = \tfrac{1}{2}\left(m_1\dot{x}_p^2 + m_1\dot{y}_p^2 + m_2\dot{x}_g^2 + m_2\dot{y}_g^2\right) \tag{2.11}$$

$$U = \tfrac{1}{2}\left\{k_{s1}x_p^2 + k_{s1}y_p^2 + k_{s2}x_g^2 + k_{s2}y_g^2 + k_m(\delta_x^2 + \delta_y^2)\right\} \tag{2.12}$$

And

$$D = \tfrac{1}{2}\left[c_{s1}\dot{x}_p^2 + c_{s1}\dot{y}_p^2 + c_{s2}\dot{x}_g^2 + c_{s2}\dot{y}_g^2 + c_m\left(\dot{\delta}_x^2 + \dot{\delta}_y^2\right)\right] \tag{2.13}$$

where m_1 and m_2 are the mass of the pinion and the gear, respectively; k_{s1} and k_{s2} are pinion and gear shaft stiffness, respectively; and c_{s1} and c_{s2} are the pinion and gear shaft damping, respectively. On substituting Eqns. (2.3), (2.6), (2.7) into Eqns. (2.11), (2.12) and (2.13), we get

$$\begin{aligned} T = {} & \tfrac{1}{2}m_1\left\{\dot{x}_1 - e_p\omega_p\sin(\omega_p t + \phi_p)\right\}^2 + \tfrac{1}{2}m_1\left\{\dot{y}_1 - e_p\omega_p\cos(\omega_p t + \phi_p)\right\}^2 + \\ & \tfrac{1}{2}m_2\left\{\dot{x}_2 - e_g\omega_g\sin(\omega_g t + \phi_g)\right\}^2 + \tfrac{1}{2}m_2\left\{\dot{y}_2 + e_g\omega_g\cos(\omega_g t + \phi_g)\right\}^2 \end{aligned} \tag{2.14}$$

$$\begin{aligned} U = {} & \tfrac{1}{2}k_{s1}\left\{x_1 + e_p\cos(\omega_p t + \phi_p)\right\}^2 + \tfrac{1}{2}k_{s1}\left\{y_1 - e_p\sin(\omega_p t + \phi_p)\right\}^2 + \\ & \tfrac{1}{2}k_{s2}\left\{x_2 + e_g\cos(\omega_g t + \phi_g)\right\}^2 + \tfrac{1}{2}k_{s2}\left\{y_2 + e_g\sin(\omega_g t + \phi_g)\right\}^2 + \\ & \tfrac{1}{2}k_m\left\{x_1 - x_2 + e_p\cos(\omega_p t + \phi_p) - e_g\cos(\omega_g t + \phi_g) - e_x(t)\right\}^2 + \\ & \tfrac{1}{2}k_m\left\{y_1 - y_2 - e_p\sin(\omega_p t + \phi_p) - e_g\sin(\omega_g t + \phi_g) - e_y(t)\right\}^2 \end{aligned} \tag{2.15}$$

and

$$D = \tfrac{1}{2}c_{s1}(\dot{x}_1 - e_p\omega_p \sin(\omega_p t + \phi_p))^2 + \tfrac{1}{2}c_{s1}(\dot{y}_1 - e_p\omega_p \cos(\omega_p t + \phi_p))^2 +$$
$$\tfrac{1}{2}c_{s2}(\dot{x}_2 - e_g\omega_g \sin(\omega_g t + \phi_g))^2 + \tfrac{1}{2}c_{s2}(\dot{y}_2 + e_g\omega_g \cos(\omega_g t + \phi_g))^2 + \qquad (2.16)$$
$$\tfrac{1}{2}c_m \begin{Bmatrix} \left(\dot{x}_1 - \dot{x}_2 + r_{b1}\omega_p - r_{b2}\omega_g - e_p\omega_p \sin(\omega_p t + \phi_p) + e_g\omega_g \sin(\omega_g t + \phi_g) - \dot{e}_x(t)\right)^2 + \\ \left(\dot{y}_1 - \dot{y}_2 + r_{b1}\omega_p - r_{b2}\omega_g - e_p\omega_p \cos(\omega_p t + \phi_p) - e_g\omega_g \cos(\omega_g t + \phi_g) - \dot{e}_y(t)\right)^2 \end{Bmatrix}$$

The gravity loading in the system model for the pinion and the gear can be written as

$$P_{x1} = 0; \qquad P_{y1} = -m_1 g; \qquad P_{x2} = 0; \qquad P_{y2} = -m_2 g \qquad (2.17)$$

According to the extended Lagrangian formulation by including dissipation function (D) to include non-conservative forces, the differential equations of motion of geared rotor system are derived as follows:

$$\frac{d}{dt}\left(\frac{\partial L}{\partial \dot{q}_i}\right) - \frac{\partial L}{\partial q_i} + \frac{\partial D}{\partial \dot{q}_i} = P_i \quad \text{with} \quad L = T - U \qquad (2.18)$$

where T represents the kinetic energy, U represents the potential energy for the system, and P_i is the external force. By substituting L in equation (2.18) can be written as

$$\frac{d}{dt}\left(\frac{\partial T}{\partial \dot{q}_i}\right) - \frac{d}{dt}\left(\frac{\partial U}{\partial \dot{q}_i}\right) - \frac{\partial T}{\partial q_i} + \frac{\partial U}{\partial q_i} + \frac{\partial D}{\partial \dot{q}_i} = P_i \quad \text{with} \quad \eta_i = \begin{bmatrix} x_1 & y_1 & x_2 & y_2 \end{bmatrix} \qquad (2.19)$$

On using Eqns. (2.14), (2.15), (2.16) and (2.17) in various terms of Eqn. (2.18), we can get

$$\frac{\partial T}{\partial \dot{x}_1} = m_1(\dot{x}_1 - e_p\omega_p \sin(\omega_p t + \phi_p)); \qquad \frac{\partial T}{\partial \dot{y}_1} = m_1(\dot{y}_1 - e_p\omega_p \cos(\omega_p t + \phi_p));$$

$$\frac{\partial T}{\partial \dot{x}_2} = m_2(\dot{x}_2 - e_g\omega_g \sin(\omega_g t + \phi_g)); \qquad \frac{\partial T}{\partial \dot{y}_2} = m_2(\dot{y}_2 + e_g\omega_g \cos(\omega_g t + \phi_g)) \tag{2.20}$$

$$\frac{d}{dt}\left(\frac{\partial T}{\partial \dot{x}_1}\right) = m_1\ddot{x}_1 - m_1 e_p\omega_p^2 \cos(\omega_p t + \phi_p); \qquad \frac{d}{dt}\left(\frac{\partial T}{\partial \dot{y}_1}\right) = m_1\ddot{y}_1 + m_1 e_p\omega_p^2 \sin(\omega_p t + \phi_p);$$

$$\frac{d}{dt}\left(\frac{\partial T}{\partial \dot{x}_2}\right) = m_2\ddot{x}_2 - m_2 e_g\omega_g^2 \cos(\omega_g t + \phi_g); \qquad \frac{d}{dt}\left(\frac{\partial T}{\partial \dot{y}_2}\right) = m_2\ddot{y}_2 - m_2 e_g\omega_g^2 \sin(\omega_g t + \phi_g) \tag{2.21}$$

$$\frac{\partial T}{\partial x_1} = 0; \quad \frac{\partial T}{\partial y_1} = 0; \quad \frac{\partial T}{\partial x_2} = 0; \quad \frac{\partial T}{\partial y_2} = 0 \tag{2.22}$$

$$\frac{d}{dt}\left(\frac{\partial U}{\partial \dot{x}_1}\right) = 0; \quad \frac{d}{dt}\left(\frac{\partial U}{\partial \dot{y}_1}\right) = 0; \quad \frac{d}{dt}\left(\frac{\partial U}{\partial \dot{x}_2}\right) = 0; \quad \frac{d}{dt}\left(\frac{\partial U}{\partial \dot{y}_2}\right) = 0 \tag{2.23}$$

$$\frac{\partial U}{\partial x_1} = k_{s1}x_1 + k_m\left\{x_1 - x_2 + r_{b1}\omega_p t - r_{b2}\omega_g t + e_p \cos(-\omega_p t + \phi_p) - e_g \cos(\omega_g t + \phi_g) - e_x(t)\right\};$$
$$\frac{\partial U}{\partial y_1} = k_{s1}y_1 + k_m\left\{y_1 - y_2 + r_{b1}\omega_p t - r_{b2}\omega_g t + e_p \sin(-\omega_p t + \phi_p) - e_g \sin(\omega_g t + \phi_g) - e_y(t)\right\} \tag{2.24}$$

$$\frac{\partial U}{\partial x_2} = k_{s2}x_2 - k_m\left\{x_1 - x_2 + r_{b1}\omega_p t - r_{b2}\omega_g t + e_p\cos(-\omega_p t + \phi_p) - e_g\cos(\omega_g t + \phi_g) - e_x(t)\right\};$$
$$\frac{\partial U}{\partial y_2} = k_{s2}y_2 - k_m\left\{y_1 - y_2 + r_{b1}\omega_p t - r_{b2}\omega_g t + e_p\sin(-\omega_p t + \phi_p) - e_g\sin(\omega_g t + \phi_g) - e_y(t)\right\} \quad (2.24)$$

$$\frac{\partial D}{\partial \dot{x}_1} = c_{s1}\dot{x}_1 + c_m\left\{\dot{x}_1 - \dot{x}_2 + r_{b1}\omega_p - r_{b2}\omega_g - e_p\omega_p\sin(\omega_p t + \phi_p) + e_g\omega_g\sin(\omega_g t + \phi_g) - \dot{e}_x(t)\right\};$$
$$\frac{\partial D}{\partial \dot{y}_1} = c_{s1}\dot{y}_1 + c_m\left\{\dot{y}_1 - \dot{y}_2 + r_{b1}\omega_p - r_{b2}\omega_g - e_p\omega_p\cos(\omega_p t + \phi_p) - e_g\omega_g\cos(\omega_g t + \phi_g) - \dot{e}_y(t)\right\};$$
$$\frac{\partial D}{\partial \dot{x}_2} = c_{s2}\dot{x}_2 - c_m\left\{\dot{x}_1 - \dot{x}_2 + r_{b1}\omega_p - r_{b2}\omega_g - e_p\omega_p\sin(\omega_p t + \phi_p) + e_g\omega_g\sin(\omega_g t + \phi_g) - \dot{e}_x(t)\right\}; \quad (2.25)$$
$$\frac{\partial D}{\partial \dot{y}_2} = c_{s2}\dot{y}_2 - c_m\left\{\dot{y}_1 - \dot{y}_2 + r_{b1}\omega_p - r_{b2}\omega_g - e_p\omega_p\cos(\omega_p t + \phi_p) - e_g\omega_g\cos(\omega_g t + \phi_g) - \dot{e}_y(t)\right\}$$

From equations (2.19) through (2.26), the equations of motion for the lateral vibration of geared rotor pair are written as

$$m_1\ddot{x}_1 + c_{s1}\left\{\dot{x}_1 - e_p\omega_p\sin(\omega_p t + \phi_p)\right\} + c_m\left\{\dot{x}_1 - \dot{x}_2 - e_p\omega_p\sin(\omega_p t + \phi_p) + e_g\omega_g\sin(\omega_g t + \phi_g) - \dot{e}_x(t)\right\} +$$
$$k_{s1}\left\{x_1 + e_p\cos(\omega_p t + \phi_p)\right\} + k_m\left\{x_1 - x_2 + e_p\cos(\omega_p t + \phi_p) - e_g\cos(\omega_g t + \phi_g) - e_x(t)\right\} = \quad (2.26)$$
$$m_1 e_p\omega_p^2\cos(\omega_p t + \phi_p)$$

$$m_1\ddot{y}_1 + c_{s1}\left\{\dot{y}_1 - e_p\omega_p\cos(\omega_p t + \phi_p)\right\} + c_m\left\{\dot{y}_1 - \dot{y}_2 - e_p\omega_p\cos(\omega_p t + \phi_p) - e_g\omega_g\cos(\omega_g t + \phi_g) - \dot{e}_x(t)\right\} +$$
$$k_{s1}\left\{y_1 - e_p\sin(\omega_p t + \phi_p)\right\} + k_m\left\{y_1 - y_2 - e_p\sin(\omega_p t + \phi_p) - e_g\sin(\omega_g t + \phi_g) - e_y(t)\right\} = \quad (2.27)$$
$$-m_1 g - m_1 e_p\omega_p^2\sin(\omega_p t + \phi_p)$$

$$m_2\ddot{x}_2 + c_{s2}\left\{\dot{x}_2 - e_g\omega_g\sin(\omega_g t+\phi_g)\right\} - c_m\left\{\dot{x}_1 - \dot{x}_2 - e_p\omega_p\sin(\omega_p t+\phi_p) + e_g\omega_g\sin(\omega_g t+\phi_g) - \dot{e}_x(t)\right\} +$$
$$k_{s2}\left\{x_2 + e_g\cos(\omega_g t+\phi_g)\right\} - k_m\left\{x_1 - x_2 + e_p\cos(\omega_p t+\phi_p) - e_g\cos(\omega_g t+\phi_g) - e_x(t)\right\} = \quad (2.28)$$
$$m_2 e_g\omega_g^2\cos(\omega_g t+\phi_g)$$

$$m_2\ddot{y}_2 + c_{s2}\left\{\dot{y}_2 + e_g\omega_g\cos(\omega_g t+\phi_g)\right\} - c_m\left\{\dot{y}_1 - \dot{y}_2 - e_p\omega_p\cos(\omega_p t+\phi_p) - e_g\omega_g\cos(\omega_g t+\phi_g) - \dot{e}_y(t)\right\} +$$
$$k_{s2}\left\{y_2 + e_g\sin(\omega_g t+\phi_g)\right\} - k_m\left\{y_1 - y_2 - e_p\sin(\omega_p t+\phi_p) - e_g\sin(\omega_g t+\phi_g) - e_y(t)\right\} = \quad (2.29)$$
$$-m_2 g + m_2 e_g\omega_g^2\sin(\omega_g t+\phi_g)$$

By rearranging terms to convert the equations of motion in the standard form with force vectors due to the STE, gear runouts and mass unbalance due to runouts (Eqn. 2.4), as

$$\begin{aligned} &m_1\ddot{x}_1 + (c_{s1}+c_m)\dot{x}_1 - c_m\dot{x}_2 + (k_{s1}+k_m)x_1 - k_m x_2 = \\ &m_1 e_p\omega_p^2\cos(\omega_p t+\phi_p) + c_{s1}e_p\omega_p\sin(\omega_p t+\phi_p) - k_{s1}e_p\cos(\omega_p t+\phi_p) \\ &+c_m\left\{e_p\omega_p\sin(\omega_p t+\phi_p) - e_g\omega_g\sin(\omega_g t+\phi_g) + \dot{e}_x(t)\right\} \\ &+k_m\left\{-e_p\cos(\omega_p t+\phi_p) + e_g\cos(\omega_g t+\phi_g) + e_x(t)\right\} \end{aligned} \quad (2.30)$$

$$\begin{aligned} &m_1\ddot{y}_1 + (c_{s1}+c_m)\dot{y}_1 - c_m\dot{y}_2 + (k_{s1}+k_m)y_1 - k_m y_2 = \\ &-m_1 g - m_1 e_p\omega_p^2\sin(\omega_p t+\phi_p) + c_{s1}e_p\omega_p\cos(\omega_p t+\phi_p) + k_{s1}e_p\sin(\omega_p t+\phi_p) \\ &+c_m\left\{e_p\omega_p\cos(\omega_p t+\phi_p) + e_g\omega_g\cos(\omega_g t+\phi_g) + \dot{e}_x(t)\right\} \\ &+k_m\left\{e_p\sin(\omega_p t+\phi_p) + e_g\sin(\omega_g t+\phi_g) + e_y(t)\right\} \end{aligned} \quad (2.31)$$

$$\begin{aligned} &m_2\ddot{x}_2 + (c_{s2}+c_m)\dot{x}_2 - c_m\dot{x}_1 + (k_{s2}+k_m)x_2 - k_m x_1 = \\ &m_2 e_g\omega_g^2\cos(\omega_g t+\phi_g) + c_{s2}e_g\omega_g\sin(\omega_g t+\phi_g) - k_{s2}e_g\cos(\omega_g t+\phi_g) \\ &-c_m\left\{e_p\omega_p\sin(\omega_p t+\phi_p) - e_g\omega_g\sin(\omega_g t+\phi_g) + \dot{e}_x(t)\right\} \\ &-k_m\left\{-e_p\cos(\omega_p t+\phi_p) + e_g\cos(\omega_g t+\phi_g) + e_x(t)\right\} \end{aligned} \quad (2.32)$$

$$
\begin{aligned}
&m_2\ddot{y}_2 + (c_{s2} + c_m)\dot{y}_2 - c_m\dot{y}_1 + (k_{s2} + k_m)y_2 - k_m y_1 = \\
&-m_2 g + m_2 e_g \omega_g^2 \sin(\omega_g t + \phi_g) - c_{s2} e_g \omega_g \cos(\omega_g t + \phi_g) - k_{s2} e_g \sin(\omega_g t + \phi_g) \\
&-c_m \left\{ e_p \omega_p \cos(\omega_p t + \phi_p) + e_g \omega_g \cos(\omega_g t + \phi_g) + \dot{e}_x(t) \right\} \\
&-k_m \left\{ e_p \sin(\omega_p t + \phi_p) + e_g \sin(\omega_g t + \phi_g) + e_y(t) \right\}
\end{aligned}
\tag{2.33}
$$

The above equations can be put in a matrix form as

$$
\mathbf{M}\,\ddot{\boldsymbol{\eta}}(t) + \mathbf{C}\,\dot{\boldsymbol{\eta}}(t) + \mathbf{K}\,\boldsymbol{\eta}(t) = \mathbf{f}_r(t) \tag{2.34}
$$

with

$$
\mathbf{M} = \begin{bmatrix} m_1 & 0 & 0 & 0 \\ 0 & m_1 & 0 & 0 \\ 0 & 0 & m_2 & 0 \\ 0 & 0 & 0 & m_2 \end{bmatrix}; \quad \mathbf{C} = \begin{bmatrix} c_{s1} + c_m & 0 & -c_m & 0 \\ 0 & c_{s1} + c_m & 0 & -c_m \\ -c_m & 0 & c_{s2} + c_m & 0 \\ 0 & -c_m & 0 & c_{s2} + c_m \end{bmatrix}; \tag{2.35}
$$

$$
\mathbf{K} = \begin{bmatrix} k_{s1} + k_m & 0 & -k_m & 0 \\ 0 & k_{s1} + k_m & 0 & -k_m \\ -k_m & 0 & k_{s2} + k_m & 0 \\ 0 & -k_m & 0 & k_{s2} + k_m \end{bmatrix}; \quad \boldsymbol{\eta} = \begin{Bmatrix} x_1 \\ y_1 \\ x_2 \\ y_2 \end{Bmatrix}; \tag{2.36}
$$

$$\mathbf{f}_r(t)=\begin{Bmatrix} f_{x1}(t)\\ f_{y1}(t)\\ f_{x2}(t)\\ f_{y2}(t)\end{Bmatrix}=\begin{Bmatrix} m_1e_p\omega_p^2\cos(\omega_pt+\phi_p)+c_m\left\{e_p\omega_p\sin(\omega_pt+\phi_p)-e_g\omega_g\sin(\omega_gt+\phi_g)+\dot{e}_x(t)\right\}\\ +k_m\left\{-e_p\cos(\omega_pt+\phi_p)+e_g\cos(\omega_gt+\phi_g)+e_x(t)\right\}\\ +c_{s1}e_p\omega_p\sin(\omega_pt+\phi_p)-k_{s1}e_p\cos(\omega_pt+\phi_p)\\ \\ -m_1e_p\omega_p^2\sin(\omega_pt+\phi_p)+c_m\left\{e_p\omega_p\cos(\omega_pt+\phi_p)+e_g\omega_g\cos(\omega_gt+\phi_g)+\dot{e}_x(t)\right\}\\ +k_m\left\{e_p\sin(\omega_pt+\phi_p)+e_g\sin(\omega_gt+\phi_g)+e_y(t)\right\}\\ +c_{s1}e_p\omega_p\cos(\omega_pt+\phi_p)+k_{s1}e_p\sin(\omega_pt+\phi_p)-m_1g\\ \\ m_2e_g\omega_g^2\cos(\omega_gt+\phi_g)-c_m\left\{e_p\omega_p\sin(\omega_pt+\phi_p)-e_g\omega_g\sin(\omega_gt+\phi_g)+\dot{e}_x(t)\right\}\\ -k_m\left\{-e_p\cos(\omega_pt+\phi_p)+e_g\cos(\omega_gt+\phi_g)+e_x(t)\right\}\\ +c_{s1}e_p\omega_p\cos(\omega_pt+\phi_p)+k_{s1}e_p\sin(\omega_pt+\phi_p)\\ \\ m_2e_g\omega_g^2\sin(\omega_gt+\phi_g)-c_m\left\{e_p\omega_p\cos(\omega_pt+\phi_p)+e_g\omega_g\cos(\omega_gt+\phi_g)+\dot{e}_x(t)\right\}\\ -k_m\left\{e_p\sin(\omega_pt+\phi_p)+e_g\sin(\omega_gt+\phi_g)+e_y(t)\right\}\\ -c_{s2}e_g\omega_g\cos(\omega_gt+\phi_g)-k_{s2}e_g\sin(\omega_gt+\phi_g)-m_2g\end{Bmatrix} \tag{2.37}$$

where **M**, **C** and **K** are the mass, damping and stiffness matrices; and $\mathbf{f}_r(t)$ is the force vector, which results due to excitation at the pitch point of the gear mesh due to transmission error and runouts of gears. In the matrix form the mass, damping and stiffness matrices are symmetric. On substituting Eqn. (2.8) and (2.9) in force vector, Eqn. (2.37), we get

$$
\mathbf{f}_r(t) = \begin{Bmatrix}
m_1 e_p \omega_p^2 \cos(\omega_p t + \phi_p) \\
+c_m \left(e_p \omega_p \sin(\omega_p t + \phi_p) - e_g \omega_g \sin(\omega_g t + \phi_g) + \sum_{i=1}^{n} e_{fxi} i\omega_e \cos(i\omega_e t + \phi_{e_{xi}}) \right) \\
+k_m \left(-e_p \cos(\omega_p t + \phi_p) + e_g \cos(\omega_g t + \phi_g) + (e_m + \sum_{i=1}^{n} e_{fxi} \sin(i\omega_e t + \phi_{e_{xi}}) \right) \\
+c_{s1} e_p \omega_p \sin(\omega_p t + \phi_p) - k_{s1} e_p \cos(\omega_p t + \phi_p) \\
\\
-m_1 g - m_1 e_p \omega_p^2 \sin(\omega_p t + \phi_p) \\
+c_m \left(e_p \omega_p \cos(\omega_p t + \phi_p) + e_g \omega_g \cos(\omega_g t + \phi_g) + \sum_{i=1}^{n} e_{fyi} i\omega_e \cos(i\omega_e t + \phi_{e_{yi}}) \right) \\
+k_m \left(e_p \sin(\omega_p t + \phi_p) + e_g \sin(\omega_g t + \phi_g) + (e_m + \sum_{i=1}^{n} e_{fyi} \sin(i\omega_e t + \phi_{e_{yi}}) \right) \\
+c_{s1} e_p \omega_p \cos(\omega_p t + \phi_p) + k_{s1} e_p \sin(\omega_p t + \phi_p) \\
\\
m_2 e_g \omega_g^2 \cos(\omega_g t + \phi_g) \\
-c_m \left(e_p \omega_p \sin(\omega_p t + \phi_p) - e_g \omega_g \sin(\omega_g t + \phi_g) + \sum_{i=1}^{n} e_{fxi} i\omega_e \cos(i\omega_e t + \phi_{e_{xi}}) \right) \\
-k_m \left(-e_p \cos(\omega_p t + \phi_p) + e_g \cos(\omega_g t + \phi_g) + (e_m + \sum_{i=1}^{n} e_{fxi} \sin(i\omega_e t + \phi_{e_{xi}}) \right) \\
+c_{s2} e_g \omega_g \sin(\omega_g t + \phi_g) - k_{s2} e_g \cos(\omega_g t + \phi_g) \\
\\
-m_2 g + m_2 e_g \omega_g^2 \sin(\omega_g t + \phi_g) \\
-c_m \left(e_p \omega_p \cos(\omega_p t + \phi_p) + e_g \omega_g \cos(\omega_g t + \phi_g) + \sum_{i=1}^{n} e_{fyi} i\omega_e \cos(i\omega_e t + \phi_{e_{yi}}) \right) \\
-k_m \left(e_p \sin(\omega_p t + \phi_p) + e_g \sin(\omega_g t + \phi_g) + (e_m + \sum_{i=1}^{n} e_{fyi} \sin(i\omega_e t + \phi_{e_{yi}}) \right) \\
-c_{s2} e_g \omega_g \cos(\omega_g t + \phi_g) - k_{s2} e_g \sin(\omega_g t + \phi_g)
\end{Bmatrix} \tag{2.38}
$$

Geared rotor equations of motion have been derived using the Lagrangian dynamics with the asymmetric transmission error excitation. With the derived equations of motion, response can be calculated in time domain for chosen geared rotor parameters. Complex nature of gear vibration problem needs frequency domain analysis to understand various frequency components present in the response spectrum and for facilitating for identification of these dynamic gear mesh parameter modelled in this chapter.

2.5 Summary

A TE based geared rotor transverse vibration problem is modelled with asymmetric transmission error considered at the gear mesh in two mutually perpendicular directions. Also, system level influence on asymmetric STE excitations at the gear mesh are modelled as DTE by including gear runouts, gear mesh stiffness and damping to study their influence on geared rotor response. The equations of motion of the proposed system model are derived using Lagrangian dynamics for analysing the transverse vibration of a geared rotor in the coming chapters. The aim will be to detect (qualitatively) and identify (quantitatively) asymmetric transmission error using frequency domain spectrum analysis both by numerical simulation and experimental investigation.

To give overall picture of subsequent chapters for which the present chapter is the base, now these chapters are briefly described. These time domain linear differential equations of motions are then converted into frequency domain in the coming Chapter 3 to analyse the forward and backward whirling of gear-pair. In Chapter 4, the time domain equations of motion derived in this chapter are solved numerically using assumed gear mesh parameters and the geared rotor response is analysed in time and frequency domain using the orbit and full spectrum plots. In Chapter 5, the frequency domain system equations derived in Chapter 3 are used for identifying the DTE gear mesh parameters modelled in this chapter. In Chapter 6, experimental geared rotor experimental rig design and development will be discussed along with the experimental rig gear mesh parameters identification and its validation using test measured response.

CHAPTER 3

TRANSFORMATION OF EQUATIONS OF MOTION OF GEARED ROTOR INTO FREQUENCY DOMAIN

3.1 Introduction

Frequency domain is a term used to describe the analysis of mathematical functions or signals with respect to frequency, rather than time. The most common purpose for analysis of signals in the frequency domain is the analysis of signal properties. Coming to the gear vibration problem, the loaded gears are known to have vibration that leads to tonal noise. Analysis of gear vibration problem in frequency domain needs transformation of time domain equations of motion into frequency domain to study the spectrum and determine DTE fault frequencies that are present in the input signal, which facilitates the detection of faults. Furthermore, these transformed equations will be used for qualitative identification of critical gear mesh parameters in subsequent chapters.

3.2 Frequency Domain Transformation

The gear mesh consists of the pinion and gear rotating at different speeds, which gives rise to two angular velocity components in frequency domain. The other derived angular velocity component using either number of teeth on the driver or drive gear is the gear meshing angular velocity component. These components are seen in the derived equations of motion in Eqn. (2.38).

Going back to fundamentals of complex mathematics, we have from Euler's equations

$$e^{\mathrm{j}(\omega_p t+\phi_p)} = \left\{\cos(\omega_p t+\phi_p) + \mathrm{j}\sin(\omega_p t+\phi_p)\right\}; \quad e^{-\mathrm{j}(\omega_p t+\phi_p)} = \left\{\cos(\omega_p t+\phi_p) - \mathrm{j}\sin(\omega_p t+\phi_p)\right\} \tag{3.1}$$

$$e^{\mathrm{j}(\omega_g t+\phi_g)}=\{\cos(\omega_g t+\phi_g)+\mathrm{j}\sin(\omega_g t+\phi_g)\};\qquad e^{-\mathrm{j}(\omega_g t+\phi_g)}=\{\cos(\omega_g t+\phi_g)-\mathrm{j}\sin(\omega_g t+\phi_g)\} \tag{3.2}$$

$$e^{\mathrm{j}(\omega_e t+\phi_e)}=\{\cos(\omega_e t+\phi_e)+\mathrm{j}\sin(\omega_e t+\phi_e)\};\qquad e^{-\mathrm{j}(\omega_e t+\phi_e)}=\{\cos(\omega_e t+\phi_e)-\mathrm{j}\sin(\omega_e t+\phi_e)\} \tag{3.3}$$

which gives

$$\sin(\omega_p t+\phi_p)=(e^{\mathrm{j}(\omega_p t+\phi_p)}-e^{-\mathrm{j}(\omega_p t+\phi_p)})/2\mathrm{j};\quad \cos(\omega_p t+\phi_p)=(e^{\mathrm{j}(\omega_p t+\phi_p)}+e^{-\mathrm{j}(\omega_p t+\phi_p)})/2 \tag{3.4}$$

$$\sin(\omega_g t+\phi_g)=(e^{\mathrm{j}(\omega_g t+\phi_g)}-e^{-\mathrm{j}(\omega_g t+\phi_g)})/2\mathrm{j};\quad \cos(\omega_g t+\phi_g)=(e^{\mathrm{j}(\omega_g t+\phi_g)}+e^{-\mathrm{j}(\omega_g t+\phi_g)})/2 \tag{3.5}$$

$$\sin(\omega_e t+\phi_e)=(e^{\mathrm{j}(\omega_e t+\phi_e)}-e^{-\mathrm{j}(\omega_e t+\phi_e)})/2\mathrm{j};\quad \cos(\omega_e t+\phi_e)=(e^{\mathrm{j}(\omega_e t+\phi_e)}+e^{-\mathrm{j}(\omega_e t+\phi_e)})/2 \tag{3.6}$$

On substituting equations (3.4) through (3.6) in the force vector of Eqn. (2.38), $\mathbf{f}_r(t)$, we get

$$\mathbf{f}_r(t)=\begin{Bmatrix} f_{x1}(t) \\ f_{y1}(t) \\ f_{x2}(t) \\ f_{y2}(t) \end{Bmatrix}=\left\{\begin{array}{l} k_m e_m+0.5m_1 e_p \omega_p^2 (e^{\mathrm{j}(\omega_p t+\phi_p)}+e^{-\mathrm{j}(\omega_p t+\phi_p)}) \\ +(0.5c_m/\mathrm{j})\begin{pmatrix} e_p\omega_p(e^{\mathrm{j}(\omega_p t+\phi_p)}-e^{-\mathrm{j}(\omega_p t+\phi_p)})-e_g\omega_g(e^{\mathrm{j}(\omega_g t+\phi_g)}-e^{-\mathrm{j}(\omega_g t+\phi_g)}) \\ +\mathrm{j}\sum_{i=1}^{n} e_{f_{xi}} i\omega_e(e^{\mathrm{j}(i\omega_e t+\phi_{exi})}+e^{-\mathrm{j}(i\omega_e t+\phi_{exi})}) \end{pmatrix} \\ +(0.5k_m/\mathrm{j})\begin{pmatrix} -\mathrm{j}e_p(e^{\mathrm{j}(\omega_p t+\phi_p)}+e^{-\mathrm{j}(\omega_p t+\phi_p)})+\mathrm{j}e_g(e^{\mathrm{j}(\omega_g t+\phi_g)}+e^{-\mathrm{j}(\omega_g t+\phi_g)}) \\ +(\sum_{i=1}^{n} e_{f_{xi}}(e^{\mathrm{j}(i\omega_e t+\phi_{exi})}-e^{-\mathrm{j}(i\omega_e t+\phi_{exi})})) \end{pmatrix} \\ +(0.5c_{s1}/\mathrm{j})\left(e_p\omega_p(e^{\mathrm{j}(\omega_p t+\phi_p)}-e^{-\mathrm{j}(\omega_p t+\phi_p)})\right)-(0.5k_{s1})\left(e_p(e^{\mathrm{j}(\omega_p t+\phi_p)}+e^{-\mathrm{j}(\omega_p t+\phi_p)})\right) \\ \\ -m_1 g+k_m e_m-0.5m_1 e_p\omega_p^2(e^{\mathrm{j}(\omega_p t+\phi_p)}-e^{-\mathrm{j}(\omega_p t+\phi_p)})/\mathrm{j} \\ +(0.5c_m/\mathrm{j})\begin{pmatrix} \mathrm{j}e_p\omega_p(e^{\mathrm{j}(\omega_p t+\phi_p)}+e^{-\mathrm{j}(\omega_p t+\phi_p)})+\mathrm{j}e_g\omega_g(e^{\mathrm{j}(\omega_g t+\phi_g)}+e^{-\mathrm{j}(\omega_g t+\phi_g)}) \\ +\mathrm{j}\sum_{i=1}^{n} e_{f_{yi}} i\omega_e(e^{\mathrm{j}(i\omega_e t+\phi_{eyi})}+e^{-\mathrm{j}(i\omega_e t+\phi_{eyi})}) \end{pmatrix} \\ +(0.5k_m/\mathrm{j})\begin{pmatrix} e_p(e^{\mathrm{j}(\omega_p t+\phi_p)}-e^{-\mathrm{j}(\omega_p t+\phi_p)})+e_g(e^{\mathrm{j}(\omega_g t+\phi_g)}-e^{-\mathrm{j}(\omega_g t+\phi_g)}) \\ +\sum_{i=1}^{n} e_{f_{yi}}(e^{\mathrm{j}(i\omega_e t+\phi_{eyi})}-e^{-\mathrm{j}(i\omega_e t+\phi_{eyi})}) \end{pmatrix} \\ +(0.5c_{s1})\left(e_p\omega_p(e^{\mathrm{j}(\omega_p t+\phi_p)}+e^{-\mathrm{j}(\omega_p t+\phi_p)})\right)+(0.5k_{s1}/\mathrm{j})\left(e_p(e^{\mathrm{j}(\omega_p t+\phi_p)}-e^{-\mathrm{j}(\omega_p t+\phi_p)})\right) \\ \\ -k_m e_m+0.5m_2 e_g\omega_g^2(e^{\mathrm{j}(\omega_g t+\phi_g)}+e^{-\mathrm{j}(\omega_g t+\phi_g)}) \\ -(0.5c_m/\mathrm{j})\begin{pmatrix} e_p\omega_p(e^{\mathrm{j}(\omega_p t+\phi_p)}-e^{-\mathrm{j}(\omega_p t+\phi_p)})-e_g\omega_g(e^{\mathrm{j}(\omega_g t+\phi_g)}-e^{-\mathrm{j}(\omega_g t+\phi_g)}) \\ +\mathrm{j}\sum_{i=1}^{n} e_{f_{xi}} i\omega_e(e^{\mathrm{j}(i\omega_e t+\phi_{exi})}+e^{-\mathrm{j}(i\omega_e t+\phi_{exi})}) \end{pmatrix} \\ -(0.5k_m/\mathrm{j})\begin{pmatrix} -e_p\mathrm{j}(e^{\mathrm{j}(\omega_p t+\phi_p)}+e^{-\mathrm{j}(\omega_p t+\phi_p)})+e_g\mathrm{j}(e^{\mathrm{j}(\omega_g t+\phi_g)}+e^{-\mathrm{j}(\omega_g t+\phi_g)}) \\ +\sum_{i=1}^{n} e_{f_{xi}}(e^{\mathrm{j}(i\omega_e t+\phi_{exi})}-e^{-\mathrm{j}(i\omega_e t+\phi_{exi})}) \end{pmatrix} \\ +(0.5c_{s2}/\mathrm{j})\left(e_g\omega_g(e^{\mathrm{j}(\omega_g t+\phi_g)}-e^{-\mathrm{j}(\omega_g t+\phi_g)})\right)-(0.5k_{s2})\left(e_g(e^{\mathrm{j}(\omega_g t+\phi_g)}+e^{-\mathrm{j}(\omega_g t+\phi_g)})\right) \\ \\ -m_2 g-k_m e_m+0.5m_2 e_g\omega_g^2(e^{\mathrm{j}(\omega_g t+\phi_g)}-e^{-\mathrm{j}(\omega_g t+\phi_g)})/\mathrm{j} \\ -(0.5c_m/\mathrm{j})\begin{pmatrix} \mathrm{j}e_p\omega_p(e^{\mathrm{j}(\omega_p t+\phi_p)}+e^{-\mathrm{j}(\omega_p t+\phi_p)})+\mathrm{j}e_g\omega_g(e^{\mathrm{j}(\omega_g t+\phi_g)}+e^{-\mathrm{j}(\omega_g t+\phi_g)}) \\ +\mathrm{j}\sum_{i=1}^{n} e_{f_{yi}} i\omega_e(e^{\mathrm{j}(i\omega_e t+\phi_{eyi})}+e^{-\mathrm{j}(i\omega_e t+\phi_{eyi})}) \end{pmatrix} \\ -(0.5k_m/\mathrm{j})\begin{pmatrix} e_p(e^{\mathrm{j}(\omega_p t+\phi_p)}-e^{-\mathrm{j}(\omega_p t+\phi_p)})+e_g(e^{\mathrm{j}(\omega_g t+\phi_g)}-e^{-\mathrm{j}(\omega_g t+\phi_g)}) \\ +\sum_{i=1}^{n} e_{f_{yi}}(e^{\mathrm{j}(i\omega_e t+\phi_{eyi})}-e^{-\mathrm{j}(i\omega_e t+\phi_{eyi})}) \end{pmatrix} \\ -(0.5c_{s2})\left(e_g\omega_g(e^{\mathrm{j}(\omega_g t+\phi_g)}+e^{-\mathrm{j}(\omega_g t+\phi_g)})\right)-(0.5k_{s2}/\mathrm{j})\left(e_g(e^{\mathrm{j}(\omega_g t+\phi_g)}-e^{-\mathrm{j}(\omega_g t+\phi_g)})\right) \end{array}\right\} \tag{3.7}$$

The force given in Eqn. (2.38) is acting at the gear mesh pitch point, which is resolved in the *x* and *y* components. Forces are now split into various identical components as follows,

$$\mathbf{f}_r(t)=\begin{Bmatrix} f_{x1}(t)\\ f_{y1}(t)\\ f_{x2}(t)\\ f_{y2}(t)\end{Bmatrix}=\begin{Bmatrix} k_m e_m\\ -m_1 g+k_m e_m\\ -k_m e_m\\ -m_2 g-k_m e_m\end{Bmatrix}+\frac{1}{2\mathrm{j}}\begin{Bmatrix} \mathrm{j}m_1 e_p\omega_p^2(e^{\mathrm{j}(\omega_p t+\phi_p)}+e^{-\mathrm{j}(\omega_p t+\phi_p)})\\ -m_1 e_p\omega_p^2(e^{\mathrm{j}(\omega_p t+\phi_p)}-e^{-\mathrm{j}(\omega_p t+\phi_p)})\\ \mathrm{j}m_2 e_g\omega_g^2(e^{\mathrm{j}(\omega_g t+\phi_g)}+e^{-\mathrm{j}(\omega_g t+\phi_g)})\\ m_2 e_g\omega_g^2(e^{\mathrm{j}(\omega_g t+\phi_g)}-e^{-\mathrm{j}(\omega_g t+\phi_g)})\end{Bmatrix}+$$

$$\begin{Bmatrix} \frac{c_{s1}}{2\mathrm{j}}e_p\omega_p(e^{\mathrm{j}(\omega_p t+\phi_p)}-e^{-\mathrm{j}(\omega_p t+\phi_p)})\\ \frac{c_{s1}}{2\mathrm{j}}\mathrm{j}e_p\omega_p(e^{\mathrm{j}(\omega_p t+\phi_p)}+e^{-\mathrm{j}(\omega_p t+\phi_p)})\\ \frac{c_{s2}}{2\mathrm{j}}e_g\omega_g(e^{\mathrm{j}(\omega_g t+\phi_g)}-e^{-\mathrm{j}(\omega_g t+\phi_g)})\\ -\frac{c_{s2}}{2\mathrm{j}}\mathrm{j}e_g\omega_g(e^{\mathrm{j}(\omega_g t+\phi_g)}+e^{-\mathrm{j}(\omega_g t+\phi_g)})\end{Bmatrix}+\begin{Bmatrix} -\frac{k_{s1}}{2\mathrm{j}}\mathrm{j}e_p(e^{\mathrm{j}(\omega_p t+\phi_p)}+e^{-\mathrm{j}(\omega_p t+\phi_p)})\\ \frac{k_{s1}}{2\mathrm{j}}e_p(e^{\mathrm{j}(\omega_p t+\phi_p)}-e^{-\mathrm{j}(\omega_p t+\phi_p)})\\ -\frac{k_{s2}}{2\mathrm{j}}\mathrm{j}e_g(e^{\mathrm{j}(\omega_g t+\phi_g)}+e^{-\mathrm{j}(\omega_g t+\phi_g)})\\ -\frac{k_{s2}}{2\mathrm{j}}e_g(e^{\mathrm{j}(\omega_g t+\phi_g)}-e^{-\mathrm{j}(\omega_g t+\phi_g)})\end{Bmatrix}+$$

$$\frac{c_m}{2\mathrm{j}}\begin{Bmatrix} e_p\omega_p(e^{\mathrm{j}(\omega_p t+\phi_p)}-e^{-\mathrm{j}(\omega_p t+\phi_p)})-e_g\omega_g(e^{\mathrm{j}(\omega_g t+\phi_g)}-e^{-\mathrm{j}(\omega_g t+\phi_g)})\\ \mathrm{j}e_p\omega_p(e^{\mathrm{j}(\omega_p t+\phi_p)}+e^{-\mathrm{j}(\omega_p t+\phi_p)})+\mathrm{j}e_g\omega_g(e^{\mathrm{j}(\omega_g t+\phi_g)}+e^{-\mathrm{j}(\omega_g t+\phi_g)})\\ -e_p\omega_p(e^{\mathrm{j}(\omega_p t+\phi_p)}-e^{-\mathrm{j}(\omega_p t+\phi_p)})+e_g\omega_g(e^{\mathrm{j}(\omega_g t+\phi_g)}-e^{-\mathrm{j}(\omega_g t+\phi_g)})\\ -\mathrm{j}e_p\omega_p(e^{\mathrm{j}(\omega_p t+\phi_p)}+e^{-\mathrm{j}(\omega_p t+\phi_p)})-\mathrm{j}e_g\omega_g(e^{\mathrm{j}(\omega_g t+\phi_g)}+e^{-\mathrm{j}(\omega_g t+\phi_g)})\end{Bmatrix}+$$

$$\frac{c_m}{2\mathrm{j}}\sum_{i=1}^{n}\begin{Bmatrix} \mathrm{j}\left(e_{fxi}i\omega_e(e^{\mathrm{j}(i\omega_e t+\phi_{exi})}+e^{-\mathrm{j}(i\omega_e t+\phi_{exi})})\right)\\ \mathrm{j}\left(e_{fyi}i\omega_e(e^{\mathrm{j}(i\omega_e t+\phi_{eyi})}+e^{-\mathrm{j}(i\omega_e t+\phi_{eyi})})\right)\\ \mathrm{j}\left(-e_{fxi}i\omega_e(e^{\mathrm{j}(i\omega_e t+\phi_{exi})}+e^{-\mathrm{j}(i\omega_e t+\phi_{exi})})\right)\\ \mathrm{j}\left(-ie_{fyi}i\omega_e(e^{\mathrm{j}(i\omega_e t+\phi_{eyi})}+e^{-\mathrm{j}(i\omega_e t+\phi_{eyi})})\right)\end{Bmatrix}+$$

$$\frac{k_m}{2\mathrm{j}}\begin{Bmatrix} -\mathrm{j}e_p(e^{\mathrm{j}(\omega_p t+\phi_p)}+e^{-\mathrm{j}(\omega_p t+\phi_p)})+\mathrm{j}e_g(e^{\mathrm{j}(\omega_g t+\phi_g)}+e^{-\mathrm{j}(\omega_g t+\phi_g)})\\ e_p(e^{\mathrm{j}(\omega_p t+\phi_p)}-e^{-\mathrm{j}(\omega_p t+\phi_p)})+e_g(e^{\mathrm{j}(\omega_g t+\phi_g)}-e^{-\mathrm{j}(\omega_g t+\phi_g)})\\ \mathrm{j}e_p(e^{\mathrm{j}(\omega_p t+\phi_p)}+e^{-\mathrm{j}(\omega_p t+\phi_p)})-\mathrm{j}e_g\omega_g(e^{\mathrm{j}(\omega_g t+\phi_g)}+e^{-\mathrm{j}(\omega_g t+\phi_g)})\\ -e_p(e^{\mathrm{j}(\omega_p t+\phi_p)}-e^{-\mathrm{j}(\omega_p t+\phi_p)})-e_g(e^{\mathrm{j}(\omega_g t+\phi_g)}-e^{-\mathrm{j}(\omega_g t+\phi_g)})\end{Bmatrix}+\frac{k_m}{2\mathrm{j}}\sum_{i=1}^{n}\begin{bmatrix} e_{fxi}(e^{\mathrm{j}(i\omega_e t+\phi_{exi})}-e^{-\mathrm{j}(i\omega_e t+\phi_{exi})})\\ e_{fyi}(e^{\mathrm{j}(i\omega_e t+\phi_{eyi})}-e^{-\mathrm{j}(i\omega_e t+\phi_{eyi})})\\ -e_{fxi}(e^{\mathrm{j}(i\omega_e t+\phi_{exi})}-e^{-\mathrm{j}(i\omega_e t+\phi_{exi})})\\ -e_{fyi}(e^{\mathrm{j}(i\omega_e t+\phi_{eyi})}-e^{-\mathrm{j}(i\omega_e t+\phi_{eyi})})\end{bmatrix}$$

(3.8)

Equations of motion in time domain can be converted directly to frequency domain by defining complex displacements, as

$$r_1 = x_1 + \mathrm{j}y_1 \quad \text{and} \quad r_2 = x_2 + \mathrm{j}y_2 \tag{3.9}$$

On substituting equation (3.9) into equation (2.35), equations of motion in complex form can be written as

$$m_1\ddot{r}_1 + (c_{s1} + c_m)\dot{r}_1 - c_m\dot{r}_2 + (k_{s1} + k_m)r_1 - k_m r_2 = f_{r1}(t) \tag{3.10}$$

And

$$m_2\ddot{r}_2 + (c_{s2} - c_m)\dot{r}_2 - c_m\dot{r}_1 + (k_{s2} + k_m)r_2 - k_m r_1 = f_{r2}(t) \tag{3.11}$$

With

$$f_{r1}(t) = f_{x1} + \mathrm{j}\, f_{y1} \quad \text{and} \quad f_{r2}(t) = f_{x2} + \mathrm{j}\, f_{y2} \tag{3.12}$$

Now, defining a complex force vector, as

$$\mathbf{f}_{rc}(t) = \begin{Bmatrix} f_{r1}(t) \\ f_{r2}(t) \end{Bmatrix} = \begin{Bmatrix} f_{x1} + \mathrm{j}f_{y1} \\ f_{x2} + \mathrm{j}f_{y2} \end{Bmatrix} \tag{3.13}$$

On substituting for force component expressions from equation (3.8), we get

$$\mathbf{f}_{rc}(t) = \begin{Bmatrix} (k_m e_m) + \mathrm{j}(-m_1 g + k_m e_m) \\ (-k_m e_m) + \mathrm{j}(-m_2 g - k_m e_m) \end{Bmatrix} + \frac{1}{2}\begin{Bmatrix} m_1 e_p \omega_p^2 (e^{\mathrm{j}(\omega_p t + \phi_p)} + e^{-\mathrm{j}(\omega_p t + \phi_p)}) - m_1 e_p \omega_p^2 (e^{\mathrm{j}(\omega_p t + \phi_p)} - e^{-\mathrm{j}(\omega_p t + \phi_p)}) \\ m_2 e_g \omega_g^2 (e^{\mathrm{j}(\omega_g t + \phi_g)} + e^{-\mathrm{j}(\omega_g t + \phi_g)}) + m_2 e_g \omega_g^2 (e^{\mathrm{j}(\omega_g t + \phi_g)} - e^{-\mathrm{j}(\omega_g t + \phi_g)}) \end{Bmatrix}$$

$$+\begin{Bmatrix} \frac{c_{s1}}{2\mathrm{j}} e_p \omega_p (e^{\mathrm{j}(\omega_p t+\phi_p)} - e^{-\mathrm{j}(\omega_p t+\phi_p)}) + \mathrm{j}\frac{c_{s1}}{2\mathrm{j}} \mathrm{j} e_p \omega_p (e^{\mathrm{j}(\omega_p t+\phi_p)} + e^{-\mathrm{j}(\omega_p t+\phi_p)}) \\ \frac{c_{s2}}{2\mathrm{j}} e_g \omega_g (e^{\mathrm{j}(\omega_g t+\phi_g)} - e^{-\mathrm{j}(\omega_g t+\phi_g)}) - \mathrm{j}\frac{c_{s2}}{2\mathrm{j}} \mathrm{j} e_g \omega_g (e^{\mathrm{j}(\omega_g t+\phi_g)} + e^{-\mathrm{j}(\omega_g t+\phi_g)}) \end{Bmatrix}$$

$$+\begin{Bmatrix} -\frac{k_{s1}}{2\mathrm{j}} \mathrm{j} e_p (e^{\mathrm{j}(\omega_p t+\phi_p)} + e^{-\mathrm{j}(\omega_p t+\phi_p)}) + \mathrm{j}\frac{k_{s1}}{2\mathrm{j}} e_p (e^{\mathrm{j}(\omega_p t+\phi_p)} - e^{-\mathrm{j}(\omega_p t+\phi_p)}) \\ -\frac{k_{s2}}{2\mathrm{j}} \mathrm{j} e_g (e^{\mathrm{j}(\omega_g t+\phi_g)} + e^{-\mathrm{j}(\omega_g t+\phi_g)}) - \mathrm{j}\frac{k_{s2}}{2\mathrm{j}} e_g (e^{\mathrm{j}(\omega_g t+\phi_g)} - e^{-\mathrm{j}(\omega_g t+\phi_g)}) \end{Bmatrix}$$

$$+\frac{c_m}{2}\begin{Bmatrix} -\mathrm{j} e_p \omega_p (e^{\mathrm{j}(\omega_p t+\phi_p)} - e^{-\mathrm{j}(\omega_p t+\phi_p)}) + \mathrm{j} e_g \omega_g (e^{\mathrm{j}(\omega_g t+\phi_g)} - e^{-\mathrm{j}(\omega_g t+\phi_g)}) \\ +\mathrm{j} e_p \omega_p (e^{\mathrm{j}(\omega_p t+\phi_p)} + e^{-\mathrm{j}(\omega_p t+\phi_p)}) + \mathrm{j} e_g \omega_g (e^{\mathrm{j}(\omega_g t+\phi_g)} + e^{-\mathrm{j}(\omega_g t+\phi_g)}) \\ \mathrm{j} e_p \omega_p (e^{\mathrm{j}(\omega_p t+\phi_p)} - e^{-\mathrm{j}(\omega_p t+\phi_p)}) - \mathrm{j} e_g \omega_g (e^{\mathrm{j}(\omega_g t+\phi_g)} - e^{-\mathrm{j}(\omega_g t+\phi_g)}) \\ -\mathrm{j} e_p \omega_p (e^{\mathrm{j}(\omega_p t+\phi_p)} + e^{-\mathrm{j}(\omega_p t+\phi_p)}) - \mathrm{j} e_g \omega_g (e^{\mathrm{j}(\omega_g t+\phi_g)} + e^{-\mathrm{j}(\omega_g t+\phi_g)}) \end{Bmatrix}$$

$$+\frac{k_m}{2}\begin{Bmatrix} -e_p (e^{\mathrm{j}(\omega_p t+\phi_p)} + e^{-\mathrm{j}(\omega_p t+\phi_p)}) + e_g (e^{\mathrm{j}(\omega_g t+\phi_g)} + e^{-\mathrm{j}(\omega_g t+\phi_g)}) \\ +e_p (e^{\mathrm{j}(\omega_p t+\phi_p)} - e^{-\mathrm{j}(\omega_p t+\phi_p)}) + e_g (e^{\mathrm{j}(\omega_g t+\phi_g)} - e^{-\mathrm{j}(\omega_g t+\phi_g)}) \\ e_p (e^{\mathrm{j}(\omega_p t+\phi_p)} + e^{-\mathrm{j}(\omega_p t+\phi_p)}) - e_g \omega_g (e^{\mathrm{j}(\omega_g t+\phi_g)} + e^{-\mathrm{j}(\omega_g t+\phi_g)}) \\ -e_p (e^{\mathrm{j}(\omega_p t+\phi_p)} - e^{-\mathrm{j}(\omega_p t+\phi_p)}) - e_g (e^{\mathrm{j}(\omega_g t+\phi_g)} - e^{-\mathrm{j}(\omega_g t+\phi_g)}) \end{Bmatrix}$$

$$+\frac{c_m}{2}\sum_{i=1}^{n}\begin{Bmatrix} \left(e_{fxi} i\omega_e (e^{\mathrm{j}(i\omega_e t+\phi_{exi})} + e^{-\mathrm{j}(i\omega_e t+\phi_{exi})})\right) \\ +\mathrm{j}\left(e_{fyi} i\omega_e (e^{\mathrm{j}(i\omega_e t+\phi_{eyi})} + e^{-\mathrm{j}(i\omega_e t+\phi_{eyi})})\right) \\ \left(-e_{fxi} i\omega_e (e^{\mathrm{j}(i\omega_e t+\phi_{exi})} + e^{-\mathrm{j}(i\omega_e t+\phi_{exi})})\right) \\ +\mathrm{j}\left(-e_{fyi} i\omega_e (e^{\mathrm{j}(i\omega_e t+\phi_{eyi})} + e^{-\mathrm{j}(i\omega_e t+\phi_{eyi})})\right) \end{Bmatrix} + \frac{k_m}{2}\sum_{i=1}^{n}\begin{Bmatrix} -\mathrm{j}\left(e_{fxi} (e^{\mathrm{j}(i\omega_e t+\phi_{exi})} - e^{-\mathrm{j}(i\omega_e t+\phi_{exi})})\right) \\ +\left(e_{fyi} (e^{\mathrm{j}(i\omega_e t+\phi_{eyi})} - e^{-\mathrm{j}(i\omega_e t+\phi_{eyi})})\right) \\ \left(+\mathrm{j} e_{fxi} (e^{\mathrm{j}(i\omega_e t+\phi_{exi})} - e^{-\mathrm{j}(i\omega_e t+\phi_{exi})})\right) \\ +\left(-e_{fyi} (e^{\mathrm{j}(i\omega_e t+\phi_{eyi})} - e^{-\mathrm{j}(i\omega_e t+\phi_{eyi})})\right) \end{Bmatrix} \tag{3.14}$$

On collecting similar exponential terms, we get

$$\mathbf{f}_{rc}(t) = \begin{Bmatrix} (k_m e_m) + \mathrm{j}(-m_1 g + k_m e_m) \\ (-k_m e_m) + \mathrm{j}(-m_2 g - k_m e_m) \end{Bmatrix}$$

$$
+\begin{Bmatrix}
m_1 e_p \omega_p^2 e^{-\mathrm{j}\phi_p} e^{-\mathrm{j}\omega_p t} + \mathrm{j} c_m e_p \omega_p e^{-\mathrm{j}\phi_p} e^{-\mathrm{j}\omega_p t} + \mathrm{j} c_m e_g \omega_g e^{\mathrm{j}\phi_g} e^{\mathrm{j}\omega_g t} \\
-k_m e_p e^{-\mathrm{j}\phi_p} e^{-\mathrm{j}\omega_p t} + k_m e_g e^{\mathrm{j}\phi_g} e^{\mathrm{j}\omega_g t} \\
\\
m_2 e_g \omega_g^2 e^{\mathrm{j}\phi_g} e^{\mathrm{j}\omega_g t} - \mathrm{j} c_m e_p \omega_p e^{-\mathrm{j}\phi_p} e^{-\mathrm{j}\omega_p t} - \mathrm{j} c_m e_g \omega_g e^{\mathrm{j}\phi_g} e^{\mathrm{j}\omega_g t} \\
+k_m e_p e^{-\mathrm{j}\phi_p} e^{-\mathrm{j}\omega_p t} - k_m e_g e^{\mathrm{j}\phi_g} e^{\mathrm{j}\omega_g t}
\end{Bmatrix}
$$

$$
+\begin{Bmatrix}
\frac{c_{s1}}{2\mathrm{j}} e_p \omega_p e^{\mathrm{j}\phi_p} e^{\mathrm{j}\omega_p t} - \frac{c_{s1}}{2\mathrm{j}} e_p \omega_p e^{-\mathrm{j}\phi_p} e^{-\mathrm{j}\omega_p t} - \frac{c_{s1}}{2\mathrm{j}} e_p \omega_p e^{\mathrm{j}\phi_p} e^{\mathrm{j}\omega_p t} - \frac{c_{s1}}{2\mathrm{j}} e_p \omega_p e^{-\mathrm{j}\phi_p} e^{-\mathrm{j}\omega_p t} \\
\frac{c_{s2}}{2\mathrm{j}} e_g \omega_g e^{\mathrm{j}\phi_g} e^{\mathrm{j}\omega_g t} - \frac{c_{s2}}{2\mathrm{j}} e_g \omega_g e^{-\mathrm{j}\phi_g} e^{-\mathrm{j}\omega_g t} + \frac{c_{s2}}{2\mathrm{j}} e_g \omega_g e^{\mathrm{j}\phi_g} e^{\mathrm{j}\omega_g t} + \frac{c_{s2}}{2\mathrm{j}} e_g \omega_g e^{-\mathrm{j}\phi_g} e^{-\mathrm{j}\omega_g t}
\end{Bmatrix}
$$

$$
+\begin{Bmatrix}
-\frac{k_{s1}}{2} e_p e^{\mathrm{j}\phi_p} e^{\mathrm{j}\omega_p t} - \frac{k_{s1}}{2} e_p e^{-\mathrm{j}\phi_p} e^{-\mathrm{j}\omega_p t} + \frac{k_{s1}}{2} e_p e^{\mathrm{j}\phi_p} e^{\mathrm{j}\omega_p t} - \frac{k_{s1}}{2} e_p e^{-\mathrm{j}\phi_p} e^{-\mathrm{j}\omega_p t} \\
-\frac{k_{s2}}{2} e_g e^{\mathrm{j}\phi g} e^{\mathrm{j}\omega_g t} - \frac{k_{s2}}{2} e_g e^{-\mathrm{j}\phi g} e^{-\mathrm{j}\omega_g t} - \frac{k_{s2}}{2} e_g e^{\mathrm{j}\phi g} e^{\mathrm{j}\omega_g t} + \frac{k_{s2}}{2} e_g e^{-\mathrm{j}\phi g} e^{-\mathrm{j}\omega_g t}
\end{Bmatrix}
$$

$$
+\sum_{i=1}^{n} \frac{i\omega_e c_m}{2} \begin{Bmatrix}
\left(e_{fxi} e^{\mathrm{j}(\phi_{exi})} + \mathrm{j} e_{fyi} e^{\mathrm{j}(\phi_{eyi})}\right) e^{\mathrm{j}(i\omega_e t)} + \left(e_{fxi} e^{-\mathrm{j}(\phi_{exi})} + \mathrm{j} e_{fyi} e^{-\mathrm{j}(\phi_{eyi})}\right) e^{-\mathrm{j}(i\omega_e t)} \\
-\left(e_{fxi} e^{\mathrm{j}(\phi_{exi})} + \mathrm{j} e_{fyi} e^{\mathrm{j}(\phi_{eyi})}\right) e^{\mathrm{j}(i\omega_e t)} - \left(e_{fxi} e^{-\mathrm{j}(\phi_{exi})} + \mathrm{j} e_{fyi} e^{-\mathrm{j}(\phi_{eyi})}\right) e^{-\mathrm{j}(i\omega_e t)}
\end{Bmatrix}
$$

$$
+\frac{k_m}{2} \sum_{i=1}^{n} \begin{Bmatrix}
\left(-\mathrm{j} e_{fxi} e^{\mathrm{j}(\phi_{exi})} + e_{fyi} e^{\mathrm{j}(\phi_{eyi})}\right) e^{\mathrm{j}(i\omega_e t)} + \left(\mathrm{j} e_{fxi} e^{-\mathrm{j}(\phi_{exi})} - e_{fyi} e^{-\mathrm{j}(\phi_{eyi})}\right) e^{-\mathrm{j}(i\omega_e t)} \\
\left(\mathrm{j} e_{fxi} e^{\mathrm{j}(\phi_{exi})} - e_{fyi} e^{\mathrm{j}(\phi_{eyi})}\right) e^{\mathrm{j}(i\omega_e t)} + \left(-\mathrm{j} e_{fxi} e^{-\mathrm{j}(\phi_{exi})} + e_{fyi} e^{-\mathrm{j}(\phi_{eyi})}\right) e^{-\mathrm{j}(i\omega_e t)}
\end{Bmatrix} \tag{3.15}
$$

By separating the excitation into different frequency components, like the pinion rotation frequency, gear rotation frequency and gear meshing frequencies in both forward and backward whirls, we get

$$
\mathbf{f}_{rc}(t) = \begin{Bmatrix} (k_m e_m) + \mathrm{j}(-m_1 g + k_m e_m) \\ (-k_m e_m) + \mathrm{j}(-m_2 g - k_m e_m) \end{Bmatrix} + \begin{Bmatrix} 0 \\ 0 \end{Bmatrix} e^{-\mathrm{j}\omega_p t}
$$

$$
+\begin{Bmatrix} (m_1 e_p \omega_p^2 e^{-\mathrm{j}\phi_p} - k_m e_p e^{-\mathrm{j}\phi_p}) + \mathrm{j}(c_m e_p \omega_p e^{-\mathrm{j}\phi_p} + c_{s1} e_p e^{-\mathrm{j}\phi_p}) - k_{s1} e_p e^{-\mathrm{j}\phi_p} \\ k_m e_p e^{-\mathrm{j}\phi_p} - \mathrm{j}(c_m e_p \omega_p e^{-\mathrm{j}\phi_p}) \end{Bmatrix} e^{-\mathrm{j}\omega_p t}
$$

$$+\begin{Bmatrix} k_m e_g e^{j\phi_g} + j(c_m e_g \omega_g e^{j\phi_g}) \\ (m_2 e_g \omega_g^2 e^{j\phi_g} - k_m e_g e^{j\phi_g}) - j(c_m e_g \omega_g e^{j\phi_g} + c_{s2} e_g \omega_g e^{j\phi_g}) - k_{s2} e_g e^{j\phi_g} \end{Bmatrix} e^{j\omega_g t} + \begin{Bmatrix} 0 \\ 0 \end{Bmatrix} e^{-j\omega_g t}$$

$$+\sum_{i=1}^{n} \begin{Bmatrix} \frac{i\omega_e c_m}{2}\left(e_{fxi} e^{j(\phi_{exi})} + j e_{fyi} e^{j(\phi_{eyi})}\right) + \frac{k_m}{2}\left(-j e_{fxi} e^{j(\phi_{exi})} + e_{fyi} e^{j(\phi_{eyi})}\right) \\ -\frac{i\omega_e c_m}{2}\left(e_{fxi} e^{j(\phi_{exi})} + j e_{fyi} e^{j(\phi_{eyi})}\right) - \frac{k_m}{2}\left(-j e_{fxi} e^{j(\phi_{exi})} + e_{fyi} e^{j(\phi_{eyi})}\right) \end{Bmatrix} e^{j(i\omega_e t)}$$

$$+\sum_{i=1}^{n} \begin{Bmatrix} \frac{i\omega_e c_m}{2}\left(e_{fxi} e^{-j(\phi_{exi})} + j e_{fyi} e^{-j(\phi_{eyi})}\right) - \frac{k_m}{2}\left(-j e_{fxi} e^{-j(\phi_{exi})} + e_{fyi} e^{-j(\phi_{eyi})}\right) \\ -\frac{i\omega_e c_m}{2}\left(e_{fxi} e^{-j(\phi_{exi})} + j e_{fyi} e^{-j(\phi_{eyi})}\right) + \frac{k_m}{2}\left(-j e_{fxi} e^{-j(\phi_{exi})} + e_{fyi} e^{-j(\phi_{eyi})}\right) \end{Bmatrix} e^{-j(i\omega_e t)}$$

(3.16)

Removing the nullified frequency components, the forcing vector is written as,

$$\boldsymbol{f}_{rc}(t) = \begin{Bmatrix} (k_m e_m) + j(-m_1 g + k_m e_m) \\ (-k_m e_m) + j(-m_2 g - k_m e_m) \end{Bmatrix}$$

$$+\begin{Bmatrix} (m_1 e_p \omega_p^2 e^{-j\phi_p} - k_m e_p e^{-j\phi_p}) + j(c_m e_p \omega_p e^{-j\phi_p} + c_{s1} e_p e^{-j\phi_p}) - k_{s1} e_p e^{-j\phi_p} \\ k_m e_p e^{-j\phi_p} - j(c_m e_p \omega_p e^{-j\phi_p}) \end{Bmatrix} e^{-j\omega_p t}$$

$$+\begin{Bmatrix} k_m e_g e^{j\phi_g} + j(c_m e_g \omega_g e^{j\phi_g}) \\ (m_2 e_g \omega_g^2 e^{j\phi_g} - k_m e_g e^{j\phi_g}) - j(c_m e_g \omega_g e^{j\phi_g} + c_{s2} e_g \omega_g e^{j\phi_g}) - k_{s2} e_g e^{j\phi_g} \end{Bmatrix} e^{j\omega_g t}$$

$$+\sum_{i=1}^{n} \begin{Bmatrix} \frac{i\omega_e c_m}{2}\left(e_{fxi} e^{j(\phi_{exi})} + j e_{fyi} e^{j(\phi_{eyi})}\right) + \frac{k_m}{2}\left(-j e_{fxi} e^{j(\phi_{exi})} + e_{fyi} e^{j(\phi_{eyi})}\right) \\ -\frac{i\omega_e c_m}{2}\left(e_{fxi} e^{j(\phi_{exi})} + j e_{fyi} e^{j(\phi_{eyi})}\right) - \frac{k_m}{2}\left(-j e_{fxi} e^{j(\phi_{exi})} + e_{fyi} e^{j(\phi_{eyi})}\right) \end{Bmatrix} e^{j(i\omega_e t)}$$

$$+\sum_{i=1}^{n} \begin{Bmatrix} \frac{i\omega_e c_m}{2}\left(e_{fxi} e^{-j(\phi_{exi})} + j e_{fyi} e^{-j(\phi_{eyi})}\right) - \frac{k_m}{2}\left(-j e_{fxi} e^{-j(\phi_{exi})} + e_{fyi} e^{-j(\phi_{eyi})}\right) \\ -\frac{i\omega_e c_m}{2}\left(e_{fxi} e^{-j(\phi_{exi})} + j e_{fyi} e^{-j(\phi_{eyi})}\right) + \frac{k_m}{2}\left(-j e_{fxi} e^{-j(\phi_{exi})} + e_{fyi} e^{-j(\phi_{eyi})}\right) \end{Bmatrix} e^{-j(i\omega_e t)}$$

(3.17)

The static, forward and backward whirl components are present in Eqn. (3.17).

For the simplicity, the static components of force vector are expressed for both input and output shafts, as

$$S_1 = S_{1r} + jS_{1j} = \left(k_m e_m\right) + \mathrm{j}\left(-m_1 g + k_m e_m\right)$$
$$S_2 = S_{2r} + jS_{2j} = \left(-k_m e_m\right) + \mathrm{j}\left(-m_2 g - k_m e_m\right) \tag{3.18}$$

Similarly, for the forward whirl of gear meshing frequency coefficients are expressed as,

For input shaft, we get

$$S_{f_{e1}} = S_{f_{e1r}} + \mathrm{j}S_{f_{e1j}} = +\sum_{i=1}^{n}\left\{\frac{i\omega_e c_m}{2}\left(e_{fxi}e^{\mathrm{j}(\phi_{e_{xi}})} + \mathrm{j}e_{fyi}e^{\mathrm{j}(\phi_{e_{yi}})}\right) + \frac{k_m}{2}\left(-\mathrm{j}e_{fxi}e^{\mathrm{j}(\phi_{e_{xi}})} + e_{fyi}e^{\mathrm{j}(\phi_{e_{yi}})}\right)\right\} \tag{3.19}$$

where subscript *f* represents the forward whirl, *r* represents the real part and j represents the imaginary part. So, on separating the real and imaginary components from Eqn. (3.19) by using Euler's equation similar to Eqn. 3.1, we get

$$\begin{aligned} S_{f_{e1r}} &= \sum_{i=1}^{n}\frac{i\omega_e c_m}{2}\left\{e_{fxi}\cos\phi_{e_{xi}} - e_{fyi}\sin\phi_{e_{yi}}\right\} + \frac{k_m}{2}\left\{e_{fxi}\sin\phi_{e_{xi}} + e_{fyi}\cos\phi_{e_{yi}}\right\}; \\ S_{f_{e1j}} &= \sum_{i=1}^{n}\frac{i\omega_e c_m}{2}\left\{e_{fxi}\sin\phi_{e_{xi}} + e_{fyi}\cos\phi_{e_{yi}}\right\} - \frac{k_m}{2}\left\{e_{fxi}\cos\phi_{e_{xi}} - e_{fyi}\sin\phi_{e_{yi}}\right\} \end{aligned} \tag{3.20}$$

Similarly, for output shaft, we get

$$S_{f_{e2}} = S_{f_{e2r}} + \mathrm{j}S_{f_{e2j}} = \sum_{i=1}^{n}\left\{-\frac{i\omega_e c_m}{2}\left(e_{fxi}e^{\mathrm{j}(\phi_{e_{xi}})} + \mathrm{j}e_{fyi}e^{\mathrm{j}(\phi_{e_{yi}})}\right) + \frac{k_m}{2}\left(\mathrm{j}e_{fxi}e^{\mathrm{j}(\phi_{e_{xi}})} - e_{fyi}e^{\mathrm{j}(\phi_{e_{yi}})}\right)\right\} \tag{3.21}$$

On separating the real and imaginary components, we can write

$$S_{f_{e2r}} = \sum_{i=1}^{n} \frac{-i\omega_e c_m}{2}\left\{e_{fxi}\cos\phi_{e_{xi}} - e_{fyi}\sin\phi_{e_{yi}}\right\} - \frac{k_m}{2}\left\{e_{fxi}\sin\phi_{e_{xi}} + e_{fyi}\cos\phi_{e_{yi}}\right\};$$
$$S_{f_{e2j}} = \sum_{i=1}^{n} \frac{-i\omega_e c_m}{2}\left\{e_{fxi}\sin\phi_{e_{xi}} + e_{fyi}\cos\phi_{e_{yi}}\right\} + \frac{k_m}{2}\left\{e_{fxi}\cos\phi_{e_{xi}} - e_{fyi}\sin\phi_{e_{yi}}\right\} \quad (3.22)$$

It is observed that Eqn. (3.20) and Eqn. (3.22) are quantitatively the same with opposite sign

In the same way, for the backward whirl of the gear meshing frequency, we have

For the input shaft, we define

$$S_{b_{e1}} = S_{b_e 1r} + \mathrm{j}S_{b_e 1j} = \sum_{i=1}^{n}\left\{\frac{i\omega_e c_m}{2}\left(e_{fxi}e^{-\mathrm{j}(\phi_{e_{xi}})} + \mathrm{j}e_{fyi}e^{-\mathrm{j}(\phi_{e_{yi}})}\right) - \frac{k_m}{2}\left(-\mathrm{j}e_{fxi}e^{-\mathrm{j}(\phi_{e_{xi}})} + e_{fyi}e^{-\mathrm{j}(\phi_{e_{yi}})}\right)\right\} \quad (3.23)$$

On separating the real and imaginary components, we can write

$$S_{b_e 1r} = \sum_{i=1}^{n} \frac{i\omega_e c_m}{2}\left\{e_{fxi}\cos\phi_{e_{xi}} + e_{fyi}\sin\phi_{e_{yi}}\right\} - \frac{k_m}{2}\left\{-e_{fxi}\sin\phi_{e_{xi}} + e_{fyi}\cos\phi_{e_{yi}}\right\};$$
$$S_{b_e 1j} = \sum_{i=1}^{n} \frac{i\omega_e c_m}{2}\left\{-e_{fxi}\sin\phi_{e_{xi}} + e_{fyi}\cos\phi_{e_{yi}}\right\} + \frac{k_m}{2}\left\{e_{fxi}\cos\phi_{e_{xi}} + e_{fyi}\sin\phi_{e_{yi}}\right\} \quad (3.24)$$

For output shaft

$$S_{b_{e2}} = S_{b_e 2r} + \mathrm{j}S_{b_e 2j} = \sum_{i=1}^{n}\left\{-\frac{i\omega_e c_m}{2}\left(e_{fxi}e^{-\mathrm{j}(\phi_{e_{xi}})} + \mathrm{j}e_{fyi}e^{-\mathrm{j}(\phi_{e_{yi}})}\right) - \frac{k_m}{2}\left(\mathrm{j}e_{fxi}e^{-\mathrm{j}(\phi_{e_{xi}})} - e_{fyi}e^{-\mathrm{j}(\phi_{e_{yi}})}\right)\right\} \quad (3.25)$$

On separating the real and imaginary components, we can write

$$S_{b_e 2r} = -\sum_{i=1}^{n} \frac{i\omega_e c_m}{2}\left\{e_{fxi}\cos\phi_{e_{xi}} + e_{fyi}\sin\phi_{e_{yi}}\right\} - \frac{k_m}{2}\left\{-e_{fxi}\sin\phi_{e_{xi}} + e_{fyi}\cos\phi_{e_{yi}}\right\};$$
$$S_{b_e 2j} = -\sum_{i=1}^{n} \frac{i\omega_e c_m}{2}\left\{-e_{fxi}\sin\phi_{e_{xi}} + e_{fyi}\cos\phi_{e_{yi}}\right\} + \frac{k_m}{2}\left\{e_{fxi}\cos\phi_{e_{xi}} + e_{fyi}\sin\phi_{e_{yi}}\right\} \quad (3.26)$$

where subscript *b* signifies the backward whirl.

It is observed that Eqn. (3.24) and Eqn. (3.26) are quantitatively same with opposite sign

As there are no forward whirl components of the pinion runout frequency component, we can write from Eqn. (3.16)

$$R_{f_{p1}} = 0 \quad (3.27)$$

$$R_{f_{p2}} = 0 \quad (3.28)$$

We can write their real and imaginary components for the input (pinion) shaft as,

$$R_{f_{p1}r} = 0 \quad (3.29)$$

and

$$R_{f_{p1}j} = 0 \quad (3.30)$$

Similarly, for the output (gear) shaft as,

$$R_{f_{p2}r} = 0 \quad (3.31)$$

and

$$R_{f_{p2}j} = 0 \quad (3.32)$$

Similarly, for the backward whirl of pinion runout frequency, we define

$$R_{b_{p1}} = R_{b_{p1r}} + \mathrm{j}R_{b_{p1j}} = (m_1 e_p \omega_p^2 - k_m e_p - k_{s1} e_p) e^{-\mathrm{j}\phi_p} + \mathrm{j}(c_m e_p \omega_p + c_{s1} e_p) e^{-\mathrm{j}\phi_p} \tag{3.33}$$

$$R_{b_{p2}} = R_{b_{p2r}} + \mathrm{j}R_{b_{p2j}} = k_m e_p e^{-\mathrm{j}\phi_p} - \mathrm{j}c_m e_p \omega_p e^{-\mathrm{j}\phi_p} \tag{3.34}$$

The real and imaginary terms, for the input (pinion) shaft, are written as

$$R_{b_{p1r}} = (m_1 e_p \omega_p^2 - k_m e_p - k_{s1} e_p)\cos\phi_p + (c_m e_p \omega_p + c_{s1} e_p \omega_p)\sin\phi_p \tag{3.35}$$

and

$$R_{b_{p1j}} = (c_m e_p \omega_p + c_{s1} e_p \omega_p)\cos\phi_p + (-m_1 e_p \omega_p^2 + k_m e_p + k_{s1} e_p)\sin\phi_p \tag{3.36}$$

Similarly, for the output (gear) shaft as,

$$R_{b_{p2r}} = (k_m e_p)\cos\phi_p - (c_m e_p \omega_p)\sin\phi_p \tag{3.37}$$

and

$$R_{b_{p2j}} = (-c_m e_p \omega_p)\cos\phi_p - (k_m e_p)\sin\phi_p \tag{3.38}$$

For the forward whirl of the gear runout frequency, on defining the following terms

$$R_{f_{g1}} = R_{f_{g1r}} + \mathrm{j}R_{f_{g1j}} = (k_m e_g) e^{\mathrm{j}\phi_g} + \mathrm{j}(c_m e_g \omega_g) e^{\mathrm{j}\phi_g} \tag{3.39}$$

The real and imaginary terms, for the input (pinion) shaft, are written as

$$R_{f_{g1r}} = k_m e_g \cos\phi_g - (c_m e_g \omega_g)\sin\phi_g \tag{3.40}$$

and

$$R_{f_{g1j}} = (c_m e_g \omega_g)\cos\phi_g + k_m e_g \sin\phi_g \tag{3.41}$$

Similarly, for the output (gear) shaft the forward whirl gear runout frequency components are written as,

$$R_{f_{g2}} = R_{f_{g2r}} + \mathrm{j}R_{f_{g2j}} = (m_2 e_g \omega_g^2 - k_m e_g - k_{s2} e_g)e^{\mathrm{j}\phi_g} - \mathrm{j}(c_m e_g \omega_g + c_{s2} e_g \omega_g)e^{\mathrm{j}\phi_g} \tag{3.42}$$

One separating the real and imaginary parts, we get

$$R_{f_{g2r}} = (m_2 e_g \omega_g^2 - k_m e_g - k_{s2} e_g)\cos\phi_g + (c_m e_g \omega_g + c_{s2} e_g \omega_g)\sin\phi_g \tag{3.43}$$

and

$$R_{f_{g2j}} = (-c_m e_g \omega_g - c_{s2} e_g \omega_g)\cos\phi_g + (m_2 e_g \omega_g^2 - k_m e_g - k_{s2} e_g)\sin\phi_g \tag{3.44}$$

As there is no backward whirl of the gear runout frequency, so we can write

$$R_{b_{g1}} = 0; \tag{3.45}$$

$$R_{b_{g2}} = 0 \tag{3.46}$$

where subscript *b* represents backward whirl. From Eqn. (3.45) and (3.46) we get

$$R_{b_{g1}r} = 0 \tag{3.47}$$

and

$$R_{b_{g1}j} = 0 \tag{3.48}$$

$$R_{b_{g2}r} = 0 \tag{3.49}$$

and

$$R_{b_{g2}j} = 0 \tag{3.50}$$

Similarly, frequency components are collected and expressed them in frequency domain for the static, forward and backward whirl components, as follows

On substituting these coefficients from Eqns. (3.18) through (3.50) into Eqn. (3.17), we get

$$\mathbf{f}_{rc} = \begin{Bmatrix} S_{1r} + \mathrm{j}S_{1j} \\ S_{2r} + \mathrm{j}S_{2j} \end{Bmatrix} + \begin{Bmatrix} R_{f_{p1r}} + \mathrm{j}R_{f_{p1j}} \\ R_{f_{p2r}} + \mathrm{j}R_{f_{p2j}} \end{Bmatrix} e^{\mathrm{j}\omega_p t} + \begin{Bmatrix} R_{b_{p1r}} + \mathrm{j}R_{b_{p1j}} \\ R_{b_{p2r}} + \mathrm{j}R_{b_{p2j}} \end{Bmatrix} e^{-\mathrm{j}\omega_p t} + \begin{Bmatrix} R_{f_{g1r}} + \mathrm{j}R_{f_{g1j}} \\ R_{f_{g2r}} + \mathrm{j}R_{f_{g2j}} \end{Bmatrix} e^{\mathrm{j}\omega_g t}$$

$$+ \begin{Bmatrix} R_{b_{g1r}} + \mathrm{j}R_{b_{g1j}} \\ R_{b_{g2r}} + \mathrm{j}R_{b_{g2j}} \end{Bmatrix} e^{-\mathrm{j}\omega_g t} + \sum_{i=1}^{n} \left(\begin{Bmatrix} S_{f_{e1r}} + jS_{f_{e1j}} \\ S_{f_{e2r}} + jS_{f_{e2j}} \end{Bmatrix} e^{j(i\omega_e t)} + \begin{Bmatrix} S_{b_{e1r}} + jS_{b_{e1j}} \\ S_{b_{e2r}} + jS_{b_{e2j}} \end{Bmatrix} e^{-j(i\omega_e t)} \right) \tag{3.51}$$

with

$$S_{1r} = k_m e_m; \quad S_{1j} = -m_1 g + k_m e_m; \quad S_{2r} = -k_m e_m; \quad S_{2j} = -m_2 g - k_m e_m \tag{3.52}$$

$$\begin{aligned}
S_{f_{e1r}} &= (i\omega_e c_m R_{f_{er}} + k_m R_{f_{ej}})/2; & S_{f_{e1j}} &= (i\omega_e c_m R_{f_{ej}} - k_m R_{f_{er}})/2 \\
S_{f_{e2r}} &= (-i\omega_e c_m R_{f_{er}} - k_m R_{f_{ej}})/2; & S_{f_{e2j}} &= (-i\omega_e c_m R_{f_{ej}} + k_m R_{f_{er}})/2 \\
S_{b_{e1r}} &= (i\omega_e c_m R_{b_{er}} - k_m R_{b_{ej}})/2; & S_{b_{e1j}} &= (i\omega_e c_m R_{b_{ej}} + k_m R_{b_{er}})/2 \\
S_{b_{e2r}} &= (-i\omega_e c_m R_{b_{er}} + k_m R_{b_{ej}})/2; & S_{b_{e2j}} &= (-i\omega_e c_m R_{b_{ej}} - k_m R_{b_{er}})/2
\end{aligned} \tag{3.53}$$

where, from Eqn. (3.20), (3.22), (3.24) and (3.26)

$$\begin{aligned}
R_{f_e r} &= e_{xi}\cos\phi_{e_{xi}} - e_{yi}\sin\phi_{e_{yi}}; & R_{f_e j} &= e_{xi}\sin\phi_{e_{xi}} + e_y\cos\phi_{e_{yi}} \\
R_{b_e r} &= e_{xi}\cos\phi_{e_{xi}} + e_{yi}\sin\phi_{e_{yi}}; & R_{b_e j} &= -e_{xi}\sin\phi_{e_{xi}} + e_{yi}\cos\phi_{e_{yi}}
\end{aligned} \tag{3.54}$$

On substituting force Eqn. (3.51) into Eqn. (3.10) and (3.11), equations of motion now can be written in a matrix form, as follows

$$\begin{bmatrix} m_1 & 0 \\ 0 & m_2 \end{bmatrix}\begin{Bmatrix} \ddot{r}_1 \\ \ddot{r}_2 \end{Bmatrix} + \begin{bmatrix} c_{s1}+c_m & -c_m \\ -c_m & c_{s2}+c_m \end{bmatrix}\begin{Bmatrix} \dot{r}_1 \\ \dot{r}_2 \end{Bmatrix} + \begin{bmatrix} k_{s1}+k_m & -k_m \\ -k_m & k_{s2}+k_m \end{bmatrix}\begin{Bmatrix} r_1 \\ r_2 \end{Bmatrix} =$$

$$\begin{Bmatrix} S_1 \\ S_2 \end{Bmatrix} + \begin{Bmatrix} R_{f_{p1}r} + \mathrm{j}R_{f_{p1}j} \\ R_{f_{p2}r} + \mathrm{j}R_{f_{p2}j} \end{Bmatrix} e^{\mathrm{j}\omega_p t} + \begin{Bmatrix} R_{b_{p1}r} + \mathrm{j}R_{b_{p1}j} \\ R_{b_{p2}r} + \mathrm{j}R_{b_{p2}j} \end{Bmatrix} e^{-\mathrm{j}\omega_p t} + \begin{Bmatrix} R_{f_{g1}r} + \mathrm{j}R_{f_{g1}j} \\ R_{f_{g2}r} + \mathrm{j}R_{f_{g2}j} \end{Bmatrix} e^{\mathrm{j}\omega_g t} + \tag{3.55}$$

$$\begin{Bmatrix} R_{b_{g1}r} + \mathrm{j}R_{b_{g1}j} \\ R_{b_{g2}r} + \mathrm{j}R_{b_{g2}j} \end{Bmatrix} e^{-\mathrm{j}\omega_g t} + \sum_{i=1}^{n} \left(\begin{Bmatrix} S_{f_e 1r} + \mathrm{j}S_{f_e 1j} \\ S_{f_e 2r} + \mathrm{j}S_{f_e 2j} \end{Bmatrix} e^{\mathrm{j}(i\omega_e t)} + \begin{Bmatrix} S_{b_e 1r} + \mathrm{j}S_{b_e 1j} \\ S_{b_e 2r} + \mathrm{j}S_{b_e 2j} \end{Bmatrix} e^{-\mathrm{j}(i\omega_e t)} \right)$$

Here S, $S_{f_{er}}$, $S_{f_{ej}}$, $S_{b_{er}}$ and $S_{b_{ej}}$ includes the TE amplitude and its phase of the gear mesh. Index *i* represents the harmonics of gear order and *n* represents total number of harmonics considered in the TE. For presumed value of TE parameters, Eqn. (3.55) can be solved to get the response of the geared rotor system. Since

equations of motion are linear, assumed solution for each harmonic can be added up using the principle of superposition, as

For *i* th harmonic, Eqn. (3.55) can be written as

$$m_1\ddot{r}_1 + (c_{s1} + c_m)\dot{r}_1 - c_m\dot{r}_2 + (k_{s1} + k_m)r_1 - k_m r_2 = S_1 + S_{f_{e1}} e^{\mathrm{j}(i\omega_e t)} + S_{b_{e1}} e^{-\mathrm{j}(i\omega_e t)} + R_{f_{p1}} e^{\mathrm{j}\omega_p t} + R_{f_{p1}} e^{-\mathrm{j}\omega_p t} + R_{f_{g1}} e^{\mathrm{j}\omega_g t} + R_{f_{g1}} e^{-\mathrm{j}\omega_g t} \quad (3.56)$$

and

$$m_2\ddot{r}_2 + (c_{s2} + c_m)\dot{r}_2 - c_m\dot{r}_1 + (k_{s2} + k_m)r_2 - k_m r_1 = S_2 + S_{f_{e2}} e^{\mathrm{j}(i\omega_e t)} + S_{b_{e2}} e^{-\mathrm{j}(i\omega_e t)} + R_{f_{p2}} e^{\mathrm{j}\omega_p t} + R_{f_{p2}} e^{-\mathrm{j}\omega_p t} + R_{f_{g2}} e^{\mathrm{j}\omega_g t} + R_{f_{g2}} e^{-\mathrm{j}\omega_g t} \quad (3.57)$$

with

$$S_1 = k_m e_m + \mathrm{j}(-m_1 g + k_m e_m);\ S_2 = -(k_m e_m) + \mathrm{j}(-m_2 g - k_m e_m) \quad (3.58)$$

and

$$S_{f_{e1}} = S_{f_{e1r}} + \mathrm{j}S_{f_{e1j}};\qquad S_{b_{e1}} = S_{b_{e1r}} + \mathrm{j}S_{b_{e1j}};$$
$$S_{f_{e2}} = S_{f_{e2r}} + \mathrm{j}S_{f_{e2j}};\qquad S_{b_{e2}} = S_{b_{e2r}} + \mathrm{j}S_{b_{e2j}} \quad (3.59)$$

where S_1 and S_2 are static components; $S_{f_{e1}}$, $S_{b_{e1}}$ and $S_{f_{e2}}$, $S_{b_{e2}}$ are time varying components with the gear mesh frequency or its harmonics. Subscripts *f* and *b* represent the forward and backward whirls. Equation (3.56) and (3.57), we can write

Only static force, it will give

$$\left(k_{s1}+k_m\right)r_1-k_m r_2=S_1;\qquad \left(k_{s2}+k_m\right)r_2-k_m r_1=S_2 \tag{3.60}$$

For the forward whirl force, we have

$$\begin{aligned} &m_1\ddot{r}_1+\left(c_{s1}+c_m\right)\dot{r}_1-c_m\dot{r}_2+\left(k_{s1}+k_m\right)r_1-k_m r_2= \\ &(S_{f_{e1r}}+\mathrm{j}S_{f_{e1j}})e^{\mathrm{j}(i\omega_e t)}+(R_{f_{p1r}}+\mathrm{j}R_{f_{p1j}})e^{\mathrm{j}\omega_p t}+(R_{f_{g1r}}+\mathrm{j}R_{f_{g1j}})e^{\mathrm{j}\omega_g t} \end{aligned} \tag{3.61}$$

and

$$\begin{aligned} &m_2\ddot{r}_2+\left(c_{s2}+c_m\right)\dot{r}_2-c_m\dot{r}_1+\left(k_{s2}+k_m\right)r_2-k_m r_1= \\ &(S_{f_{e2r}}+\mathrm{j}S_{f_{e2j}})e^{\mathrm{j}(i\omega_e t)}+(R_{f_{p2r}}+\mathrm{j}R_{f_{p2j}})e^{\mathrm{j}\omega_p t}+(R_{f_{g2r}}+\mathrm{j}R_{f_{g2j}})e^{\mathrm{j}\omega_g t} \end{aligned} \tag{3.62}$$

For the backward whirl force, we have

$$\begin{aligned} &m_1\ddot{r}_1+\left(c_{s1}+c_m\right)\dot{r}_1-c_m\dot{r}_2+\left(k_{s1}+k_m\right)r_1-k_m r_2= \\ &(S_{b1r}+\mathrm{j}S_{b1j})e^{-\mathrm{j}(i\omega_e t)}+(R_{b_{p1r}}+\mathrm{j}R_{b_{p1j}})e^{-\mathrm{j}\omega_p t}+(R_{b_{g1r}}+\mathrm{j}R_{b_{g1j}})e^{-\mathrm{j}\omega_g t} \end{aligned} \tag{3.63}$$

and

$$m_2\ddot{r}_2 + (c_{s2} + c_m)\dot{r}_2 - c_m\dot{r}_1 + (k_{s2} + k_m)r_2 - k_m r_1 =$$

$$(S_{b2r} + \mathrm{j}S_{b2j})e^{-\mathrm{j}(i\omega_e t)} + (R_{b_{p2r}} + \mathrm{j}R_{b_{p2j}})e^{-\mathrm{j}\omega_p t} + (R_{b_{g2r}} + \mathrm{j}R_{b_{g2j}})e^{-\mathrm{j}\omega_g t} \quad (3.64)$$

Assuming solution due to the static force for Eqns. (3.60) as

$$r_1 = P_{s1} = P_{s1r} + \mathrm{j}P_{s1j} \qquad \text{and} \qquad r_2 = P_{s2} = P_{s1r} + \mathrm{j}P_{s1j} \quad (3.65)$$

where P_{s1} and P_{s2} are in complex form as $P_s = P_{sr} + jP_{sj}$.

Presuming solutions for the forward whirl of Eqns. (3.61) and (3.62), as

$$\begin{aligned}
r_1(t) &= P_{f_{e1}}e^{\mathrm{j}(i\omega_e t)} + P_{f_{p1}}e^{\mathrm{j}(\omega_p t)} + P_{f_{g1}}e^{\mathrm{j}(\omega_g t)} \\
r_2(t) &= P_{f_{e2}}e^{\mathrm{j}(i\omega_e t)} + P_{f_{p2}}e^{\mathrm{j}(\omega_p t)} + P_{f_{g2}}e^{\mathrm{j}(\omega_g t)} \\
\dot{r}_1(t) &= \mathrm{j}i\omega_e P_{f_{e1}}e^{\mathrm{j}(i\omega_e t)} + \mathrm{j}\omega_p P_{f_{p1}}e^{\mathrm{j}(\omega_p t)} + \mathrm{j}\omega_g P_{f_{g1}}e^{\mathrm{j}(\omega_g t)} \\
\dot{r}_2(t) &= \mathrm{j}i\omega_e P_{f_{e2}}e^{\mathrm{j}(i\omega_e t)} + \mathrm{j}\omega_p P_{f_{p2}}e^{\mathrm{j}(\omega_p t)} + \mathrm{j}\omega_g P_{f_{g2}}e^{\mathrm{j}(\omega_g t)}
\end{aligned} \quad (3.66)$$

$$\begin{aligned}
\ddot{r}_1(t) &= -(i\omega_e)^2 P_{f_{e1}}e^{\mathrm{j}(i\omega_e t)} - (\omega_p)^2 P_{f_{p1}}e^{\mathrm{j}(\omega_p t)} - (\omega_g)^2 P_{f_{g1}}e^{\mathrm{j}(\omega_g t)} \\
\ddot{r}_2(t) &= -(i\omega_e)^2 P_{f_{e2}}e^{\mathrm{j}(i\omega_e t)} - (\omega_p)^2 P_{f_{p2}}e^{\mathrm{j}(\omega_p t)} - (\omega_g)^2 P_{f_{g2}}e^{\mathrm{j}(\omega_g t)}
\end{aligned}$$

where P_{f1} and P_{f2} are in complex form as $P_f = P_{fr} + jP_{fj}$.

Presuming solution for the backward whirl of Eqns. (3.63) and (3.64) as,

$$
\begin{aligned}
r_1(t) &= P_{b_e 1} e^{-\mathrm{j}(i\omega_e t)} + P_{b_p 1} e^{-\mathrm{j}(\omega_p t)} + P_{b_g 1} e^{-\mathrm{j}(\omega_g t)} \\
r_2(t) &= P_{b_e 2} e^{-\mathrm{j}(i\omega_e t)} + P_{b_p 2} e^{-\mathrm{j}(\omega_p t)} + P_{b_g 2} e^{-\mathrm{j}(\omega_g t)} \\
\dot{r}_1(t) &= -\mathrm{j}i\omega_e P_{b_e 1} e^{-\mathrm{j}(i\omega_e t)} - \mathrm{j}\omega_p P_{b_p 1} e^{-\mathrm{j}(\omega_p t)} - \mathrm{j}\omega_g P_{b_g 1} e^{-\mathrm{j}(\omega_g t)} \\
\dot{r}_2(t) &= -\mathrm{j}i\omega_e P_{b_e 2} e^{-\mathrm{j}(i\omega_e t)} - \mathrm{j}\omega_p P_{b_p 2} e^{-\mathrm{j}(\omega_p t)} - \mathrm{j}\omega_g P_{b_g 2} e^{-\mathrm{j}(\omega_g t)} \\
\ddot{r}_1(t) &= (i\omega_e)^2 P_{b_e 1} e^{-\mathrm{j}(i\omega_e t)} + (\omega_p)^2 P_{b_p 1} e^{-\mathrm{j}(\omega_p t)} + (\omega_g)^2 P_{b_g 1} e^{-\mathrm{j}(\omega_g t)} \\
\ddot{r}_2(t) &= (i\omega_e)^2 P_{b_e 2} e^{-\mathrm{j}(i\omega_e t)} + (\omega_p)^2 P_{b_p 2} e^{-\mathrm{j}(\omega_p t)} + (\omega_g)^2 P_{b_g 2} e^{-\mathrm{j}(\omega_g t)}
\end{aligned}
\tag{3.67}
$$

where P_b is in complex form as $P_b = P_{br} + jP_{bj}$.

3.2.1 Grouping of static components

On substituting back Eqn. (3.65) in Eqn. (3.60), we get

For the static force, we get

$$
\left(k_{s1} + k_m\right) P_{s1} - k_m P_{s2} = S_1; \qquad \left(k_{s2} + k_m\right) P_{s2} - k_m P_{s1} = S_2 \tag{3.68}
$$

Now Eqn. (3.68) can be arranged in the real and imaginary parts, as

$$
\left(k_{s1} + k_m\right)\left(P_{s1r} + \mathrm{j}P_{s1j}\right) - k_m\left(P_{s2r} + \mathrm{j}P_{s2j}\right) = S_{1r} + \mathrm{j}S_{1j} \tag{3.69}
$$

and

$$
\left(k_{s2} + k_m\right)\left(P_{s2r} + \mathrm{j}P_{s2j}\right) - k_m\left(P_{s1r} + \mathrm{j}P_{s1j}\right) = S_{2r} + \mathrm{j}S_{2j} \tag{3.70}
$$

On separating the real and imaginary components on both sides of Eqn. (3.69) and (3.70), we get the static force real and imaginary components, as

$$\left(k_{s1}+k_m\right)P_{s1r}-k_mP_{s2r}=S_{1r};\qquad -k_mP_{s1r}+\left(k_{s2}+k_m\right)P_{s2r}=S_{2r} \tag{3.71}$$

and

$$\left(k_{s1}+k_m\right)P_{s1j}-k_mP_{s2j}=S_{1j};\qquad -k_mP_{s1j}+\left(k_{s2}+k_m\right)P_{s2j}=S_{2j} \tag{3.72}$$

On combining Eqns. (3.71) and (3.72) in a matrix form, we get

$$\mathbf{A}_s\mathbf{p}_s=\mathbf{s}_s \tag{3.73}$$

with

$$\mathbf{A}_{si}=\begin{bmatrix} k_{s1}+k_m & 0 & -k_m & 0 \\ 0 & k_{s1}+k_m & 0 & -k_m \\ -k_m & 0 & k_{s2}+k_m & 0 \\ 0 & -k_m & 0 & k_{s2}+k_m \end{bmatrix};\ \mathbf{p}_s=\begin{Bmatrix} P_{s1r} \\ P_{s1j} \\ P_{s2r} \\ P_{s2j} \end{Bmatrix};\ \mathbf{s}_s=\begin{Bmatrix} S_{1r} \\ S_{1j} \\ S_{2r} \\ S_{2j} \end{Bmatrix} \tag{3.74}$$

3.2.2 Grouping of forward whirl components

On substituting back equation (3.66) into equations (3.61) and (3.62), for the forward whirl force, we get

$$-m_1i^2\omega_e^2P_{f_{e1}}+\mathrm{j}i\omega_e\left(c_{s1}+c_m\right)P_{f_{e1}}-\mathrm{j}i\omega_ec_mP_{f_{e2}}+\left(k_{s1}+k_m\right)P_{f_{e1}}-k_mP_{f_{e2}}=S_{f_{e1}} \tag{3.75}$$

$$-m_1i^2\omega_p^2P_{f_{p1}}+\mathrm{j}\omega_p\left(c_{s1}+c_m\right)P_{f_{p1}}-\mathrm{j}\omega_pc_mP_{f_{p2}}+\left(k_{s1}+k_m\right)P_{f_{p1}}-k_mP_{f_{p2}}=R_{f_{p1}} \tag{3.76}$$

$$-m_1i^2\omega_g^2P_{f_{g1}}+\mathrm{j}\omega_g\left(c_{s1}+c_m\right)P_{f_{g1}}-\mathrm{j}\omega_gc_mP_{f_{g2}}+\left(k_{s1}+k_m\right)P_{f_{g1}}-k_mP_{f_{g2}}=R_{f_{g1}} \tag{3.77}$$

and

$$-m_2i^2\omega_e^2P_{f_{e2}}+\mathrm{j}\omega_e\left(c_{s2}+c_m\right)P_{f_{e2}}-\mathrm{j}\omega_ec_mP_{f_{e1}}+\left(k_{s2}+k_m\right)P_{f_{e2}}-k_mP_{f_{e1}}=S_{f_{e2}} \tag{3.78}$$

$$-m_2 i^2 \omega_p^2 P_{f_{p2}} + \mathrm{j}\omega_p \left(c_{s2} + c_m\right) P_{f_{p2}} - \mathrm{j}\omega_p c_m P_{f_{p1}} + \left(k_{s2} + k_m\right) P_{f_{p2}} - k_m P_{f_{p1}} = R_{f_{p2}} \tag{3.79}$$

$$-m_2 i^2 \omega_g^2 P_{f_{g2}} + \mathrm{j}\omega_g \left(c_{s2} + c_m\right) P_{f_{g2}} - \mathrm{j}\omega_g c_m P_{f_{g1}} + \left(k_{s2} + k_m\right) P_{f_{g2}} - k_m P_{f_{g1}} = R_{f_{g2}} \tag{3.80}$$

with

$i = 1, 2, \cdots, n$

Now, these are organized into the real and imaginary components, as

$$\begin{aligned} &-m_1 i^2 \omega_e^2 \left(P_{f_{e1r}} + \mathrm{j}P_{f_{e1j}}\right) + (\mathrm{j}i\omega_e)\left(c_{s1} + c_m\right)\left(P_{f_{e1r}} + \mathrm{j}P_{f_{e1j}}\right) - (\mathrm{j}i\omega_e)c_m \left(P_{f_{e2r}} + \mathrm{j}P_{f_{e2j}}\right) \\ &+ \left(k_{s1} + k_m\right)\left(P_{f_{e1r}} + \mathrm{j}P_{f_{e1j}}\right) - k_m \left(P_{f_{e2r}} + \mathrm{j}P_{f_{e2j}}\right) = \left(S_{f_{e1r}} + \mathrm{j}S_{f_{e1j}}\right) \end{aligned} \tag{3.81}$$

$$\begin{aligned} &-m_1 i^2 \omega_p^2 \left(P_{f_{p1r}} + jP_{f_{p1j}}\right) + \mathrm{j}\omega_p \left(c_{s1} + c_m\right)\left(P_{f_{p1r}} + \mathrm{j}P_{f_{p1j}}\right) - \mathrm{j}\omega_p c_m \left(P_{f_{p2r}} + \mathrm{j}P_{f_{p2j}}\right) \\ &+ \left(k_{s1} + k_m\right)\left(P_{f_{p1r}} + \mathrm{j}P_{f_{p1j}}\right) - k_m \left(P_{f_{p2r}} + \mathrm{j}P_{f_{p2j}}\right) = \left(R_{f_{p1r}} + \mathrm{j}R_{f_{p1j}}\right) \end{aligned} \tag{3.82}$$

$$\begin{aligned} &-m_1 i^2 \omega_g^2 \left(P_{f_{g1r}} + \mathrm{j}P_{f_{g1j}}\right) + \mathrm{j}\omega_g \left(c_{s1} + c_m\right)\left(P_{f_{g1r}} + \mathrm{j}P_{f_{g1j}}\right) - \mathrm{j}\omega_g c_m \left(P_{f_{g2r}} + \mathrm{j}P_{f_{g2j}}\right) \\ &+ \left(k_{s1} + k_m\right)\left(P_{f_{g1r}} + \mathrm{j}P_{f_{g1j}}\right) - k_m \left(P_{f_{g2r}} + \mathrm{j}P_{f_{g2j}}\right) = \left(R_{f_{g1r}} + \mathrm{j}R_{f_{g1j}}\right) \end{aligned} \tag{3.83}$$

and

$$\begin{aligned} &-m_2 i^2 \omega_e^2 \left(P_{f_{e2r}} + \mathrm{j}P_{f_{e2j}}\right) + \mathrm{j}i\omega_e \left(c_{s2} + c_m\right)\left(P_{f_{e2r}} + \mathrm{j}P_{f_{e2j}}\right) - \mathrm{j}i\omega_e c_m \left(P_{f_{e1r}} + \mathrm{j}P_{f_{e1j}}\right) \\ &+ \left(k_{s2} + k_m\right)\left(P_{f_{e2r}} + \mathrm{j}P_{f_{e2j}}\right) - k_m \left(P_{f_{e1r}} + \mathrm{j}P_{f_{e1j}}\right) = \left(S_{f_{e2r}} + \mathrm{j}S_{f_{e2j}}\right) \end{aligned} \tag{3.84}$$

$$-m_2 i^2 \omega_p^2 \left(P_{f_{p2r}} + \mathrm{j}P_{f_{p2j}}\right) + \mathrm{j}\omega_p \left(c_{s2} + c_m\right)\left(P_{f_{p2r}} + \mathrm{j}P_{f_{p2j}}\right) - \mathrm{j}\omega_p c_m \left(P_{f_{p1r}} + \mathrm{j}P_{f_{p1j}}\right)$$
$$+\left(k_{s2} + k_m\right)\left(P_{f_{p2r}} + \mathrm{j}P_{f_{p1j}}\right) - k_m \left(P_{f_{p1r}} + \mathrm{j}P_{f_{p1j}}\right) = \left(R_{f_{p2r}} + \mathrm{j}R_{f_{p2j}}\right) \quad (3.85)$$

$$-m_2 i^2 \omega_g^2 \left(P_{f_{g2r}} + \mathrm{j}P_{f_{g2j}}\right) + \mathrm{j}\omega_g \left(c_{s2} + c_m\right)\left(P_{f_{g2r}} + \mathrm{j}P_{f_{g2j}}\right) - \mathrm{j}\omega_g c_m \left(P_{f_{g1r}} + \mathrm{j}P_{f_{g1j}}\right)$$
$$+\left(k_{s2} + k_m\right)\left(P_{f_{g2r}} + \mathrm{j}P_{f_{g2j}}\right) - k_m \left(P_{f_{g1r}} + \mathrm{j}P_{f_{g1j}}\right) = \left(R_{f_{g2r}} + \mathrm{j}R_{f_{g2j}}\right) \quad (3.86)$$

with $i = 1, 2, \cdots, n$

On separating the real and imaginary components on both sides of Eqn. (3.84) through (3.86), we get

For the forward whirl real component:

$$-m_1 i^2 \omega_e^2 P_{f_{e1r}} - i\omega_e \left(c_{s1} + c_m\right) P_{f_{e1j}} + i\omega_e c_m P_{f_{e2j}} + \left(k_{s1} + k_m\right) P_{f_{e1r}} - k_m P_{f_{e2r}} = S_{f_{e1r}} \quad (3.87)$$

$$-m_1 i^2 \omega_p^2 P_{f_{p1r}} - \omega_p \left(c_{s1} + c_m\right) P_{f_{p1j}} + \omega_p c_m P_{f_{p2j}} + \left(k_{s1} + k_m\right) P_{f_{p1r}} - k_m P_{f_{p2r}} = R_{f_{p1r}} \quad (3.88)$$

$$-m_1 i^2 \omega_g^2 P_{f_{g1r}} - \omega_g \left(c_{s1} + c_m\right) P_{f_{g1j}} + \omega_g c_m P_{f_{g2j}} + \left(k_{s1} + k_m\right) P_{f_{g1r}} - k_m P_{f_{g2r}} = R_{f_{g1r}} \quad (3.89)$$

$$-m_2 i^2 \omega_e^2 P_{f_{e2r}} - i\omega_e \left(c_{s2} + c_m\right) P_{f_{e2j}} + i\omega_e c_m P_{f_{e1j}} + \left(k_{s2} + k_m\right) P_{f_{e2r}} - k_m P_{f_{e1r}} = S_{f_{e2r}} \quad (3.90)$$

$$-m_2 i^2 \omega_p^2 P_{f_{p2r}} - \omega_p \left(c_{s2} + c_m\right) P_{f_{p2j}} + \omega_p c_m P_{f_{p1j}} + \left(k_{s2} + k_m\right) P_{f_{p2r}} - k_m P_{f_{p1r}} = R_{f_{p2r}} \quad (3.91)$$

$$-m_2 i^2 \omega_g^2 P_{f_{g2r}} - \omega_g \left(c_{s2} + c_m\right) P_{f_{g3j}} + \omega_g c_m P_{f_{g1j}} + \left(k_{s2} + k_m\right) P_{f_{g2r}} - k_m P_{f_{g1r}} = R_{f_{g2r}} \quad (3.92)$$

For the forward whirl imaginary component:

$$-m_1 i^2 \omega_e^2 P_{f_{e1j}} + i\omega_e \left(c_{s1} + c_m\right) P_{f_{e1r}} - i\omega_e c_m P_{f_{e2r}} + \left(k_{s1} + k_m\right) P_{f_{e1j}} - k_m P_{f_{e2j}} = S_{f_{e1j}} \tag{3.93}$$

$$-m_1 i^2 \omega_p^2 P_{f_{p1j}} + \omega_p \left(c_{s1} + c_m\right) P_{f_{p1r}} - \omega_p c_m P_{f_{p2r}} + \left(k_{s1} + k_m\right) P_{f_{p1j}} - k_m P_{f_{p2j}} = R_{f_{p1j}} \tag{3.94}$$

$$-m_1 i^2 \omega_g^2 P_{f_{g1j}} + \omega_g \left(c_{s1} + c_m\right) P_{f_{g1r}} - \omega_g c_m P_{f_{g2r}} + \left(k_{s1} + k_m\right) P_{f_{g1j}} - k_m P_{f_{g2j}} = R_{f_{g1j}} \tag{3.95}$$

$$-m_2 i^2 \omega_e^2 P_{f_{e2j}} + i\omega_e \left(c_{s2} + c_m\right) P_{f_{e2r}} - i\omega_e c_m P_{f_{e1r}} + \left(k_{s2} + k_m\right) P_{f_{e2j}} - k_m P_{f_{e1j}} = S_{f_{e2j}} \tag{3.96}$$

$$-m_2 i^2 \omega_p^2 P_{f_{p2j}} + \omega_p \left(c_{s2} + c_m\right) P_{f_{p2r}} - \omega_p c_m P_{f_{p1r}} + \left(k_{s2} + k_m\right) P_{f_{p2j}} - k_m P_{f_{p1j}} = R_{f_{p2j}} \tag{3.97}$$

$$-m_2 i^2 \omega_g^2 P_{f_{g2j}} + \omega_g \left(c_{s2} + c_m\right) P_{f_{g2r}} - \omega_g c_m P_{f_{g1r}} + \left(k_{s2} + k_m\right) P_{f_{g2j}} - k_m P_{f_{g1j}} = R_{f_{g2j}} \tag{3.98}$$

On combining Eqns. (3.87) through (3.98), we get

$$\mathbf{A}_{fi}\mathbf{p}_{fi} = \mathbf{s}_{fi} \tag{3.99}$$

with

$$\mathbf{A}_{fi} = \begin{bmatrix} \mathbf{A}_{f_e i} & 0 & 0 \\ 0 & \mathbf{A}_{f_p i} & 0 \\ 0 & 0 & \mathbf{A}_{f_g i} \end{bmatrix} \tag{3.100}$$

$$\mathbf{A}_{f_e i} = \begin{bmatrix} -m_1 i^2 \omega_e^2 + \left(k_{s1} + k_m\right) & -i\omega_e \left(c_{s1} + c_m\right) & -k_m & i\omega_e c_m \\ i\omega_e \left(c_{s1} + c_m\right) & -m_1 i^2 \omega_e^2 + \left(k_{s1} + k_m\right) & -i\omega_e c_m & -k_m \\ -k_m & i\omega_e c_m & -m_2 i^2 \omega_e^2 + \left(k_{s2} + k_m\right) & -i\omega_e \left(c_{s2} + c_m\right) \\ -i\omega_e c_m & -k_m & i\omega_e \left(c_{s2} + c_m\right) & -m_2 i^2 \omega_e^2 + \left(k_{s2} + k_m\right) \end{bmatrix} \tag{3.101}$$

$$\mathbf{A}_{f_p i}=\begin{bmatrix} -m_1 i^2\omega_p^2+\left(k_{s1}+k_m\right) & -i\omega_p\left(c_{s1}+c_m\right) & -k_m & i\omega_p c_m \\ i\omega_p\left(c_{s1}+c_m\right) & -m_1 i^2\omega_p^2+\left(k_{s1}+k_m\right) & -i\omega_p c_m & -k_m \\ -k_m & i\omega_p c_m & -m_2 i^2\omega_p^2+\left(k_{s2}+k_m\right) & -i\omega_p\left(c_{s2}+c_m\right) \\ -i\omega_p c_m & -k_m & i\omega_p\left(c_{s2}+c_m\right) & -m_2 i^2\omega_p^2+\left(k_{s2}+k_m\right) \end{bmatrix} \tag{3.102}$$

$$\mathbf{A}_{f_g i}=\begin{bmatrix} -m_1 i^2\omega_g^2+\left(k_{s1}+k_m\right) & -i\omega_g\left(c_{s1}+c_m\right) & -k_m & i\omega_g c_m \\ i\omega_g\left(c_{s1}+c_m\right) & -m_1 i^2\omega_g^2+\left(k_{s1}+k_m\right) & -i\omega_g c_m & -k_m \\ -k_m & i\omega_g c_m & -m_2 i^2\omega_g^2+\left(k_{s2}+k_m\right) & -i\omega_g\left(c_{s2}+c_m\right) \\ -i\omega_p c_m & -k_m & i\omega_g\left(c_{s2}+c_m\right) & -m_2 i^2\omega_g^2+\left(k_{s2}+k_m\right) \end{bmatrix} \tag{3.103}$$

$$\mathbf{p}_{fi}=\begin{Bmatrix} P_{f_e 1ri} \\ P_{f_e 1ji} \\ P_{f_e 2ri} \\ P_{f_e 2ji} \\ P_{f_p 1ri} \\ P_{f_p 1ji} \\ P_{f_p 2ri} \\ P_{f_p 2ji} \\ P_{f_g 1ri} \\ P_{f_g 1ji} \\ P_{f_g 2ri} \\ P_{f_g 2ji} \end{Bmatrix}; \qquad S_{fi}=\begin{Bmatrix} S_{f_e 1ri} \\ S_{f_e 1ji} \\ S_{f_e 2ri} \\ S_{f_e 2ji} \\ R_{f_p 1ri} \\ R_{f_p 1ji} \\ R_{f_p 2ri} \\ R_{f_p 2ji} \\ R_{f_g 1ri} \\ R_{f_g 1ji} \\ R_{f_g 2ri} \\ R_{f_g 2ji} \end{Bmatrix} \tag{3.104}$$

3.2.3 Grouping of backward whirl components

On substituting back equation (3.67) into eqns. (3.63) and (3.64), for the backward whirl force, we get

$$-m_1 i^2\omega_e^2 P_{b_{e1}}-\mathrm{j}i\omega_e\left(c_{s1}+c_m\right)P_{b_{e1}}+\mathrm{j}i\omega_e c_m P_{b_{e2}}+\left(k_{s1}+k_m\right)P_{b_{e1}}-k_m P_{b_{e2}}=S_{b_{e1}} \tag{3.105}$$

$$-m_1 i^2 \omega_p^2 P_{b_{p1}} - \mathrm{j}\omega_p \left(c_{s1} + c_m\right) P_{b_{p1}} + \mathrm{j}\omega_p c_m P_{b_{p2}} + \left(k_{s1} + k_m\right) P_{b_{p1}} - k_m P_{b_{p2}} = R_{b_{p1}} \tag{3.106}$$

$$-m_1 i^2 \omega_g^2 P_{b_{g1}} - \mathrm{j}\omega_g \left(c_{s1} + c_m\right) P_{b_{g1}} + \mathrm{j}\omega_g c_m P_{b_{g2}} + \left(k_{s1} + k_m\right) P_{b_{g1}} - k_m P_{b_{g2}} = R_{b_{g1}} \tag{3.107}$$

and

$$-m_2 i^2 \omega_e^2 P_{b_{e2}} - \mathrm{j}i\omega_e \left(c_{s2} + c_m\right) P_{b_{e2}} + \mathrm{j}i\omega_e c_m P_{b_{e1}} + \left(k_{s2} + k_m\right) P_{b_{e2}} - k_m P_{b_{e1}} = S_{b_{e2}} \tag{3.108}$$

$$-m_2 i^2 \omega_p^2 P_{b_{p2}} - \mathrm{j}\omega_p \left(c_{s2} + c_m\right) P_{b_{p2}} + \mathrm{j}\omega_p c_m P_{b_{p1}} + \left(k_{s2} + k_m\right) P_{b_{p2}} - k_m P_{b_{p1}} = R_{b_{p2}} \tag{3.109}$$

$$-m_2 i^2 \omega_g^2 P_{b_{g2}} - \mathrm{j}\omega_g \left(c_{s2} + c_m\right) P_{b_{g2}} + \mathrm{j}\omega_g c_m P_{b_{g1}} + \left(k_{s2} + k_m\right) P_{b_{g2}} - k_m P_{b_{g1}} = R_{b_{g2}} \tag{3.110}$$

with $i = 1, 2, \cdots, n$

These are organized into the real and imaginary components, as

$$\begin{aligned} &-m_1 i^2 \omega_e^2 \left(P_{b_{e1r}} + \mathrm{j}P_{b_{e1j}}\right) - \mathrm{j}i\omega_e \left(c_{s1} + c_m\right)\left(P_{b_{e1r}} + \mathrm{j}P_{b_{e1j}}\right) + \mathrm{j}i\omega_e c_m \left(P_{b_{e2r}} + \mathrm{j}P_{b_{e2j}}\right) \\ &+\left(k_{s1} + k_m\right)\left(P_{b_{e1r}} + \mathrm{j}P_{b_{e1j}}\right) - k_m \left(P_{b_{e2r}} + \mathrm{j}P_{b_{e2j}}\right) = \left(S_{b_{e1r}} + \mathrm{j}S_{b_{e1j}}\right) \end{aligned} \tag{3.111}$$

$$\begin{aligned} &-m_1 i^2 \omega_p^2 \left(P_{b_{p1r}} + \mathrm{j}P_{b_{p1j}}\right) - \mathrm{j}\omega_p \left(c_{s1} + c_m\right)\left(P_{b_{p1r}} + \mathrm{j}P_{b_{p1j}}\right) + \mathrm{j}\omega_p c_m \left(P_{b_{p2r}} + \mathrm{j}P_{b_{p2j}}\right) \\ &+\left(k_{s1} + k_m\right)\left(P_{b_{p1r}} + \mathrm{j}P_{b_{p1j}}\right) - k_m \left(P_{b_{p2r}} + \mathrm{j}P_{b_{p2j}}\right) = \left(R_{b_p 1r} + \mathrm{j}R_{b_{p1j}}\right) \end{aligned} \tag{3.112}$$

$$-m_1 i^2 \omega_g^2 \left(P_{b_{g1r}} + \mathrm{j}P_{b_{p1j}}\right) - \mathrm{j}\omega_p \left(c_{s1} + c_m\right)\left(P_{b_{p1r}} + \mathrm{j}P_{b_{g1j}}\right) + \mathrm{j}\omega_g c_m \left(P_{b_{g2r}} + \mathrm{j}P_{b_{g2j}}\right)$$
$$+\left(k_{s1} + k_m\right)\left(P_{b_{g1r}} + \mathrm{j}P_{b_{g1j}}\right) - k_m \left(P_{b_{g2r}} + \mathrm{j}P_{b_{g2j}}\right) = \left(R_{b_{g1r}} + \mathrm{j}R_{b_{g1j}}\right) \tag{3.113}$$

$$-m_2 i^2 \omega_e^2 \left(P_{b_{e2r}} + \mathrm{j}P_{b_{e2j}}\right) - \mathrm{j}i\omega_e \left(c_{s2} + c_m\right)\left(P_{b_{e2r}} + \mathrm{j}P_{b_{e2j}}\right) + \mathrm{j}i\omega_e c_m \left(P_{b_{e1r}} + \mathrm{j}P_{b_{e1j}}\right)$$
$$+\left(k_{s2} + k_m\right)\left(P_{b_{e2r}} + \mathrm{j}P_{b_{e2j}}\right) - k_m \left(P_{b_{e1r}} + \mathrm{j}P_{b_{e1j}}\right) = \left(S_{b_{e2r}} + \mathrm{j}S_{b_{e2j}}\right) \tag{3.114}$$

$$-m_2 i^2 \omega_p^2 \left(P_{b_{p2r}} + \mathrm{j}P_{b_{p2j}}\right) - \mathrm{j}\omega_p \left(c_{s2} + c_m\right)\left(P_{b_{p2r}} + \mathrm{j}P_{b_{p2j}}\right) + \mathrm{j}\omega_p c_m \left(P_{b_{p1r}} + \mathrm{j}P_{b_{p1j}}\right)$$
$$+\left(k_{s2} + k_m\right)\left(P_{b_{p2r}} + \mathrm{j}P_{b_{p2j}}\right) - k_m \left(P_{b_{p1r}} + \mathrm{j}P_{b_{p1j}}\right) = \left(R_{b_{p2r}} + \mathrm{j}R_{b_{p2j}}\right) \tag{3.115}$$

$$-m_2 i^2 \omega_g^2 \left(P_{b_{g2r}} + \mathrm{j}P_{b_{g2j}}\right) - \mathrm{j}\omega_g \left(c_{s2} + c_m\right)\left(P_{b_{g2r}} + \mathrm{j}P_{b_{g2j}}\right) + \mathrm{j}\omega_g c_m \left(P_{b_{g1r}} + \mathrm{j}P_{b_{g1j}}\right)$$
$$+\left(k_{s2} + k_m\right)\left(P_{b_{g2r}} + \mathrm{j}P_{b_{g2j}}\right) - k_m \left(P_{b_{g1r}} + \mathrm{j}P_{b_{g1j}}\right) = \left(R_{b_{g2r}} + \mathrm{j}R_{b_{g2j}}\right) \tag{3.116}$$

with $i = 1, 2, \cdots, n$

On separating the real and imaginary components on both sides of equations (3.111) to (3.116), we get

The real component of the backward whirl are

$$-m_1 i^2 \omega_e^2 P_{b_{e1r}} + i\omega_e \left(c_{s1} + c_m\right) P_{b_{e1j}} - i\omega_e c_m P_{b_{e2j}} + \left(k_{s1} + k_m\right) P_{b_{e1r}} - k_m P_{b_{e2r}} = S_{b_{e1r}} \tag{3.117}$$

$$-m_1 i^2 \omega_p^2 P_{b_{p1r}} + \omega_p \left(c_{s1} + c_m\right) P_{b_{p1j}} - \omega_p c_m P_{b_{p2j}} + \left(k_{s1} + k_m\right) P_{b_{p1r}} - k_m P_{b_{p2r}} = R_{b_{p1r}} \tag{3.118}$$

$$-m_1 i^2 \omega_g^2 P_{b_{g1r}} + \omega_g \left(c_{s1} + c_m\right) P_{b_{g1j}} - \omega_g c_m P_{b_{g2j}} + \left(k_{s1} + k_m\right) P_{b_{g1r}} - k_m P_{b_{g2r}} = R_{b_{g1r}} \tag{3.119}$$

and

$$-m_2 i^2 \omega_e^2 P_{b_e 2r} + i\omega_e \left(c_{s2} + c_m\right) P_{b_e 2j} - i\omega_e c_m P_{b_e 1j} + \left(k_{s2} + k_m\right) P_{b_e 2r} - k_m P_{b_e 1r} = S_{b_e 2r} \quad (3.120)$$

$$-m_2 i^2 \omega_p^2 P_{b_{p2r}} + \omega_p \left(c_{s2} + c_m\right) P_{b_{p2j}} - \omega_p c_m P_{b_{p1j}} + \left(k_{s2} + k_m\right) P_{b_{p2r}} - k_m P_{b_{p1r}} = R_{b_{p2r}} \quad (3.121)$$

$$-m_2 i^2 \omega_g^2 P_{b_{g2r}} + \omega_g \left(c_{s2} + c_m\right) P_{b_{g2j}} - \omega_g c_m P_{b_{g1j}} + \left(k_{s2} + k_m\right) P_{b_{g2r}} - k_m P_{b_{g1r}} = R_{b_{g2r}} \quad (3.122)$$

For the backward whirl, imaginary components are

$$-m_1 i^2 \omega_e^2 P_{b_{e1j}} - i\omega_e \left(c_{s1} + c_m\right) P_{b_{e1r}} + i\omega_e c_m P_{b_{e2r}} + \left(k_{s1} + k_m\right) P_{b_{e1j}} - k_m P_{b_{e2j}} = S_{b_{e1j}} \quad (3.123)$$

$$-m_1 i^2 \omega_p^2 P_{b_{p1j}} - \omega_p \left(c_{s1} + c_m\right) P_{b_{p1r}} + \omega_p c_m P_{b_{p2r}} + \left(k_{s1} + k_m\right) P_{b_{p1j}} - k_m P_{b_{p2j}} = R_{b_{p1j}} \quad (3.124)$$

$$-m_1 i^2 \omega_g^2 P_{b_{g1j}} - \omega_g \left(c_{s1} + c_m\right) P_{b_{g1r}} + \omega_g c_m P_{b_{g2r}} + \left(k_{s1} + k_m\right) P_{b_{g1j}} - k_m P_{b_{g2j}} = R_{b_{g1j}} \quad (3.125)$$

and

$$-m_2 i^2 \omega_e^2 P_{b_{e2j}} - i\omega_e \left(c_{s2} + c_m\right) P_{b_{e2r}} + i\omega_e c_m P_{b_{e1r}} + \left(k_{s2} + k_m\right) P_{b_{e2j}} - k_m P_{b_{e1j}} = S_{b_{e2j}} \quad (3.126)$$

$$-m_2 i^2 \omega_p^2 P_{b_{p2j}} - \omega_p \left(c_{s2} + c_m\right) P_{b_{p2r}} + \omega_p c_m P_{b_{p1r}} + \left(k_{s2} + k_m\right) P_{b_{p2j}} - k_m P_{b_{p1j}} = R_{b_{p2j}} \quad (3.127)$$

$$-m_2 i^2 \omega_g^2 P_{b_{g2j}} - \omega_g \left(c_{s2} + c_m\right) P_{b_{g2r}} + \omega_g c_m P_{b_{g1r}} + \left(k_{s2} + k_m\right) P_{b_{g2j}} - k_m P_{b_{g1j}} = R_{b_{g2j}} \quad (3.128)$$

On combining Eqns. (3.117) through Eqn. (3.128), we get

$$\mathbf{A}_{bi}\mathbf{p}_{bi} = \mathbf{s}_{bi} \tag{3.129}$$

$$\mathbf{A}_{bi} = \begin{bmatrix} \mathbf{A}_{b_e i} & 0 & 0 \\ 0 & \mathbf{A}_{b_p i} & 0 \\ 0 & 0 & \mathbf{A}_{b_g i} \end{bmatrix} \tag{3.130}$$

with

$$\mathbf{A}_{b_e i} = \begin{bmatrix} -m_1 i^2 \omega_e^2 + (k_{s1} + k_m) & i\omega_e (c_{s1} + c_m) & -k_m & -i\omega_e c_m \\ -i\omega_e (c_{s1} + c_m) & -m_1 i^2 \omega_e^2 + (k_{s1} + k_m) & i\omega_e c_m & -k_m \\ -k_m & -i\omega_e c_m & -m_2 i^2 \omega_e^2 + (k_{s2} + k_m) & i\omega_e (c_{s2} + c_m) \\ i\omega_e c_m & -k_m & -i\omega_e (c_{s2} + c_m) & -m_2 i^2 \omega_e^2 + (k_{s2} + k_m) \end{bmatrix} \tag{3.131}$$

$$\mathbf{A}_{b_p i} = \begin{bmatrix} -m_1 i^2 \omega_p^2 + (k_{s1} + k_m) & i\omega_p (c_{s1} + c_m) & -k_m & -i\omega_p c_m \\ -i\omega_p (c_{s1} + c_m) & -m_1 i^2 \omega_p^2 + (k_{s1} + k_m) & i\omega_p c_m & -k_m \\ -k_m & -i\omega_p c_m & -m_2 i^2 \omega_p^2 + (k_{s2} + k_m) & i\omega_p (c_{s2} + c_m) \\ i\omega_p c_m & -k_m & -i\omega_p (c_{s2} + c_m) & -m_2 i^2 \omega_p^2 + (k_{s2} + k_m) \end{bmatrix} \tag{3.132}$$

$$\mathbf{A}_{b_g i} = \begin{bmatrix} -m_1 i^2 \omega_g^2 + (k_{s1} + k_m) & i\omega_g (c_{s1} + c_m) & -k_m & -i\omega_g c_m \\ -i\omega_g (c_{s1} + c_m) & -m_1 i^2 \omega_g^2 + (k_{s1} + k_m) & i\omega_g c_m & -k_m \\ -k_m & -i\omega_g c_m & -m_2 i^2 \omega_g^2 + (k_{s2} + k_m) & i\omega_g (c_{s2} + c_m) \\ i\omega_g c_m & -k_m & -i\omega_g (c_{s2} + c_m) & -m_2 i^2 \omega_g^2 + (k_{s2} + k_m) \end{bmatrix} \tag{3.133}$$

The displacement and force vectors are given in the matrix form as,

$$\mathbf{p}_{bi}=\begin{Bmatrix} P_{b_{e1ri}} \\ P_{b_{e1ji}} \\ P_{b_{e2ri}} \\ P_{b_{e2ji}} \\ P_{b_{p1ri}} \\ P_{b_{p1ji}} \\ P_{b_{p2ri}} \\ P_{b_{p2ji}} \\ P_{b_{g1ri}} \\ P_{b_{g1ji}} \\ P_{b_{g2ri}} \\ P_{b_{g2ji}} \end{Bmatrix}; \quad \mathbf{s}_{bi}=\begin{Bmatrix} S_{b_{e1ri}} \\ S_{b_{e1ji}} \\ S_{b_{e2ri}} \\ S_{b_{e2ji}} \\ R_{b_{p1ri}} \\ R_{b_{p1ji}} \\ R_{b_{p2ri}} \\ R_{b_{p2ji}} \\ R_{b_{g1ri}} \\ R_{b_{g1ji}} \\ R_{b_{g2ri}} \\ R_{b_{g2ji}} \end{Bmatrix} \tag{3.134}$$

3.3 Direct Problem in the Matrix Form

For the static component, gear meshing frequency, and pinion and gear runout frequencies with centrifugal forces due to runouts, the equations of motion in frequency domain can be written in matrix form by combining Eqns. (3.73) (3.99) and (3.129), as

$$\begin{bmatrix} \mathbf{A}_s & \mathbf{0} & \mathbf{0} \\ \mathbf{0} & \mathbf{A}_{fi} & \mathbf{0} \\ \mathbf{0} & \mathbf{0} & A_{bi} \end{bmatrix} \begin{Bmatrix} \mathbf{p}_s \\ \mathbf{p}_{fi} \\ \mathbf{p}_{bi} \end{Bmatrix} = \begin{Bmatrix} \mathbf{s}_s \\ \mathbf{s}_{fi} \\ \mathbf{s}_{bi} \end{Bmatrix} \tag{3.135}$$

with i=1, 2 ,3, …, n

Herein, i depicts the index of harmonic gear order; n depicts number of harmonics, which are assumed in TE. With presumed value of TE parameters, Eqn. (3.135) can be used to numerically simulate transverse vibration response of a geared-rotor system. Here, we can observe that the equations of motion are linear

due to neglect of the torsional vibration coupling. The holistic solutions with assumed parameters of each harmonic should be summed up for i=1, 2, 3, …, n. The full solution can be written in a matrix form by combining all solutions for all value of i is written as,

$$\begin{bmatrix} \mathbf{A}_s & \mathbf{0} & \mathbf{0} & \mathbf{0} & \mathbf{0} & \mathbf{0} & \mathbf{0} \\ & \mathbf{A}_{f1} & \mathbf{0} & \mathbf{0} & \mathbf{0} & \mathbf{0} & \mathbf{0} \\ & & \ddots & \mathbf{0} & \mathbf{0} & \mathbf{0} & \mathbf{0} \\ & & & \mathbf{A}_{fn} & \mathbf{0} & \mathbf{0} & \mathbf{0} \\ & & & & \mathbf{A}_{b1} & \mathbf{0} & \mathbf{0} \\ & & & & & \ddots & \mathbf{0} \\ \text{sym} & & & & & & \mathbf{A}_{bn} \end{bmatrix} \begin{Bmatrix} \mathbf{p}_s \\ \mathbf{p}_{f1} \\ \vdots \\ \mathbf{p}_{fn} \\ \mathbf{p}_{b1} \\ \vdots \\ \mathbf{p}_{bn} \end{Bmatrix} = \begin{Bmatrix} \mathbf{s}_s \\ \mathbf{s}_{f1} \\ \vdots \\ \mathbf{s}_{fn} \\ \mathbf{s}_{b1} \\ \vdots \\ \mathbf{s}_{bn} \end{Bmatrix} \tag{3.136}$$

This can be put in a simple form as

$$\mathbf{Ap} = \mathbf{s} \tag{3.137}$$

With this we can obtain solution for geared rotor response vector from given forcing function using geared rotor physical parameters and assumed geared rotor parameters.

With chosen input gear parameters for n number of harmonics, the geared rotor response can be calculated by inverting the dynamic stiffness matrix **A.** From Eqn. (3.137), we get

$$\mathbf{p} = \mathbf{A}^{-1}\mathbf{s} \tag{3.138}$$

Eqn. (3.138) calculates the response of the forward and backward whirl gear meshing frequencies with obligatory number of harmonics based on the nature of excitation for known values of all dynamic

parameters of system model. These responses will be used to test the identification algorithm described in the next section and also for validation of experimentally identified gear mesh parameters.

Various harmonics of *p*'s (full spectrum complex amplitude) can be obtained from above for known values of the mass of gear, m_1 , and pinion, m_2 ; the mesh stiffness, k_m ; the gear mesh damping, c_m, and the shaft stiffness's, k_{s1} and k_{s2} ; and the shaft damping's, c_{s1} and c_{s2} ; transmission error and their phase; gear runouts and their phases. This inverse problem transformations are used in subsequent chapters using developed formulation of the present chapter for the identification of critical gear mesh parameters both using the simulated response and the test measured response.

3.5 Summary

Using Euler's formulae, the forcing function and equations of motion are converted into frequency domain. Presuming the solution in frequency domain from three different frequency components, namely, the gear meshing frequency, pinion rotation frequency and gear rotation frequencies, by taking advantage principle of superposition for linearised equations. The time domain equations of motions are transformed into frequency domain. The frequency domain reformations make it covenant to identify DTE parameters associated with dominant response frequencies. These frequency domain transformations will be used for development of the identification method for estimation of gear mesh dynamic parameters in the next chapter.

CHAPTER 4

DETECTION AND IDENTIFICATION OF GEAR MESH DYNAMIC TRANSMISSION ERROR PARAMETERS USING FULL SPECTRUM ANALYSIS

4.1 Introduction

The derived equations of motion using extended Lagrangian dynamics are solved numerically using assumed geared rotor physical parameters, like the geometry and mass of subassemblies of a geared rotor. The gear mesh dynamic parameters are chosen based on the physical consideration used for manufacturing existing gears in automotive transmissions. The degree of asymmetry in static TE between two orthogonal directions is chosen realistic but arbitrary as this is the new concept being studied in this research. The linear differential equations of motion obtained in Chapter 2 are numerically integrated using Runge-Kutta technique for calculating time domain responses. These time domain responses in two orthogonal directions are converted in the complex form into frequency domain using special FFT technique by shifting the zero frequency components to center to generate full spectrum responses. This facilitates the analysis of the forward and backward whirls up to desired harmonics of the gear meshing frequency. Later, the parametric analyses are done for analyzing the responses by varying the gear mesh DTE parameters to detect qualitatively the dominant source of vibration in the geared rotor. An identification algorithm is developed to estimate gear-mesh parameters based on frequency domain governing equations derived in Chapter 3. Using full spectrum responses at the gear meshing frequencies, and the pinion and gear rotational frequencies these estimates are obtained. The identification algorithm is tested against the measurement noise by introducing different levels of the white Gaussian noise into time domain signals.

4.2 Numerical Simulation of Geared Rotor Response

The time domain solution to the system of linear second order differential equations of motion (i.e. Eqns. (2.31) to (2.34)) of geared rotor are obtained using direct numerical integration Runge-Kutta technique (i.e., ode45 of MATLAB). This solver integrates the series of differential equations and is based on an explicit version of the Runge-Kutta formula, i.e. the Dormand-Prince pair. It is a one-step method that uses initial conditions and solves for conditions at the next time step. The input parameters used for solving the equations of motion are given in Table 4.1. These are physical parameters of system model, like the size of shafts, damping ratios, mass of gears and chosen gear mesh dynamic transmission error parameters. These are based on past best practices used in automotive transmission gears (Zhou et al., 2015 and Rao, 2018), like the mean TE, variable TE and their phases, gear mesh stiffness, gear mesh damping and gear runouts and their phases. The initial conditions for all variables are chosen as null and *linspace* command of MATLAB is used to set solution span and time step by selecting 15^{th} power of 2 as over sampling ratio. For solving the equations of motion, Eqns. (2.31) through (2.34) are converted into a state space form by defining displacement and velocity variables, as

$$u_1 = x_1;\ u_2 = \dot{x}_1;\ u_3 = y_1;\ u_4 = \dot{y}_1;\ u_5 = x_2;\ u_6 = \dot{x}_2;\ u_7 = y_2;\ u_8 = \dot{y}_2 \tag{4.1}$$

Table 4.1: Geared rotor data used for numerical simulation

Parameter	**Units**	**Value**
Radius of shafts	meter	0.0055
Shafts damping ratio	No units	0.01
Length of shafts	meter	0.190
Drive gear mass	Kg	0.310
Output shaft gear mass	Kg	1.270
Count of driven gear tooth	no units	35
Count of drive gear tooth	No units	16
Driving gear rpm	rpm	660.0

Modulus of elasticity of shafts	M Pa	2×10^5	
Stiffness of shafts	N/m	1×10^6	
Frequency of gear mesh	Hertz	176.0	
Stiffness of gear meshing	N/m	6×10^8	
Gear meshing damping ratio	No units	0.01	
Number of Harmonics	No units	5	
Mean TE	μm	50	
Gravitational acceleration	m/s^2	9.81	
Fluctuating TE in x (Harmonics of peak-to-peak TE)	μm	e_{rx1}	40
		e_{rx2}	25
		e_{rx3}	35
		e_{rx4}	20
		e_{rx5}	10
Phase of TE in x	radian	0.785	
Fluctuating TE in y (Harmonics of peak-to-peak TE)	μm	e_{ry1}	30
		e_{ry2}	15
		e_{ry3}	25
		e_{ry4}	10
		e_{ry5}	5
Phase of TE in y	radian	1.570	
Pinion runout	μm	200	
Gear runout	μm	300	
Phase of pinion runout	radian	1.047	
Phase of gear runout	radian	2.094	

Using coupled linear differential equations, time domain responses are calculated, and orbit plots of the input and output shafts are plotted for the driver speed of 660 rpm as shown in Fig. 4.1 (a) and Fig. 4.1 (b), respectively, during time duration of 15 s of numerical simulation. From Fig. 4.1, it can be seen that it has multiple loops indicating multiple harmonics in it. Moreover, each loop is not circular indicating

that it has the forward and backward whirls, which will be evident in full spectrum plots. To understand more about these whirling components, frequency domain spectrum analysis is required. Moreover, the effect of the dynamic transmission error parameters is analysed by treating them as the dynamic TE fault parameters in geared rotor system model as shown in Fig. 2.1.

4.3 Full Spectrum Response and its Significance

Traditionally transformation of the calculated responses into frequency domain (FFT) gives information about various frequency components existing in the vibration spectrum. It contains both magnitude and phase information of responses to analyse the system dynamics. However, the traditional FFT response spectrum does not indicate about relative phase direction between vibration signals in two orthogonal directions. In addition, traditional FFT fails to provide the direction of precession of the pinon and gear harmonics with respect to the direction of drive shaft.

The geared rotor vibration signal in the x and y directions (two transverse directions) are plotted together to get the orbit plots. It may include multiple components of the forward and backward whirls. Both magnitude and phase of various frequency components are required to get the actual shape of the rotor orbit. Full-spectrum plot is not only a convenient tool to identify whether the orbit at a frequency is of forward or backward whirl with respect to rotor spin direction (Goldman, 1999), but also it is helpful to analyze the geared rotor responses to detect qualitatively the asymmetric transmission error using the full-spectrum response. Relative phase correlation of two vibration signals is used in full-spectrum to splits the geared rotor frequency into two: the forward (positive) whirl frequency component and the backward (negative) whirl frequency component, which constitute the orbit.

In the present research, the response of Fig. 4.1 consists of multiple harmonic components of the spin speed and the static TE excitation. Some of its harmonics excite the rotor in the same sense of rotation of spin whereas the other harmonics excite the rotor in the reverse sense of spin. The harmonics, which excite the

rotor in the same direction of spin, are denoted positive and their magnitude is given by R_{+i} (forward force coefficients). The harmonics in the reverse direction as spin are considered negative and their magnitude is given by R_{-i} (reverse force coefficients). Similarly, the response coefficient magnitudes P_{+i} and P_{-i} are forward and reverse, respectively. It is not possible to directly obtain R_i or P_i (reverse force coefficients and reverse displacement coefficients, respectively) using conventional FFT. Hence, there is a need for using full-spectrum signal processing in a geared rotor for qualitative detection and qualitative identification problem of gear mesh DTE fault parameters.

A full-spectrum requires a complex time domain response as its input. For this purpose, the time domain responses calculated for both input and output shafts in the x and y directions are combined to form a complex time domain response, as

$$r_1 = x_1 + \mathrm{j}y_1 \quad \text{and} \quad r_2 = x_2 + \mathrm{j}y_2 \tag{4.2}$$

The full-spectrum converts a time domain complex signal of sample length N into a frequency domain complex signal of same sample length N and its coefficients are complex. The frequency index d (sample length of the full spectrum signal) varies from 0 to $N-1$. The index d from 0 to $N/2$ corresponds to $R(+d)$ and $N/2$ to $N-1$ corresponds to $R(-d)$, i.e. $R(N/2+d) = R(-d)$. Let R_l (force coefficient) corresponds to $R(d)$, where $2\pi d / N = i\omega$, and i = 1, 2, 3, …, l is the number of discrete data in the time history of which Δt as the time interval (sampling time). Here, i corresponds to various positive and negative harmonic components of the force at gear mesh contact. The acquisition time (T) of the time domain signal is $N\Delta t$. Samples are acquired at a sampling rate (f_s), which is $1/\Delta t$. The sampling rate also satisfies the Nyquist–Shannon sampling theorem (i.e., $f_s \geq 2 f_{\max}$), where $f_{\max}$ is the maximum frequency of interest. In a similar manner, response coefficients R (d) will be obtained.

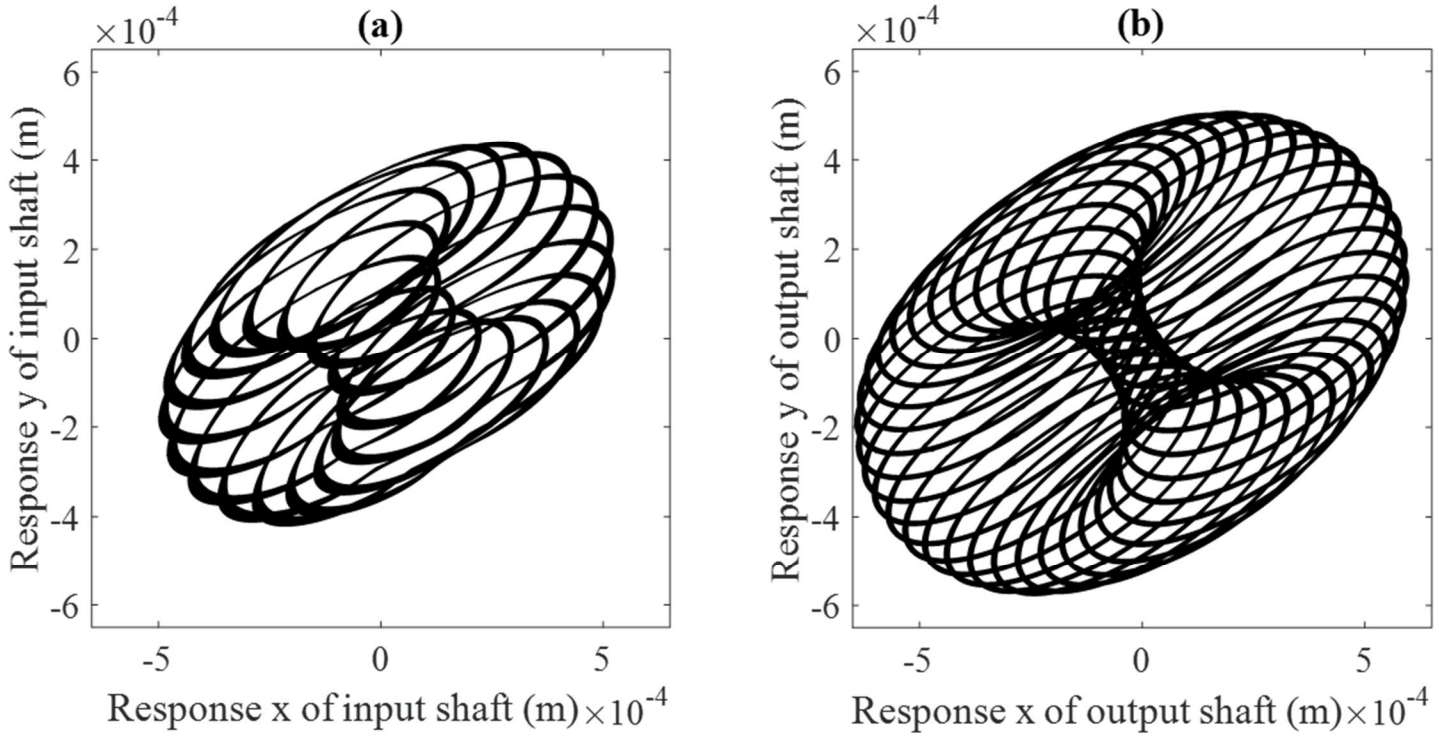

Figure 4.1: (a) Orbit plot of drive shaft; (b) Orbit plot of driven shaft

A full-spectrum can be effectively plotted by placing zero frequency component (corresponding to DC) at the centre; positive frequencies to the right and negative frequencies to the left. The frequency at $N/2$ corresponds to the Nyquist frequency. The maximum frequency or the bandwidth frequency of the full-spectrum depends on the sampling frequency or the sampling time. Based on this, the number of harmonics components in the spectrum can be chosen.

4.4 Analysis of Geared Rotor using Full Spectrum Response

Using *fftshift* of FFT function of MATLAB the full spectrum plot is generated. Figs. 4.2(a) and 4.2(b) show the full spectrum of numerically simulated responses of the input and output shafts, respectively. Here, we can observe various forward and backward whirl amplitudes of the input and output shafts due to asymmetric static TE. Five harmonic components (i.e., 176, 352, 528, 704 and 880 Hz) can be seen in the full spectrum both in the forward (positive) and backward (negative) frequencies. First three harmonics are predominant and other two are very small. The response shows the characteristics of combination of many harmonics in it. The usefulness of full spectrum to study the whirl amplitudes of various harmonics of gear drive due to the static TE is clearly demonstrated. The result of full spectrum is consistent with frequency domain formulation presented in Chapter3, where amplitudes of the pinion backward runout frequency at 11 Hz (660/60 = 11 Hz) is present in full spectrum plots whereas forward whirl amplitude is zero, and the gear forward runout frequency at (11×16/35 = 5.02 Hz) is present in these full spectrum plots, however, backward whirl amplitude is absent. This is due to the fact pinion and gear rotate in opposite directions and runout give only 1× component. However, in Fig. 4.2, the whirling has been plotted with respect to respective shaft rotation direction so both 1× components are in positive frequency. Apart from these, at zero frequency static component of deflection is evident due to the weight of gears.

To simulate the effect of measurement noise, the response is calculated by introducing 5 % white Gaussian noise to time domain signal. Using these time domain responses, the orbit plots of the input and

output shafts are plotted as shown in Fig. 4.3(a) and Fig. 4.3(b) for the input shaft speed of 660 rpm. The effect of measurement noise hardly had any effect in the full spectrum as shown in Fig. 4.4(a) and Fig. 4.4(b) in frequency range of the study, however, from orbit plots the noise effect is evident.

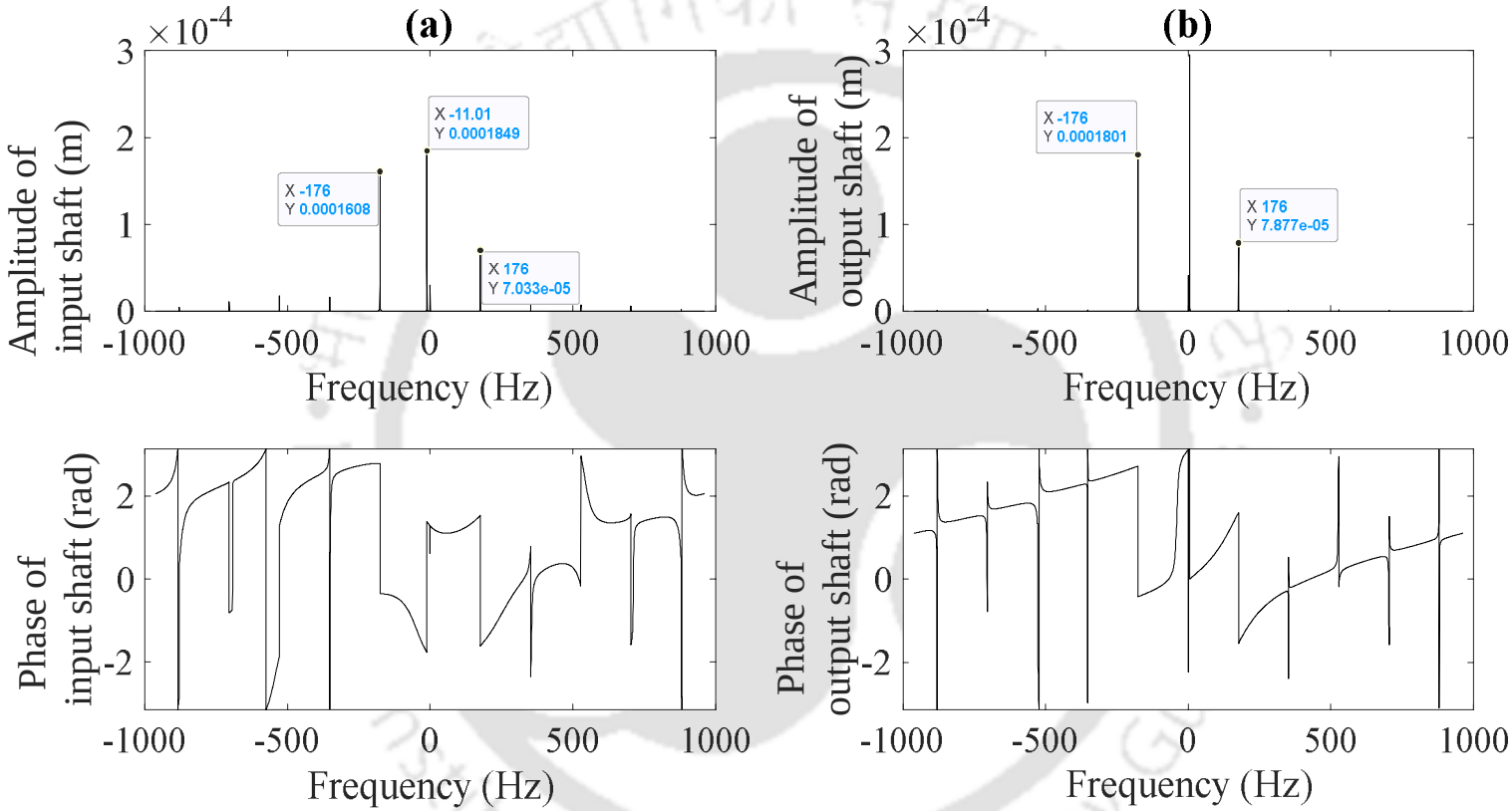

Figure 4.2: (a) Full spectrum of input shaft; (b) Full spectrum of output shaft

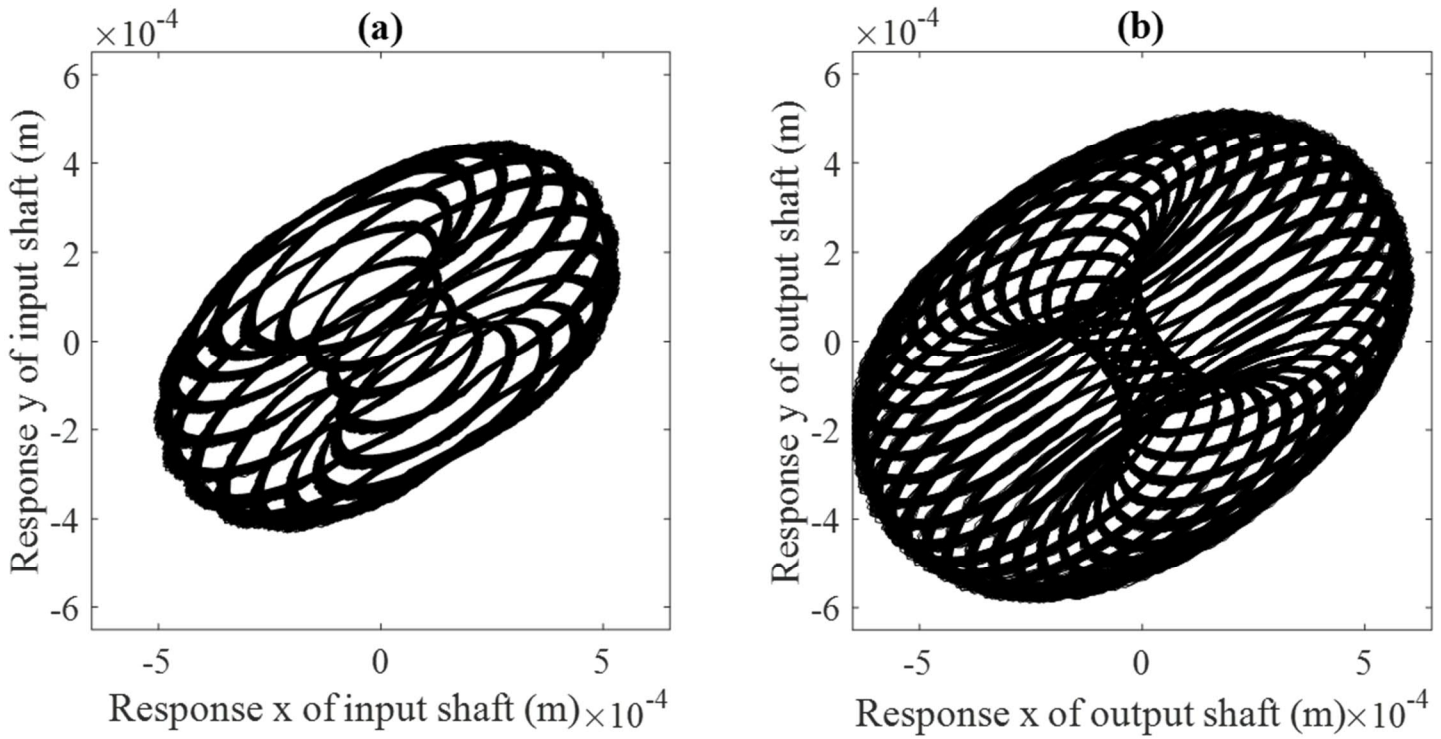

Figure 4.3:(a) Orbit response plot of input shaft with noise; (b) Orbit response plot of output shaft with noise

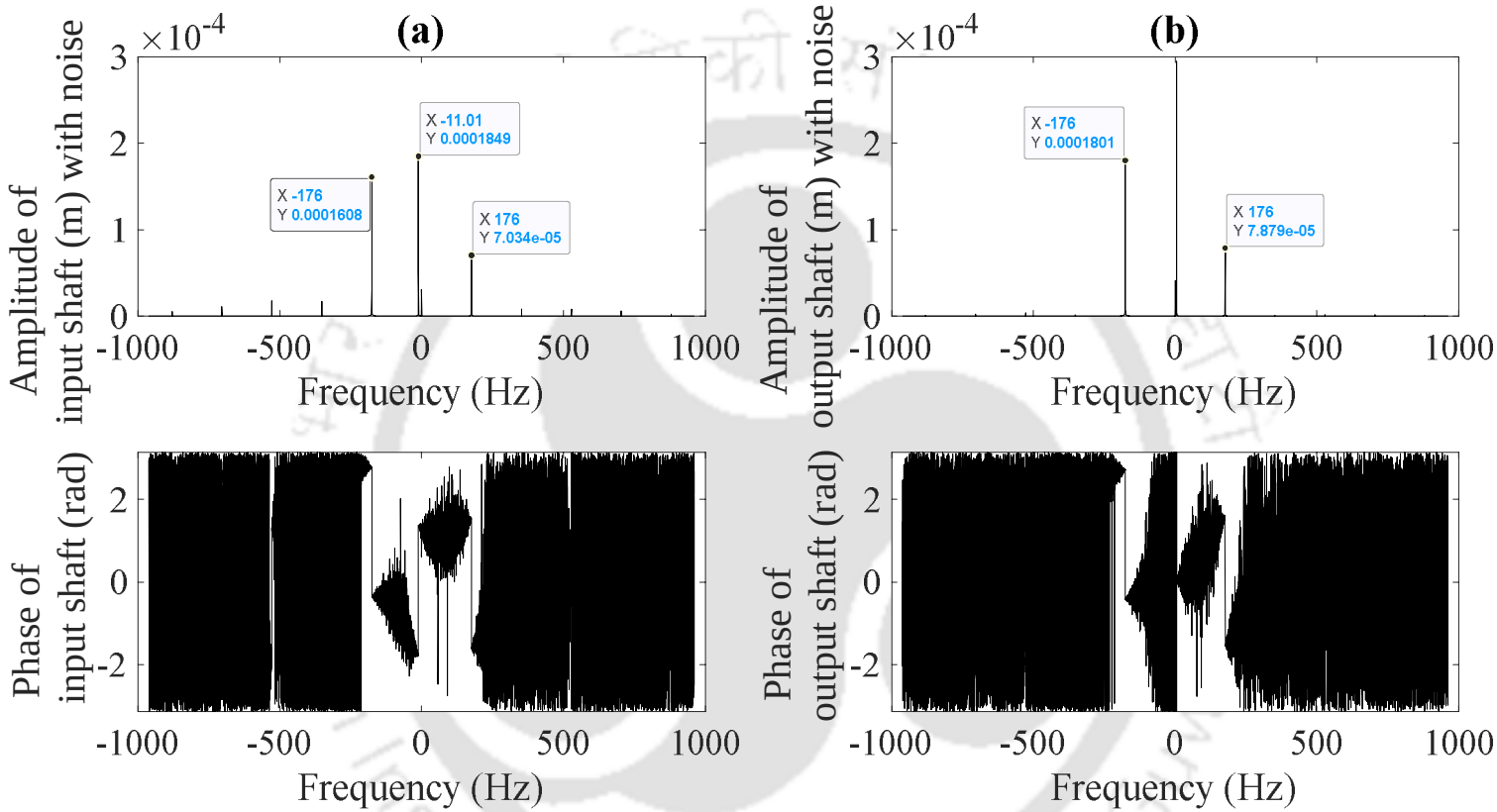

Figure 4.4:(a) Full spectrum of input shaft with noise; (b) Full spectrum of output shaft with noise

4.5 Detection of Dominant Source of Vibration in Geared Rotors using Analysis of Variation

In order to study the effect of variation in the dynamic gear mesh parameters on the orbit plots and full spectrum responses, an attempt is made to detect the dominant source of vibration in a geared rotor using parametric variation of parameters. The geared rotor physical parameters used in this section are same as the ones listed in Table 4.1, except the dynamic gear mesh parameters, which are list in Table 4.2. These dynamic gear mesh parameters along with the shaft speed are varied with randomly chosen proportions to study the dominant behaviour out of them individually and together on orbit plots and full spectrum responses.

Table 4.2: Gear mesh dynamic parameters used for detection of dominant source of vibration

Gear parameter	**Units**	**Value**
Mean transmission error	μm	60
Phase of TE in x	radian	1.047
Phase of TE in y	radian	2.094
Variable TE in x direction (Five harmonics as given in eqn. 8)	μm	e_{rx1} 50
		e_{rx2} 30
		e_{rx3} 40
		e_{rx4} 20
		e_{rx5} 10
Variable TE in y direction (Five harmonics of peak-to-peak TE)	μm	e_{ry1} 35
		e_{ry2} 25
		e_{ry3} 15
		e_{ry4} 10
		e_{ry5} 20
Pinion runout	μm	400
Gear runout	μm	500

Time domain responses calculated for three input shaft speeds (baseline speed of 11 Hz, twice and four times of the base line speed). Few orbits of those three speeds with different lines are shown in Fig. 4.5(a) and 4.5(b). Here, we can see the effect of speed on orbit response, with higher speeds the orbit is getting smoother. Fig. 4.6 (a) and 4.6(b) shows full orbits, where lines are coloured for different speeds to show them distinctly in the highly populated plots.

Frequency domain is used to get more insight understanding on the actual dynamics happening in the system due to various sources. It enables us to separate the response based on its frequency content to study the dominant source and is helpful to detect the gear vibration source using its frequency content. The time domain solution calculated in the previous section is used for the frequency domain analysis using a processing technique, called the full spectrum. Out of many available signal processing techniques the full spectrum unwraps the frequency spectrum into the forward and backward whirls. Also, it reveals more information about a frequency component orbit, like if it is a backward or forward with respect to rotor spin. As the geared rotor has two shafts, which spin in opposite directions at different speeds, analysis using full spectrum gives fair understanding of gear mesh dynamics with the forward and backward whirls to investigate the dominant sources. Figs. 4.7(a) and 4.7(b) shows the full spectrum for these three speeds. Fig. 4.8(a) and 4.8(b) shows the close view of hidden amplitudes of full spectrum for these three speeds, i.e. 660, 1320 and 2640 rpm. The first critical speed of geared rotor is 8490 rpm and is obtained by the output shaft stiffness and the mass of gear mounted on it by considering it is simply supported shaft. The full spectrum and orbits plots show reduction in the response for higher speeds. Also, it is observed that at any speed the full spectrum response amplitudes are lower for higher harmonics.

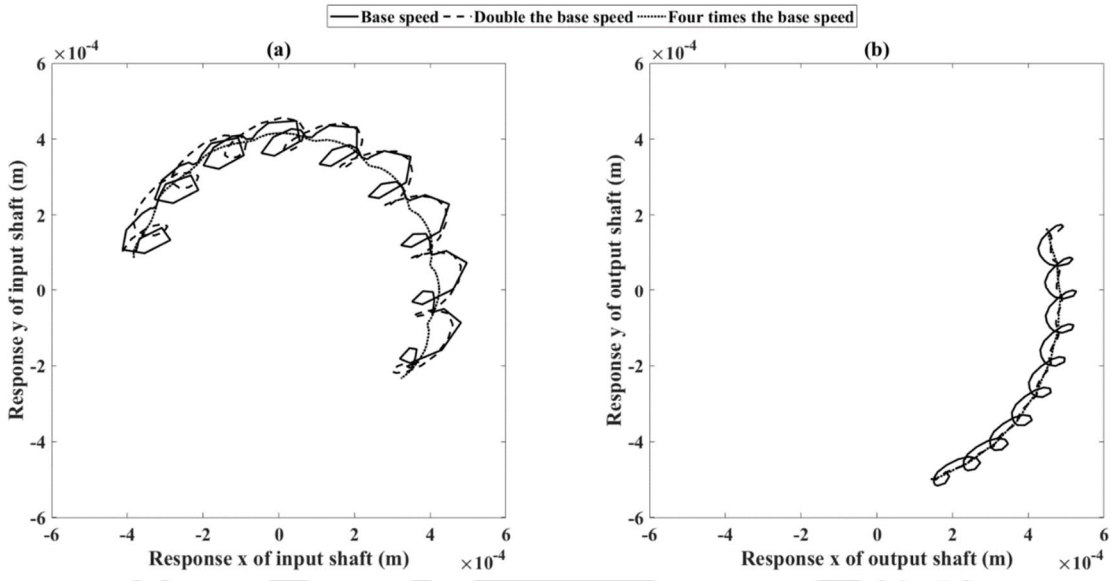

Figure 4.5: Part of orbits at three different speeds (660, 1320 and 2640 rpm) of (a) the input shaft; (b) the output shaft

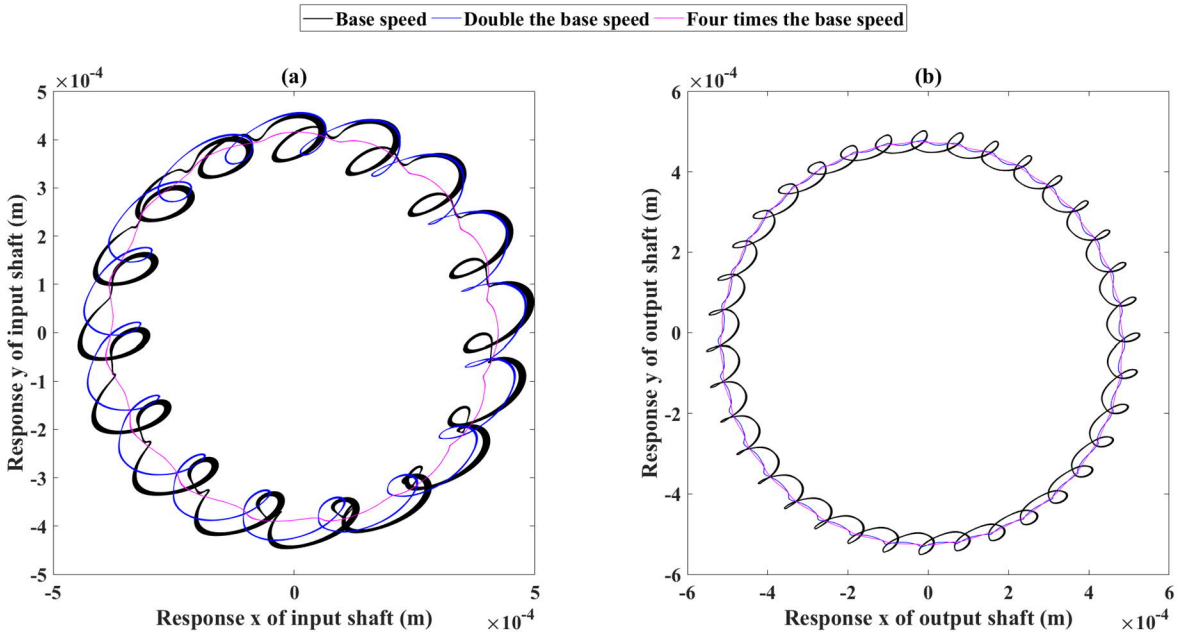

Figure 4.6: Complete response orbits at three speeds (660, 1320 and 2640 rpm) of (a) the input shaft; (b) the output shaft

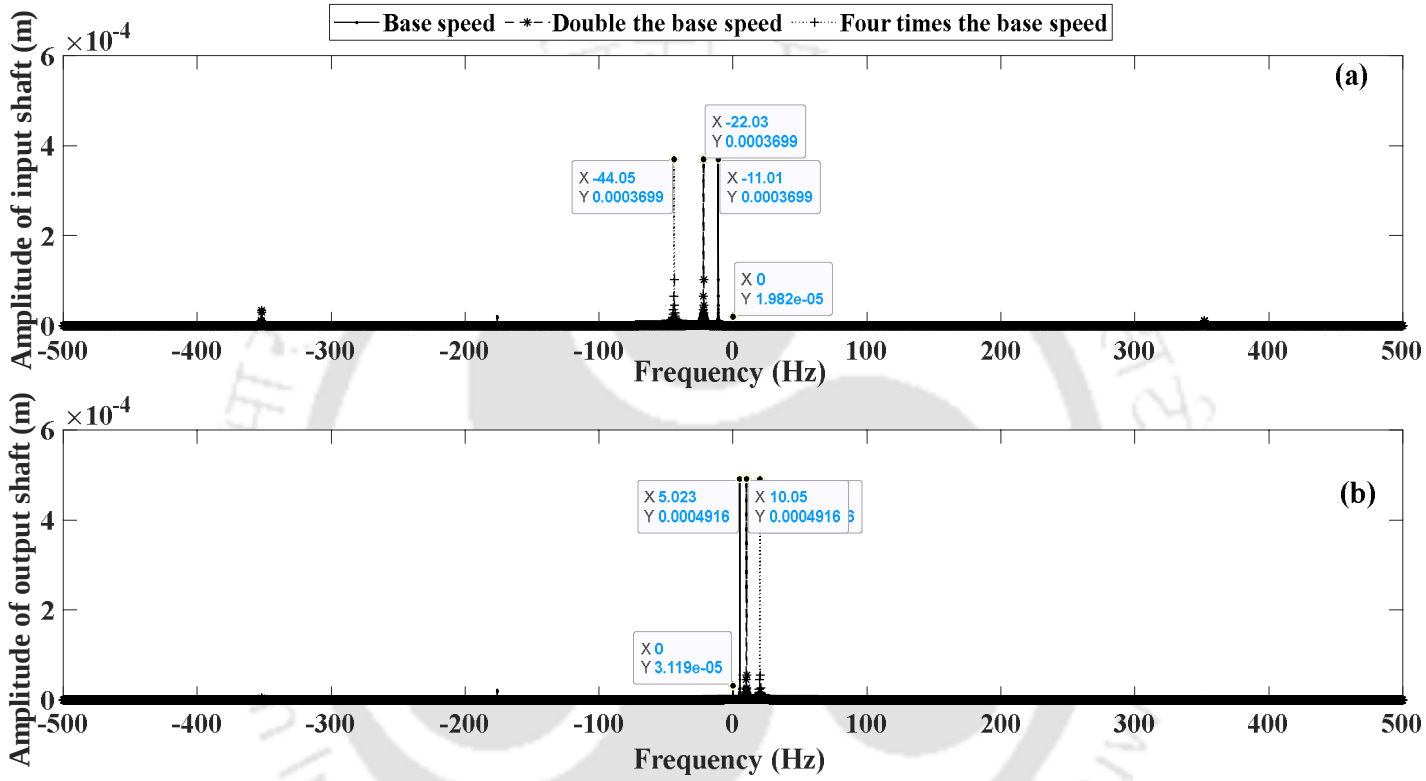

Figure 4.7: Full spectrum of response at three speeds (660, 1320 and 2640 rpm) of (a) Input shaft; (b) the Output shaft.

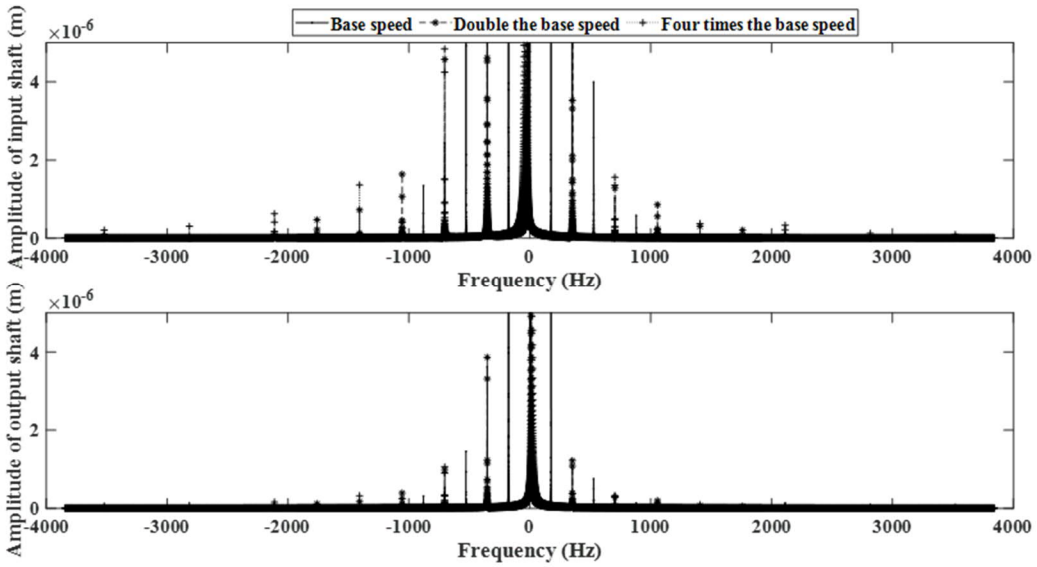

Figure 4.8: Close view of full spectrum of response at three speeds (660, 1320 and 2640 rpm) (a) input shaft; (b) output shaft

For analysing the variation of responses with other gear mesh parameters at the baseline speed, we begin with the mesh stiffness, as this parameter influences transmission error also. From literature (Kahraman, 1992), it is established fact in gear dynamics that the static TE and the gear mesh stiffness are linked together, we cannot see their effects separately as calculation of the TE depends on mesh stiffness. Higher the mesh stiffness it will have lower gear mesh vibration due to lower deformation at the gear mesh due lower TE for the same gear profile. As per Eqn. 2.6, the higher gear mesh stiffness will have lower deformation and lower transmission error, which will have a lower gear vibration. Hence, we will first study the variation of gear vibration responses with the TE. For analysis, 20% higher mesh stiffness effect is plotted with 20 % lower TE, and responses are shown in Fig. 4.9(a) for the input shaft. Similarly, to the effect of 20% higher TE is chosen to have 20% lower mesh stiffness, and corresponding plot is shown in 4.9(b) for the output shaft. The orbit plots show slightly higher response with higher TE as compared with the higher gear mesh stiffness for the same rotational speed.

The change in gear mesh damping for given change in the gear mesh stiffness can be approximated as twice the square root of product of average mass of two mating gears and the gear mesh (the pinon and gear mesh are approximated as spring-mass-damper with gear mesh stiffness and gear mesh damping). The full spectrum of responses with this variation are shown Fig. 4.10(a) and 4.10(b). Also, Fig. 4.11(a) and 4.11(b) show a close view of full spectrum with different lines for each variation. These plots show response comparison with the baseline speed, and the TE and associated mesh stiffness shows higher responses for higher TE, which establishes the fact that TE is the major dominant parameter for the gear vibration. For analysing the effect of variation in gear-runouts, responses are calculated with half the base line value and double the baseline value, respectively, in Fig. 4.12(a) and 4.12(b). These show its effect on the few orbits plot and Fig. 4.13(a) and 4.13(b) show for full orbits. The responses show that with higher runouts the orbit moves away from centre and vice-a-versa for lower runouts. This effect can also be seen in the full spectrum plots in Fig. 4.14(a) and 4.14(b). A closer look at these full spectrum plots with different marked lines are given in Fig. 4.15(a) and 4.15(b).

Now to analyse the effect of variation of gear mesh damping on responses, it is considered with the half and double the baseline gear mesh damping. Fig. 4.16(a) and 4.16(b) show few orbit responses, and Fig. 4.17(a) and 4.17(b) show full spectrum responses. Whereas Fig. 4.18(a) and 4.18(b) show a close view of the full spectrum responses with different marked lines. These plots are used for comparison of variation of responses with change in the gear mesh damping. This comparison also shows consistent results with the increase in response with lower damping and vice versa. In all these full spectrum plots the first harmonic is found to be dominant due to higher TE of 50 microns provided to the simulation model.

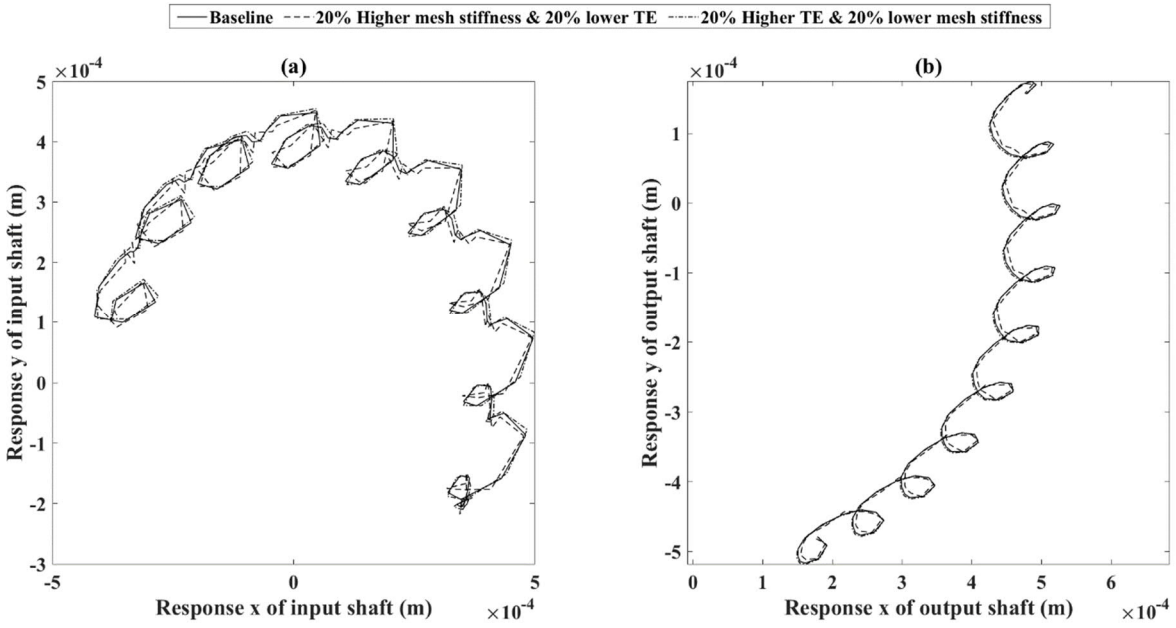

Figure 4.9: Part of orbits with 20% variation in gear mesh stiffness and TE at 660 rpm of (a) the input shaft; (b) the output shaft

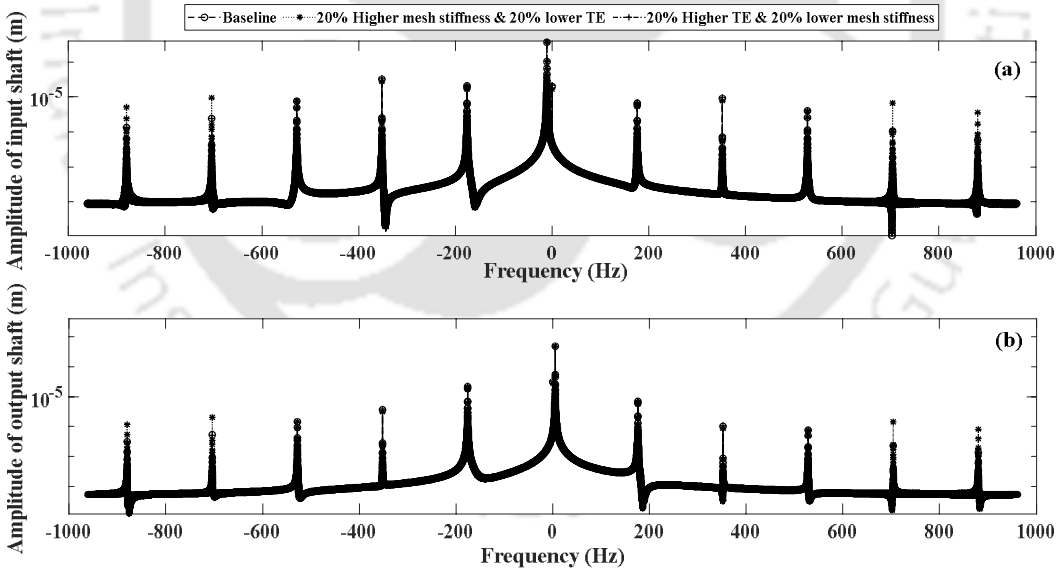

Figure 4.10: Full spectrum response with 20% variation in gear mesh stiffness and TE at 660 rpm of (a) the input shaft; (b) the output shaft

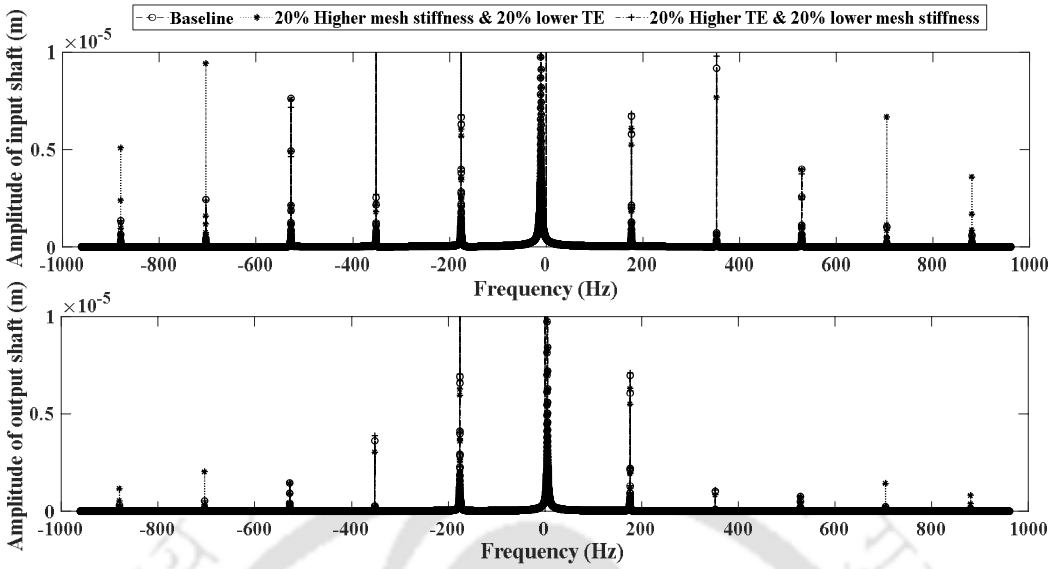

Figure 4.11: Close view of full spectrum response with 20% variation in gear mesh stiffness and TE at 660 rpm of (a) the input shaft; (b) the output shaft

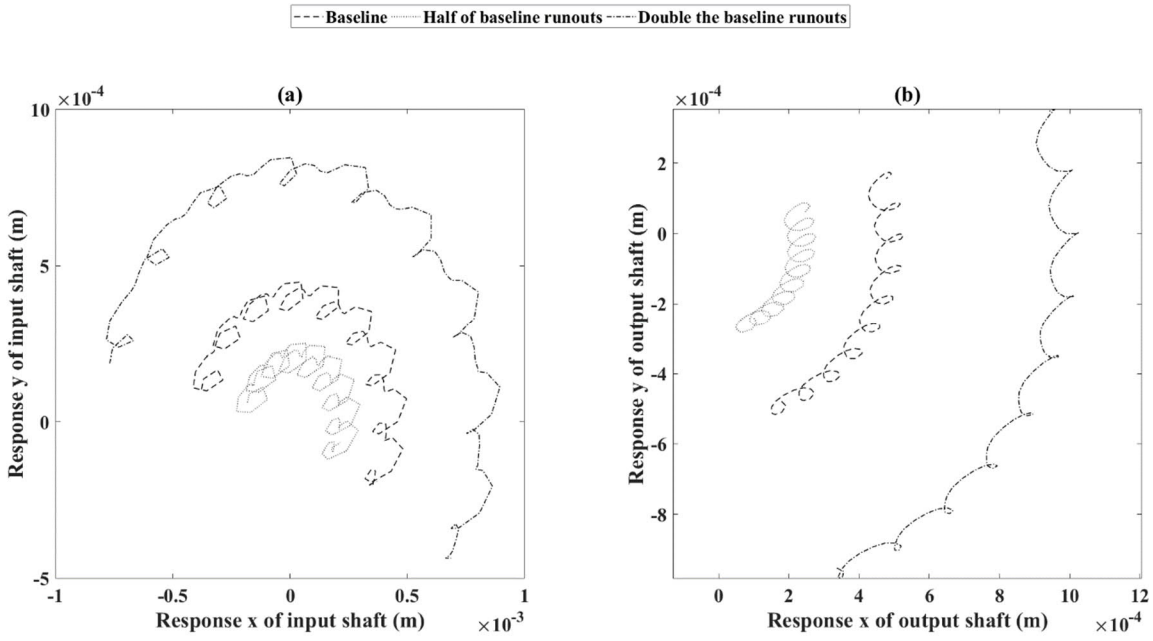

Figure 4.12: Part of orbits at (baseline, half and double) runouts 660 rpm of (a) the input shaft; (b) the output shaft

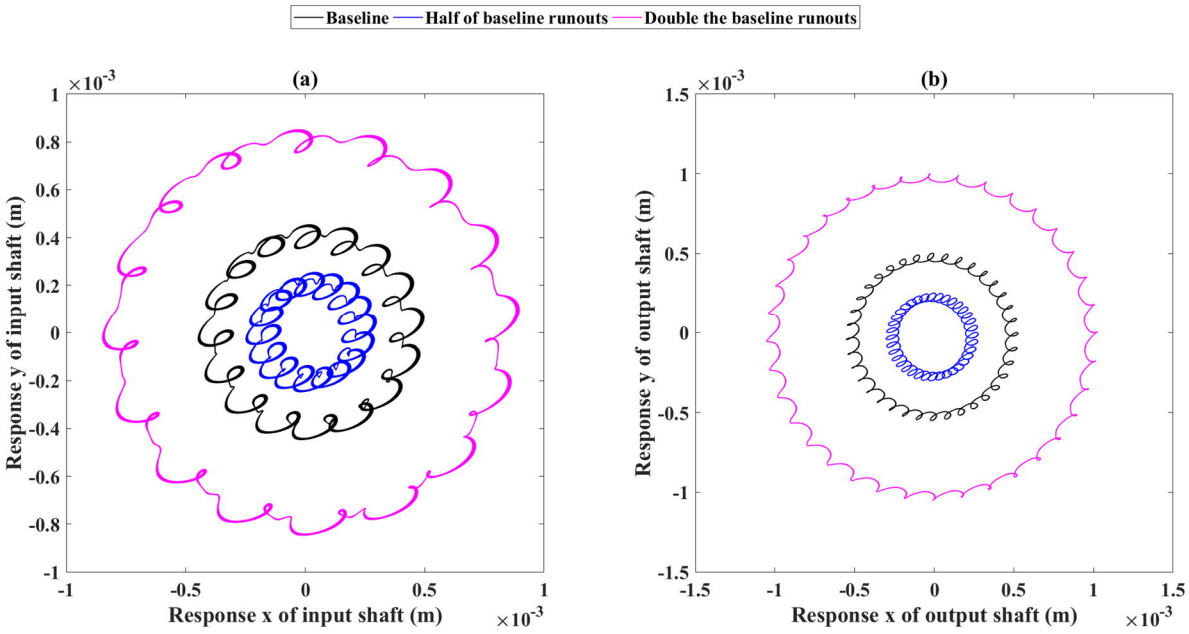

Figure 4.13: Complete response orbits at (baseline, half and double) runouts 660 rpm of (a) the input shaft; (b) the output shaft

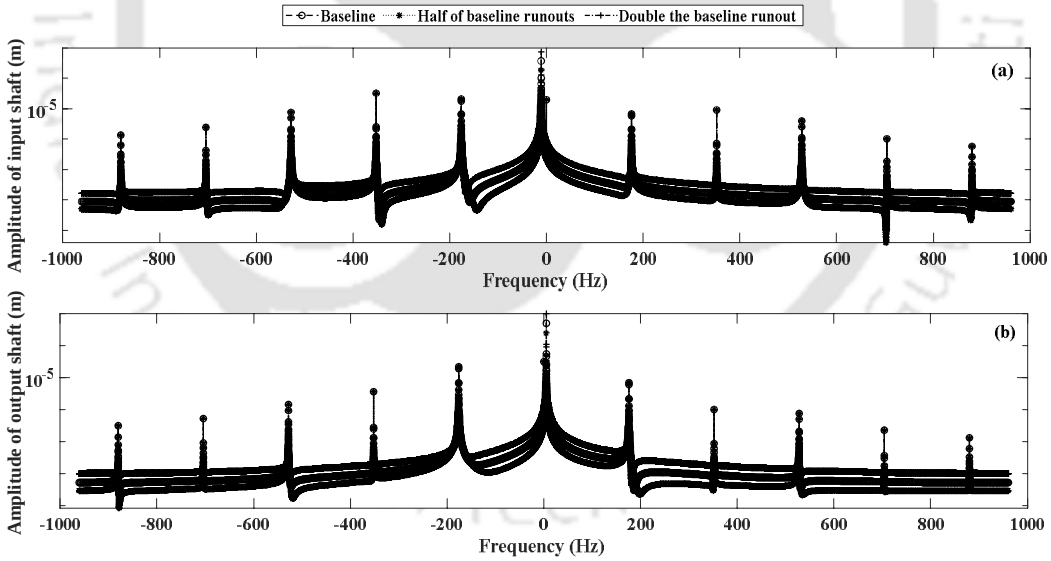

Figure 4.14: (a) Full spectrum response at (baseline, half and double) runouts 660 rpm of (a) the input shaft; (b) the output shaft

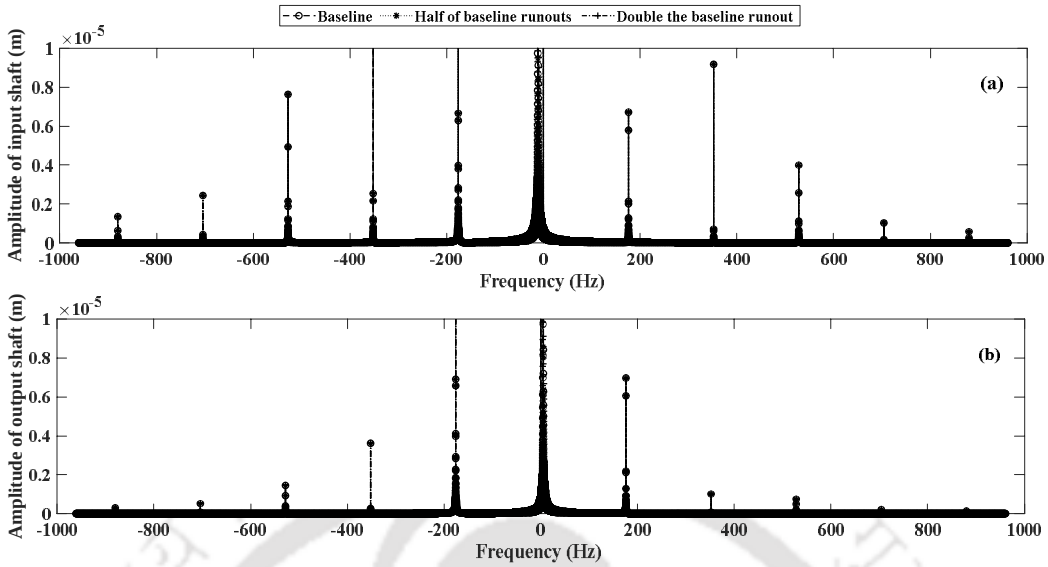

Figure 4.15: (a) Close view of full spectrum response at (baseline, half and double) runouts 660 rpm of (a) the input shaft; (b) the output shaft

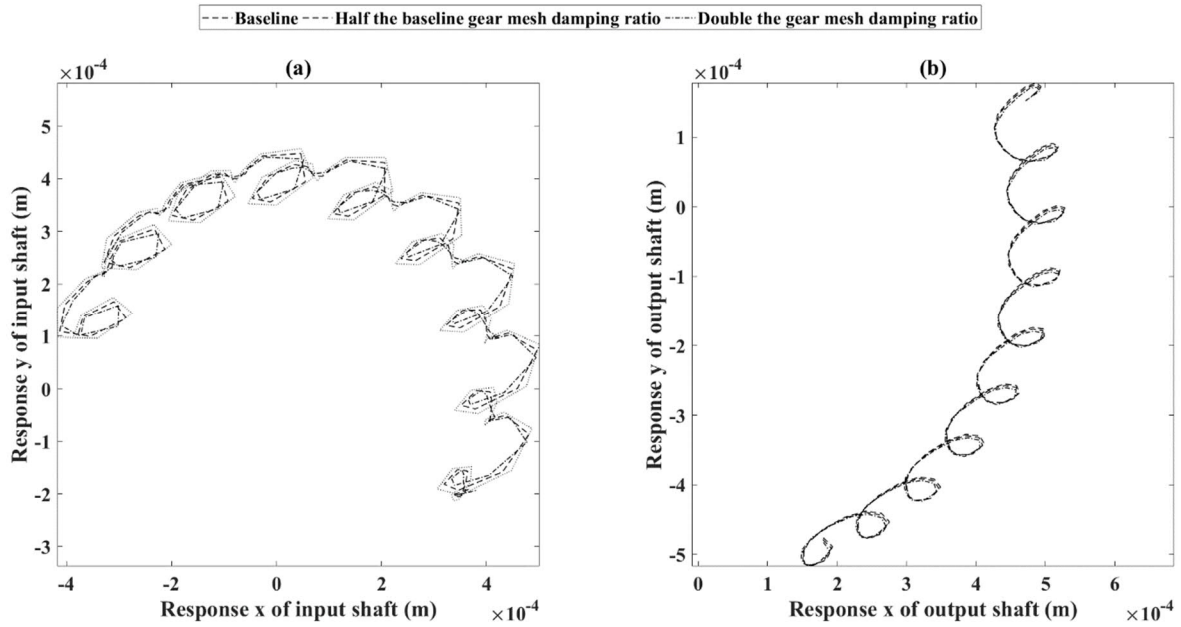

Figure 4.16: (a) Part of orbits at (baseline, half and double) gear mesh damping ratio at speed 660 rpm of (a) the input shaft; (b) the output shaft

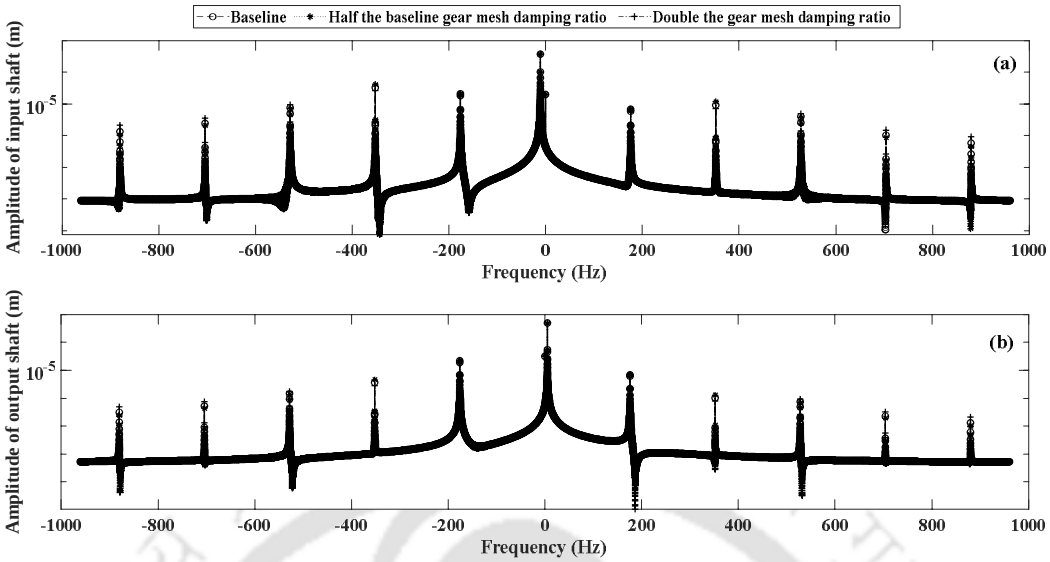

Figure 4.17: (a) Full spectrum response at (baseline, half and double) gear mesh damping ratio at speed 660 rpm of (a) the input shaft (b) the output shaft

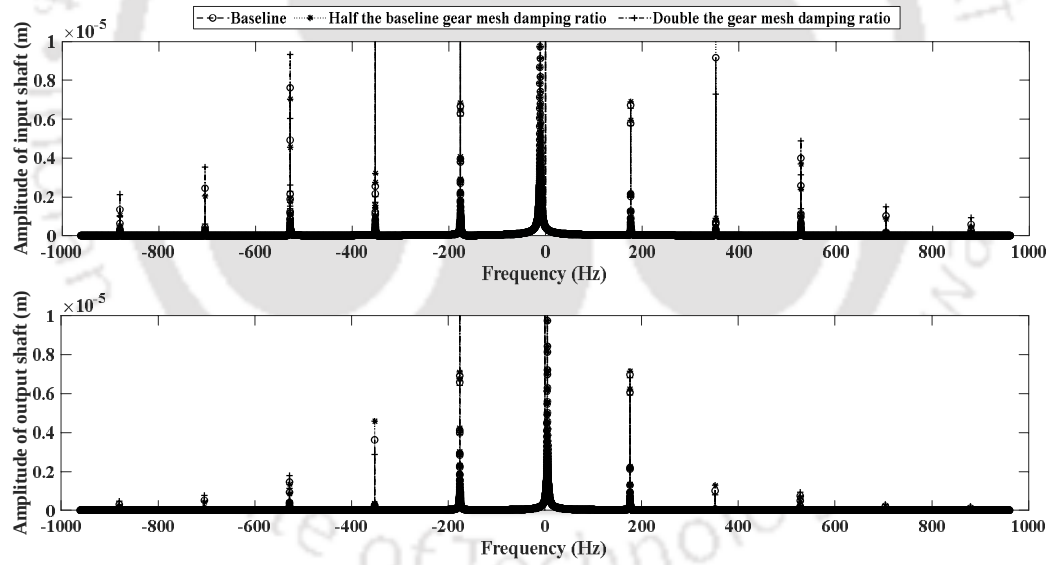

Figure 4.18: (a) Close view of full spectrum response at (baseline, half and double) gear mesh damping ratio at speed 660 rpm of (a) the input shaft (b) the output shaft

4.6 Identification Algorithm for Estimation of Gear Mesh Dynamic Transmission Error Parameters

After detecting geared rotor dominant source of vibration using the full spectrum analysis, it is attempted to identify the gear mesh dynamic TE parameters with a novel identification algorithm (IA). The algorithm uses equations of motion in frequency domain as derived in Chapter 3 and full spectrum responses calculated using the numerical simulation as shown in Fig. 4.2(a) and 4.2(b).

A three-step identification algorithm is proposed as

- In the first step, the gear mesh stiffness and the mean transmission error are estimated using static components of response taken from numerically simulated full-spectrum plots.
- In the second step, gear mesh damping is calculated with the help of estimated gear mesh stiffness and average gearing mass (details of this is given subsequently). Also, variable components of transmission errors and their initial phases are identified using the gear mesh stiffness estimated from the first step, gear mesh damping and the gear mesh frequency harmonic responses from full-spectrum plots.
- In the third step, the gear runouts and their initial phases are estimated using the estimates of first and second steps, and response at the pinion and gear meshing frequencies are taken from full-spectrum plots.

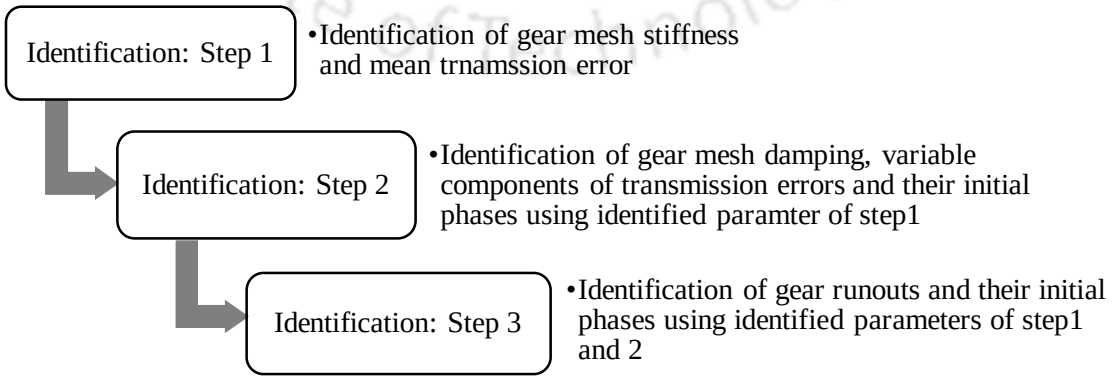

Figure 4.19: Schematic representation of the identifcation algorithm in a step down process

The pictorial representation of proposed identification algorithm is shown in Fig. 4.19.

The identification process starts with the estimation of the mean transmission error and the gear meshing stiffness using the static response components. Eqns. (3.71) and (3.72) are combined in a matrix form, as

$$\begin{Bmatrix} S_{1r} \\ S_{1j} \\ S_{2r} \\ S_{2j} \end{Bmatrix} = \begin{Bmatrix} k_{s1}P_{s1r} + k_m(P_{s1r} - P_{s2r}) \\ k_{s1}P_{s1j} + k_m(P_{s1j} - P_{s2j}) \\ k_{s2}P_{s2r} + k_m(P_{s2r} - P_{s1r}) \\ k_{s2}P_{s2j} + k_m(P_{s2j} - P_{s1j}) \end{Bmatrix} \tag{4.1}$$

On substituting Eqn. (3.52) in Eqn. (4.1), unknown terms are rearranged as

$$\begin{Bmatrix} k_m e_m \\ k_m e_m \\ k_m e_m \\ k_m e_m \end{Bmatrix} = \begin{Bmatrix} k_{s1}P_{s1r} + k_m(P_{s1r} - P_{s2r}) \\ k_{s1}P_{s1j} + k_m(P_{s1j} - P_{s2j}) + m_1 g \\ -k_{s2}P_{s2r} - k_m(P_{s2r} - P_{s1r}) \\ -k_{s2}P_{s2j} - k_m(P_{s2j} - P_{s1j}) - m_2 g \end{Bmatrix} \tag{4.2}$$

The gear mesh stiffness and mean TE are separated and written in matrix form, as

$$\begin{bmatrix} (P_{s1r} - P_{s2r}) & -1 \\ (P_{s1j} - P_{s2j}) & -1 \\ (P_{s2r} - P_{s1r}) & 1 \\ (P_{s2j} - P_{s1j}) & 1 \end{bmatrix} \begin{Bmatrix} k_m \\ k_m e_m \end{Bmatrix} = \begin{Bmatrix} -k_{s1}P_{s1r} \\ -k_{s1}P_{s1j} - m_1 g \\ -k_{s2}P_{s2r} \\ -k_{s2}P_{s2j} - m_2 g \end{Bmatrix} \tag{4.3}$$

In the first step of identification problem, the gear mesh stiffness (k_m) and the mean transmission error (e_m) are estimated using the static responses (*P* terms) that are taken from full spectrum plots as shown in Fig. 4.2 (a) for subscript 1 (input shaft) and 4.2 (b) for subscript 2 (output shaft). Also, the mass of gears; gravitational constant; the input and output shaft stiffnesses are substituted from Table 4.1. On the pseudo-inverting Eqn. 4.3, we get k_m and e_m.

In the second step of the identification process the gear meshing frequency components of frequency domain transformations are considered for the identification of the gear mesh damping, and variable transmission error with its magnitudes and initial phases. For the identification of the static TE and their phases, following forcing functions with sine and cosine terms are conveniently grouped from Eqns. (3.20), (3.22), (3.24), (3.26) and (3.54) as

$$\begin{Bmatrix} R_{f_e r} \\ R_{f_e j} \\ R_{b_e r} \\ R_{b_e j} \end{Bmatrix} = \begin{Bmatrix} e_{xi}\cos\phi_{e_{xi}} - e_{yi}\sin\phi_{e_{yi}} \\ e_{xi}\sin\phi_{e_{xi}} + e_{yi}\cos\phi_{e_{yi}} \\ e_{xi}\cos\phi_{e_{xi}} + e_{yi}\sin\phi_{e_{yi}} \\ -e_{xi}\sin\phi_{e_{xi}} + e_{yi}\cos\phi_{e_{yi}} \end{Bmatrix} \Rightarrow \begin{bmatrix} 1 & -1 & 0 & 0 \\ 0 & 0 & 1 & 1 \\ 1 & 1 & 0 & 0 \\ 0 & 0 & -1 & 1 \end{bmatrix} \begin{Bmatrix} e_{xi}\cos\phi_{e_{xi}} \\ e_{yi}\sin\phi_{e_{yi}} \\ e_{xi}\sin\phi_{e_{xi}} \\ e_{yi}\cos\phi_{e_{yi}} \end{Bmatrix} = \{T\} \tag{4.4}$$

Now, the forcing functions due to gear meshing frequency on the input and output shafts are grouped for the input shaft by substituting these equations in Eqns. (3.53) to get the defined pinion and gear force real and imaginary components (*R*) in terms of critical DTE parameters of gear mesh as,

$$\begin{Bmatrix} S_{f_{e1r}} \\ S_{f_{e1j}} \\ S_{b_{e1r}} \\ S_{b_{e1j}} \end{Bmatrix} = \frac{1}{2}\begin{bmatrix} i\omega_e c_m & k_m & 0 & 0 \\ -k_m & i\omega_e c_m & 0 & 0 \\ 0 & 0 & i\omega_e c_m & -k_m \\ 0 & 0 & k_m & i\omega_e c_m \end{bmatrix}\begin{bmatrix} 1 & -1 & 0 & 0 \\ 0 & 0 & 1 & 1 \\ 1 & 1 & 0 & 0 \\ 0 & 0 & -1 & 1 \end{bmatrix}\begin{Bmatrix} e_{xi}\cos\phi_{e_{xi}} \\ e_{yi}\sin\phi_{e_{yi}} \\ e_{xi}\sin\phi_{e_{xi}} \\ e_{yi}\cos\phi_{e_{yi}} \end{Bmatrix}$$

$$\Rightarrow \frac{1}{2}\begin{bmatrix} i\omega_e c_m & -i\omega_e c_m & k_m & k_m \\ -k_m & k_m & i\omega_e c_m & i\omega_e c_m \\ i\omega_e c_m & i\omega_e c_m & k_m & -k_m \\ k_m & k_m & -i\omega_e c_m & i\omega_e c_m \end{bmatrix}\begin{Bmatrix} e_{xi}\cos\phi_{e_{xi}} \\ e_{yi}\sin\phi_{e_{yi}} \\ e_{xi}\sin\phi_{e_{xi}} \\ e_{yi}\cos\phi_{e_{yi}} \end{Bmatrix} \tag{4.5}$$

Similarly, for the output shaft we can write

$$\begin{Bmatrix} S_{f_{e2r}} \\ S_{f_{e2j}} \\ S_{b_{e2r}} \\ S_{b_{e2j}} \end{Bmatrix} = \frac{1}{2}\begin{bmatrix} -i\omega_e c_m & -k_m & 0 & 0 \\ k_m & -i\omega_e c_m & 0 & 0 \\ 0 & 0 & -i\omega_e c_m & k_m \\ 0 & 0 & -k_m & -i\omega_e c_m \end{bmatrix}\begin{bmatrix} 1 & -1 & 0 & 0 \\ 0 & 0 & 1 & 1 \\ 1 & 1 & 0 & 0 \\ 0 & 0 & -1 & 1 \end{bmatrix}\begin{Bmatrix} e_{xi}\cos\phi_{e_{xi}} \\ e_{yi}\sin\phi_{e_{yi}} \\ e_{xi}\sin\phi_{e_{xi}} \\ e_{yi}\cos\phi_{e_{yi}} \end{Bmatrix}$$

$$\Rightarrow \frac{1}{2}\begin{bmatrix} -i\omega_e c_m & i\omega_e c_m & -k_m & -k_m \\ k_m & -k_m & -i\omega_e c_m & -i\omega_e c_m \\ -i\omega_e c_m & -i\omega_e c_m & -k_m & k_m \\ -k_m & -k_m & i\omega_e c_m & -i\omega_e c_m \end{bmatrix}\begin{Bmatrix} e_{xi}\cos\phi_{e_{xi}} \\ e_{yi}\sin\phi_{e_{yi}} \\ e_{xi}\sin\phi_{e_{xi}} \\ e_{yi}\cos\phi_{e_{yi}} \end{Bmatrix} \tag{4.6}$$

These equation formulations are used for second step of identification by substituting them into Eqns. (3.87), (3.90), (3.93), (3.96), (3.117), (3.120), (3.123) and (3.126) to get the identification equations of the input and out shafts, these are written in a matrix form by rearranging terms for the input shaft as,

$$\frac{1}{2}\begin{bmatrix} i\omega_e c_m & -i\omega_e c_m & k_m & k_m \\ -k_m & k_m & i\omega_e c_m & i\omega_e c_m \\ i\omega_e c_m & i\omega_e c_m & k_m & -k_m \\ k_m & k_m & -i\omega_e c_m & i\omega_e c_m \end{bmatrix} \begin{Bmatrix} e_{xi}\cos\phi_{e_{xi}} \\ e_{yi}\sin\phi_{e_{yi}} \\ e_{xi}\sin\phi_{e_{xi}} \\ e_{yi}\cos\phi_{e_{yi}} \end{Bmatrix}$$

$$= \begin{Bmatrix} -m_1(i\omega_e)^2 P_{f_e 1r} - (i\omega_e)c_{s1}P_{f_e 1j} + k_{s1}P_{f_e 1r} + k_m(P_{f_e 1r} - P_{f_e 2r}) - (i\omega_e c_m)(P_{f_e 1j} - P_{f_e 2j}) \\ -m_1(i\omega_e)^2 P_{f_e 1j} + i\omega_e c_{s1}P_{f_e 1r} + k_{s1}P_{f_e 1j} + k_m(P_{f_e 1j} - P_{f_e 2j}) + i\omega_e c_m(P_{f_e 1r} - P_{f_e 2r}) \\ -m_1(i\omega_e)^2 P_{b_e 1r} + i\omega_e c_{s1}P_{b_e 1j} + k_{s1}P_{b_e 1r} + k_m(P_{b_e 1r} - P_{b_e 2r}) + (i\omega_e c_m)(P_{b_e 1j} - P_{b_e 2j}) \\ -m_1(i\omega_e)^2 P_{b_e 1j} - i\omega_e c_{s1}P_{b_e 1r} + k_{s1}P_{b_e 1j} + k_m(P_{b_e 1j} - P_{b_e 2j}) + i\omega_e c_m(P_{b_e 2r} - P_{b_e 1r}) \end{Bmatrix} \quad (4.7)$$

Similarly, for the output shaft, it can be arranged as,

$$\frac{1}{2}\begin{bmatrix} -i\omega_e c_m & i\omega_e c_m & -k_m & -k_m \\ k_m & -k_m & -i\omega_e c_m & -i\omega_e c_m \\ -i\omega_e c_m & -i\omega_e c_m & -k_m & k_m \\ -k_m & -k_m & i\omega_e c_m & -i\omega_e c_m \end{bmatrix} \begin{Bmatrix} e_{xi}\cos\phi_{e_{xi}} \\ e_{yi}\sin\phi_{e_{yi}} \\ e_{xi}\sin\phi_{e_{xi}} \\ e_{yi}\cos\phi_{e_{yi}} \end{Bmatrix}$$

$$= \begin{Bmatrix} -m_2(i\omega_e)^2 P_{f_e 2r} - i\omega_e c_{s2}P_{f_e 2j} + k_{s2}P_{f_e 2r} + k_m(P_{f_e 2r} - P_{f_e 1r}) + i\omega_e c_m(P_{f_e 1j} - P_{f_e 2j}) \\ -m_2(i\omega_e)^2 P_{f_e 2j} + i\omega_e c_{s2}P_{f_e 2r} + k_{s2}P_{f_e 2j} + k_m(P_{f_e 2j} - P_{f_e 1j}) + i\omega_e c_m(P_{f_e 2r} - P_{f_e 1r}) \\ -m_2(i\omega_e)^2 P_{b_e 2r} + i\omega_e c_{s2}P_{b_e 2j} + k_{s2}P_{b_e 2r} + k_m(P_{b_e 2r} - P_{b_e 1r}) + i\omega_e c_m(P_{b_e 2j} - P_{b_e 1j}) \\ -m_2(i\omega_e)^2 P_{b_e 2j} - i\omega_e c_{s2}P_{b_e 2r} + k_{s2}P_{b_e 2j} + k_m(P_{b_e 2j} - P_{b_e 1j}) + i\omega_e c_m(P_{b_e 1r} - P_{b_e 2r}) \end{Bmatrix} \quad (4.8)$$

Herein, the gear mesh damping is estimated from gear meshing stiffness, k_m, and average pinion (m_p) and gear (m_g) masses. The average mass of pinion and gear is given by average gearing mass as,

$$m_{avg} = \frac{m_p m_g}{m_p + m_g} \quad (4.9)$$

The gear meshing damping can be calculated using free vibration damping formula with average gearing mass and gear mesh stiffness by using assumed gear mesh damping ratio (ζ_m) value of 0.01 as

$$c_m = \zeta_m 2\sqrt{k_m m_{avg}} \tag{4.10}$$

By substituting the identified value of gear mesh stiffness (k_m) and gear mesh damping (c_m) from the first step, the chosen geared rotor parameters given in Table 1 and full-spectrum responses at respective harmonics (*P* terms, which are quantitatively the real and imaginary components of the full spectrum, whose amplitudes are given in Fig. 4.2) in Eqns. (4.7) and (4.8), the resulting equations are simplified to get the combined form as,

$$\frac{1}{2}\begin{bmatrix} i\omega_e c_m & -i\omega_e c_m & k_m & k_m \\ -k_m & k_m & i\omega_e c_m & i\omega_e c_m \\ i\omega_e c_m & i\omega_e c_m & k_m & -k_m \\ k_m & k_m & -i\omega_e c_m & i\omega_e c_m \\ -i\omega_e c_m & i\omega_e c_m & -k_m & -k_m \\ k_m & -k_m & -i\omega_e c_m & -i\omega_e c_m \\ -i\omega_e c_m & -i\omega_e c_m & -k_m & k_m \\ -k_m & -k_m & i\omega_e c_m & -i\omega_e c_m \end{bmatrix} \begin{Bmatrix} e_{xi}\cos\phi_{e_{xi}} \\ e_{yi}\sin\phi_{e_{yi}} \\ e_{xi}\sin\phi_{e_{xi}} \\ e_{yi}\cos\phi_{e_{yi}} \end{Bmatrix}$$

$$= \begin{Bmatrix} -m_1(i\omega_e)^2 P_{f_e 1r} - (i\omega_e)c_{s1}P_{f_e 1j} + k_{s1}P_{f_e 1r} + k_m(P_{f_e 1r} - P_{f_e 2r}) - (i\omega_e c_m)(P_{f_e 1j} - P_{f_e 2j}) \\ -m_1(i\omega_e)^2 P_{f_e 1j} + i\omega_e c_{s1}P_{f_e 1r} + k_{s1}P_{f_e 1j} + k_m(P_{f_e 1j} - P_{f_e 2j}) + i\omega_e c_m(P_{f_e 1r} - P_{f_e 2r}) \\ -m_1(i\omega_e)^2 P_{b_e 1r} + i\omega_e c_{s1}P_{b_e 1j} + k_{s1}P_{b_e 1r} + k_m(P_{b_e 1r} - P_{b_e 2r}) + (i\omega_e c_m)(P_{b_e 1j} - P_{b_e 2j}) \\ -m_1(i\omega_e)^2 P_{b_e 1j} - i\omega_e c_{s1}P_{b_e 1r} + k_{s1}P_{b_e 1j} + k_m(P_{b_e 1j} - P_{b_e 2j}) + i\omega_e c_m(P_{b_e 2r} - P_{b_e 1r}) \\ -m_2(i\omega_e)^2 P_{f_e 2r} - i\omega_e c_{s2}P_{f_e 2j} + k_{s2}P_{f_e 2r} + k_m(P_{f_e 2r} - P_{f_e 1r}) + i\omega_e c_m(P_{f_e 1j} - P_{f_e 2j}) \\ -m_2(i\omega_e)^2 P_{f_e 2j} + i\omega_e c_{s2}P_{f_e 2r} + k_{s2}P_{f_e 2j} + k_m(P_{f_e 2j} - P_{f_e 1j}) + i\omega_e c_m(P_{f_e 2r} - P_{f_e 1r}) \\ -m_2(i\omega_e)^2 P_{b_e 2r} + i\omega_e c_{s2}P_{b_e 2j} + k_{s2}P_{b_e 2r} + k_m(P_{b_e 2r} - P_{b_e 1r}) + i\omega_e c_m(P_{b_e 2j} - P_{b_e 1j}) \\ -m_2(i\omega_e)^2 P_{b_e 2j} - i\omega_e c_{s2}P_{b_e 2r} + k_{s2}P_{b_e 2j} + k_m(P_{b_e 2j} - P_{b_e 1j}) + i\omega_e c_m(P_{b_e 1r} - P_{b_e 2r}) \end{Bmatrix} \tag{4.11}$$

Herein, subscripts 1 and 2 represent the input and output shafts. The harmonic number *i* is from 1 to 5 harmonics of gear meshing frequencies considered in modelling variable TE, the gear mesh stiffness calculated from Step 1, the input and output shaft stiffness, the masses of gears and the full spectrum responses (*P* terms) calculated numerically as shown in Fig. 4.2 (a) and 4.2 (b) are substituted in the Eqn. (4.11). On taking the pseudo-inverse of the regression equation (4.11) to identify the four unknown quantities of fluctuating part of TE and their phases as,

$$\begin{Bmatrix} e_{fxi}\cos\phi_{e_{xi}} \\ e_{fyi}\sin\phi_{e_{yi}} \\ e_{fxi}\sin\phi_{e_{xi}} \\ e_{fyi}\cos\phi_{e_{yi}} \end{Bmatrix} = \begin{Bmatrix} e_{11} \\ e_{21} \\ e_{31} \\ e_{41} \end{Bmatrix} \tag{4.12}$$

On noting Eqn. (4.12), the fluctuating part of the static TE in the *x* and *y* directions are estimated using sine and cosine trigonometric relations by combining the first and third components; then by combining the second and fourth components as

$$e_{fxi} = \sqrt{e_{11}^2 + e_{31}^2};\ \ e_{fyi} = \sqrt{e_{21}^2 + e_{41}^2} \tag{4.13}$$

From the first and second components of Eqn. (4.12), we get the initial phases of fluctuating components of the static TE in the *x* and *y* directions and are estimated as

$$\phi_{e_{xi}} = \cos^{-1}(e_{11} / e_{xi});\ \ \phi_{e_{yi}} = \sin^{-1}(e_{21} / e_{yi}) \tag{4.14}$$

In the third and final step, the gear runouts and their phases are identified with the pinion and gear meshing frequency components of frequency domain transformations. The defined pinion and gear force real and imaginary components (*R*) in Eqns. (3.35), (3.36), (3.37), (3.38), (3.40), (3.41), (3.43) and (3.44) are substituted into Eqns. (3.118), (3.121), (3.124), (3.127), (3.89), (3.95), (3.92) and (3.98), respectively, to get the backward pinion equations (forward pinion equations are nullified) and forward gear equations (backward gear equations are nullified). Now the identification equations on the input and output shafts for the first harmonic is written in a matrix form by rearranging pinion equations as,

$$\begin{bmatrix} (m_1\omega_p^2 - k_m - k_{s1}) & (c_m\omega_p + c_{s1}\omega_p) & 0 & 0 \\ (c_m\omega_p + c_{s1}\omega_p) & (-m_1\omega_p^2 + k_m + k_{s1}) & 0 & 0 \\ k_m & -c_m\omega_p & 0 & 0 \\ -c_m\omega_p & -k_m & 0 & 0 \end{bmatrix} \begin{Bmatrix} e_p\cos\varphi_p \\ e_p\sin\varphi_p \\ e_g\cos\varphi_g \\ e_g\sin\varphi_g \end{Bmatrix}$$

$$= \begin{bmatrix} -m_1(\omega_p)^2 P_{b_{p1r}} + i\omega_p c_{s1} P_{b_{p1j}} + k_{s1} P_{b_{p1r}} + k_m (P_{b_{p1r}} - P_{b_{p2r}}) + i\omega_p c_m (P_{b_{p1j}} - P_{b_{p2j}}) \\ -m_1(\omega_p)^2 P_{b_{p1j}} - i\omega_p c_{s1} P_{b_{p1r}} + k_{s1} P_{b_{p1j}} + k_m (P_{b_{p1j}} - P_{b_{p2j}}) + i\omega_p c_m (P_{b_{p2r}} - P_{b_{p1r}}) \\ -m_2(\omega_p)^2 P_{b_{p2r}} + i\omega_p c_{s2} P_{b_{p2j}} + k_{s2} P_{b_{p2r}} + k_m (P_{b_{p2r}} - P_{b_{p1r}}) + i\omega_p c_m (P_{b_{p2j}} - P_{b_{p1j}}) \\ -m_2(\omega_p)^2 P_{b_{p2j}} - i\omega_p c_{s2} P_{b_{p2r}} + k_{s2} P_{b_{p2j}} + k_m (P_{b_{p2j}} - P_{b_{p1j}}) + i\omega_p c_m (P_{b_{p1r}} - P_{b_{p2r}}) \end{bmatrix} \quad (4.15)$$

and gear equations as,

$$\begin{bmatrix} 0 & 0 & k_m & -c_m\omega_g \\ 0 & 0 & c_m\omega_g & k_m \\ 0 & 0 & m_2\omega_g^2 - k_m - k_{s2} & c_m\omega_g + c_{s2}\omega_g \\ 0 & 0 & -c_m\omega_g - c_{s2}\omega_g & m_2\omega_g^2 - k_m - k_{s2} \end{bmatrix} \begin{Bmatrix} e_p\cos\varphi_p \\ e_p\sin\varphi_p \\ e_g\cos\varphi_g \\ e_g\sin\varphi_g \end{Bmatrix}$$

$$= \begin{bmatrix} -m_1(\omega_g)^2 P_{f_{g1r}} - i\omega_g c_{s1} P_{f_{g1j}} + k_{s1} P_{f_{g1r}} + k_m (P_{f_{g1r}} - P_{f_{g2r}}) - i\omega_g c_m (P_{f_{g1j}} - P_{f_{g2j}}) \\ -m_1(\omega_g)^2 P_{f_{g1j}} + i\omega_g c_{s1} P_{f_{g1r}} + k_{s1} P_{f_{g1j}} + k_m (P_{f_g 1j} - P_{f_{g2j}}) + i\omega_g c_m (P_{f_{g1r}} - P_{f_{g2r}}) \\ -m_2(\omega_g)^2 P_{f_{g2r}} - i\omega_g c_{s2} P_{f_{g2j}} + k_{s2} P_{f_{g2r}} + k_m (P_{f_{g2r}} - P_{f_{g1r}}) + i\omega_g c_m (P_{f_{g2j}} - P_{f_{g1j}}) \\ -m_2(\omega_g)^2 P_{f_{g2j}} + i\omega_g c_{s2} P_{f_{g2r}} + k_{s2} P_{f_{g2j}} + k_m (P_{f_{g2j}} - P_{f_{g1j}}) + i\omega_g c_m (P_{f_{g2r}} - P_{f_{g1r}}) \end{bmatrix} \quad (4.16)$$

On substituting the identified value of gear mesh stiffness (k_m) and gear mesh damping (c_m) from the first and second steps, and full-spectrum responses (P terms) of the gear and pinion rotation frequencies shown in Fig. 4.2 (a) and Fig. 4.2 (b) in Eqns. (4.15) and (4.16) and resulting equations are simplified to get the combined form as,

$$\begin{bmatrix} m_1\omega_p^2 - k_m - k_{s1} & c_m\omega_p + c_{s1}\omega_p & 0 & 0 \\ c_m\omega_p + c_{s1}\omega_p & -m_1\omega_p^2 + k_m + k_{s1} & 0 & 0 \\ k_m & -c_m\omega_p & 0 & 0 \\ -c_m\omega_p & -k_m & 0 & 0 \\ 0 & 0 & k_m & -c_m\omega_g \\ 0 & 0 & c_m\omega_g & k_m \\ 0 & 0 & m_2\omega_g^2 - k_m - k_{s2} & c_m\omega_g + c_{s2}\omega_g \\ 0 & 0 & -c_m\omega_g - c_{s2}\omega_g & m_2\omega_g^2 - k_m - k_{s2} \end{bmatrix} \begin{Bmatrix} e_p\cos\varphi_p \\ e_p\sin\varphi_p \\ e_g\cos\varphi_g \\ e_g\sin\varphi_g \end{Bmatrix}$$

$$= \begin{bmatrix} -m_1(\omega_p)^2 P_{b_{p1r}} + i\omega_p c_{s1} P_{b_{p1j}} + k_{s1} P_{b_{p1r}} + k_m(P_{b_{p1r}} - P_{b_{p2r}}) + i\omega_p c_m(P_{b_{p1j}} - P_{b_{p2j}}) \\ -m_1(\omega_p)^2 P_{b_{p1j}} - i\omega_p c_{s1} P_{b_{p1r}} + k_{s1} P_{b_{p1j}} + k_m(P_{b_{p1j}} - P_{b_{p2j}}) + i\omega_p c_m(P_{b_{p2r}} - P_{b_{p1r}}) \\ -m_2(\omega_p)^2 P_{b_{p2r}} + i\omega_p c_{s2} P_{b_{p2j}} + k_{s2} P_{b_{p2r}} + k_m(P_{b_{p2r}} - P_{b_{p1r}}) + i\omega_p c_m(P_{b_{p2j}} - P_{b_{p1j}}) \\ -m_2(\omega_p)^2 P_{b_{p2j}} - i\omega_p c_{s2} P_{b_{p2r}} + k_{s2} P_{b_{p2j}} + k_m(P_{b_{p2j}} - P_{b_{p1j}}) + i\omega_p c_m(P_{b_{p1r}} - P_{b_{p2r}}) \\ -m_1(\omega_g)^2 P_{f_{g1r}} - i\omega_g c_{s1} P_{f_{g1j}} + k_{s1} P_{f_{g1r}} + k_m(P_{f_{g1r}} - P_{f_{g2r}}) - i\omega_g c_m(P_{f_{g1j}} - P_{f_{g2j}}) \\ -m_1(\omega_g)^2 P_{f_{g1j}} + i\omega_g c_{s1} P_{f_{g1r}} + k_{s1} P_{f_{g1j}} + k_m(P_{f_g 1j} - P_{f_{g2j}}) + i\omega_g c_m(P_{f_{g1r}} - P_{f_{g2r}}) \\ -m_2(\omega_g)^2 P_{f_{g2r}} - i\omega_g c_{s2} P_{f_{g2j}} + k_{s2} P_{f_{g2r}} + k_m(P_{f_{g2r}} - P_{f_{g1r}}) + i\omega_g c_m(P_{f_{g2j}} - P_{f_{g1j}}) \\ -m_2(\omega_g)^2 P_{f_{g2j}} + i\omega_g c_{s2} P_{f_{g2r}} + k_{s2} P_{f_{g2j}} + k_m(P_{f_{g2j}} - P_{f_{g1j}}) + i\omega_g c_m(P_{f_{g2r}} - P_{f_{g1r}}) \end{bmatrix} \quad (4.17)$$

In the third step of identification problem, the matrix in Eqn. (4.17) is pseudo-inverted using the regression fit for identifying the pinion and gear runouts. The resulting form of the vector is written as,

$$\begin{Bmatrix} e_p \cos\varphi_p \\ e_p \sin\varphi_p \\ e_g \cos\varphi_g \\ e_g \sin\varphi_g \end{Bmatrix} = \begin{Bmatrix} e_{p1} \\ e_{p2} \\ e_{g1} \\ e_{g2} \end{Bmatrix} \tag{4.18}$$

On noting Eqn. (4.18), the pinion and gear runouts are estimated using the sine and cosine trigonometric relations by combining the first and second components; then by combining the third and fourth components, as

$$e_p = \sqrt{e_{p1}^2 + e_{p2}^2}; \quad e_g = \sqrt{e_{g1}^2 + e_{g2}^2} \tag{4.19}$$

From the first and second components of Eqn. (4.18), we get the initial phases of the pinion and gear runout frequencies and are estimated as,

$$\phi_{e_p} = \cos^{-1}(e_{p1} / e_p); \quad \phi_{e_g} = \cos^{-1}(e_{g1} / e_g) \tag{4.20}$$

With this three-step identification algorithm, the estimation of all eleven critical gear mesh dynamic TE parameters that influences the lateral responses of the spur geared rotor with parallel shafts has been presented.

4.7 Numerical Testing of Identification Algorithm

To test the three-step identification algorithm (IA) described in Section 4.6, estimation of gear mesh dynamic TE parameters is performed using numerically generated full spectrum responses (*P* terms, which are real and imaginary components of full spectrum amplitudes) as shown in Fig. 4.2 (a) and 4.2 (b), where

magnitudes of the real and imaginary components are shown for the first harmonic of gear meshing frequency. Alternately these *P* vector can be calculated from frequency domain formulation given in Eqn. (3.318) (the real and imaginary components at all the peaks are shown in full spectrum plots separately for input and output shafts are given in Fig. A1.1 and Fig. A1.2 in Appendix A). The resulting estimates are compared with parameters chosen for simulating numerical responses as given in Table 4.1. The percentage deviation of the estimates with assumed parameters for numerical simulation are also presented. It is observed that the proposed IA estimates are perfectly matching with the assumed values without any deviation. Also, the estimations are checked by changing the harmonic number from 1 to 5. For all five harmonics the estimates are perfectly matching with assumed variables.

To test the robustness of proposed identification algorithm against noise present in measurement data, 1 % and 5 % white Gaussian noise is introduced in the numerically simulated data. The full spectrum response is plotted with 5 % Gaussian noise as shown in Fig. 4.4 in the amplitude and phase form (Bode plot) and is used for the identification purpose. The comparison of phase between these two plots Fig 4.2 and Fig. 4.4 shows the effect of adding 5% Gaussian measurement noise with quickly varying phase in the entire spectrum in Fig. 4.4.

With the same identification procedure used for without noise case, the estimates are calculated with measurement noise in the full spectrum by increasing from 1% up to 5%. It is observed that, with noise the estimate of gear mesh stiffness and mean transmission error are deviating. Table 4.3 shows the percent deviations of estimates with noise and without noise for varied presumed gear mesh parameters by changing the shaft speed, gear mesh stiffness, mean TE, variable TE, runouts and damping. It is observed that without considering measurement noise, the IA estimates are perfectly matching with presumed parameters used in numerical simulations as shown in Table 4.3 for the first harmonic. Table 4.4 show the deviation in estimates for the higher harmonic from 1 to 5. These deviations are helpful in correcting the estimates on the actual gear drive for practical purposes. Also, the deviations in estimates are checked by feeding data

from two speeds, which are 600 rpm apart to the IA to improve the least-squares fit estimates (by this way we are trying to get better regression fit by feeding more training data to the system). Last part of Table 4.4 shows that with two speeds data the deviation in phase of TE has reduced from 103 % to 40 % but the same has increased the deviation in the corresponding fluctuating TE from -4.1 to -10%.

Table 4.3: Identification of gear mesh parameters based on numerical simulation

Varied parameter		**Percentage deviation of identified parameter with assumed one (%)**										
Following parameters are varied to check the robustness of IA		k_m	e_m	c_m	$e_{fxi}(t)$	$e_{fyi}(t)$	ϕ_{exi}	ϕ_{eyi}	e_p	e_g	ϕ_p	ϕ_g
Noise	**Speed (**rpm**)**											
0	660	0	0	0	0	0	0	0	0	0	0	0
0	1320	0	0	0	0	0	0	0	0	0	0	0
1	660	-96	1.8	0	-12	-14	13	-5	0.2	0.1	-0.1	0.04
5	660	-99	10	0	-4.1	-16	103	-52	1.1	0.7	-0.6	0.2
Noise	**Gear mesh stiffness (**N/m**)**											
0	6e8	0	0	0	0	0	0	0	0	0	0	0
0	7e8	0	0	0	0	0	0	0	0	0	0	0
5	6e8	-99	10	0	-4.1	-16	103	-52	1.1	0.7	-0.6	0.2
Noise	**Mean TE (** μm **)**											
0	10	0	0	0	0	0	0	0	0	0	0	0
0	100	0	0	0	0	0	0	0	0	0	0	0
5	10	-99	10	0	-4.1	-16	103	-52	1.1	0.7	-0.6	0.2
Noise	**Variable TE (** μm **)**											
0	10	0	0	0	0	0	0	0	0	0	0	0
0	50	0	0	0	0	0	0	0	0	0	0	0
5	10	-99	10	0	-4.1	-16	103	-52	1.1	0.7	-0.6	0.2

Noise	Runouts (μm)											
0	100	0	0	0	0	0	0	0	0	0	0	0
0	200	0	0	0	0	0	0	0	0	0	0	0
5	100	-99	10	0	-4.1	-16	103	-52	1.1	0.7	-0.6	0.2
Noise	**Damping**											
0	0.01	0	0	0	0	0	0	0	0	0	0	0
0	0.02	0	0	0	0	0	0	0	0	0	0	0
5	0.01	-99	10	0	-4.1	-16	103	-52	1.1	0.7	-0.6	0.2

Table 4.4: Identification of gear mesh parameters based on numerical simulation at higher harmonics with noise

Varied parameter		**Percentage deviation of identified parameter with assumed one (%)**										
Harmonic number is varied from 1 to 5 for 660 rpm speed		k_m	e_m	c_m	$e_{fxi}(t)$	$e_{fyi}(t)$	ϕ_{exi}	ϕ_{eyi}	e_p	e_g	ϕ_p	ϕ_g
Noise	**Harmonic**											
5	1	-99	10	0	-4.1	-16	103	-52	1.1	0.7	-0.6	0.2
5	2	-99	10	0	-5.5	-5.6	7.6	-3.6	1.1	0.7	-0.6	0.2
5	3	-99	10	0	-9	-9	28	-13	1.1	0.7	-0.6	0.2
5	4	-99	10	0	-7	-7	47	-23	1.1	0.7	-0.6	0.2
5	5	-99	10	0	-2	-2	64	-31	1.1	0.7	-0.6	0.2
Two speeds data at 660 and 1260 rpm are fed to IA												
5	1	-99	10	0	-10	-15	40	-18	1.1	0.7	-0.6	0.2

Table 4.3 shows the percent deviation in the estimates increase with the measurement noise mainly due to deviation in gear mesh stiffness and slight deviation in mesh TE in all cases, which is sensitive to the static deflection. Also, it is observed that without passing the deviated gear mesh stiffness and the mean TE due

to measurement noise in the second and third steps of IA, the estimates of TE and runout parameter estimate are robust to the measurement noise. To avoid these deviations, one may calculate gear mesh stiffness using Hertzian contact formulation proposed in Choi (2001) and Flek et al. (2021) using analytically or by the FE model.

4.8 Summary

Numerical solution for the geared rotor is obtained with assumed geared rotor DTE parameters and presumed gear mesh dynamic parameters. Responses of geared rotor system model is analyzed in time domain with orbit plots and in frequency domain with the full spectrum response. Also, the parametric study is carried out to detect the dominant source of vibration in geared rotor. A novel three-step identification algorithm is proposed to identify the dynamic transmission error in a geared rotor system. The identification algorithm is tested using numerically simulated data. The identification summary is presented with varied input parameters. The estimates from identification algorithm are observed to be stable with varied gear mesh parameters. By introducing the Gaussian measurement noise in the input signal, the gear mesh stiffness and the mean TE are deviating. Herein, the mesh stiffness deviates by 99% due to deviation the static deformation with noise, mainly this has caused the further deviation of 103% in the phase of variable TE in the second step estimates. This deviation causes the slight deviations in the TE and runout estimates with measurement noise, which is considered up to 5%. The identification summary shows that the identification algorithm is robust enough for estimating geared rotor system parameters, like the TE and runouts even with measurement noise. The same is tested numerically with varied dynamic TE parameters with different speeds up to five harmonics. For validating geared rotor system model developed, an experimental rig is to be designed and fabricated and it is covered in Chapter 5.

CHAPTER 5

EXPERIMENTAL RIG DESIGN AND DEVELOPMENT FOR IDENTIFICATION OF GEARED ROTOR DYNAMIC TRANSMISSION ERROR PARAMETERS

5.1 Introduction

The geared rotor system model developed in Chapter 2 for calculating lateral vibration response need to be validated with responses form an experimental setup. Also, the identification of gear mesh dynamic transmission error (TE) parameters, as proposed in Chapter 4, needs the geared rotor experimental kit responses to estimate gear mesh parameters. To fulfil these needs a geared rotor experimental kit is designed and developed for lateral vibration measurement. The static TE is introduced in the gear set, which was fixed to the experimental kit. The output shaft of the experimental kit was fitted with magnetic torquer to load the gear mesh with nominal torque to avoid loss of contact during the torque transfer. The drive was given to input shaft with an induction motor. The lateral vibration measurements were done directly at the gears with displacement probes fitted for this purpose along with the phase measurement at the motor input shaft. The test measurements are converted to frequency domain to generate full spectrum plots for validating the system model response. Further, the test measured full spectrum amplitudes are used in the identification algorithm to validate the system model using identified test kit parameters.

5.2 Design of the Geared Rotor Experimental Rig Layout

A geared rotor experimental rig with a spur gear mesh is designed and developed at Vibration and Acoustics Laboratory of IIT Guwahati. A nominal torque transfer was applied with a magnetic brake in a single gear pair mounted at the shaft centre to replicate the system model developed in Chapter 2. The schematic view of geared rotor experimental rig is shown in Fig. 5.1. The gear set and the supporting shafts on which these gears are mounted are chosen to replicate the geared rotor system model developed Chapter 2. The physical parameters of the experimental rig are same as the parameters given in Table 4.1 of Chapter 4. Design

drawings of the pinion and the gear are shown in Figs. 5.2 and 5.3. The solid model layout of the experimental rig prepared for this purpose is shown in Fig. 5.4. The gear and the pinion are fixed at the shaft centres using the M6 bolt taps provide for it, as shown in the gear and pinion drawings in Fig. 5.2 and Fig. 5.3. Chosen gear parameters are given in Table 5.1. Other elements of the experimental rig are the ball bearings, couplings, motor and variable frequency drive (VFD). Five eddy-current proximity sensors of Bently-Nevada make were utilized for acquiring vibration displacements of the shaft at gear mounting locations and its phase. These were located in two orthogonal transverse directions near the pinion and the gear on the shafts and one sensor is fixed close to the motor on the input shaft to get the reference phase measurement.

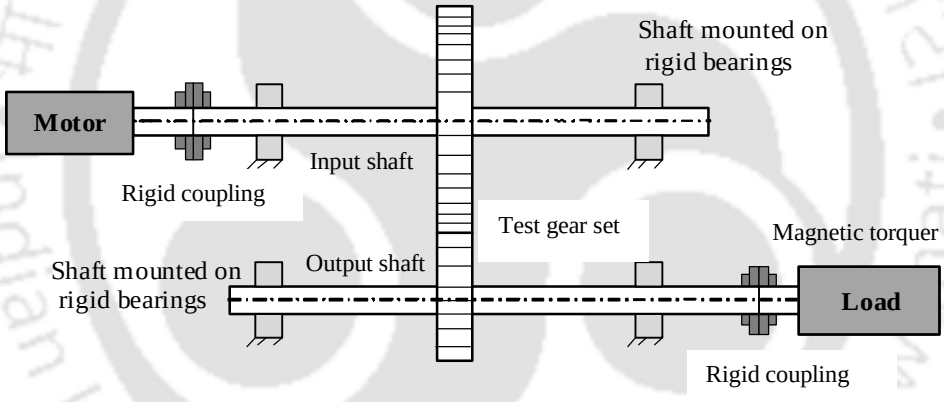

Figure 5.1: Schematic of the geared rotor experimental rig

A thick base plate was chosen to resist any base motion during the torque transfer. The baseplate was given with taps to fix the bearing blocks. The bearing block was split type to hold deep groove ball bearings along with shafts as shown in CAD model of experimental kit layout in Fig. 5.4. The mounting plate has provision to accommodate the switching gear sets having shaft centre distance (CD) varies from 45 mm to 100 mm. Threaded holes with 10 mm pitch were provided in the mounting plate to adjust the bearing blocks according to varies centre distances of the gear sets. The gear hub having 11 mm bore and

20 mm width (10 mm width is reserved for face of gear) were provided with M6 taps to fix the gear at any position on the shaft. The experimental rig consisted of two parallel shafts, the drive shaft coupled with the motor shaft and the driven shaft loaded with a magnetic torque brake.

Table 5.1: Experimental gear set design parameters

Gear design parameter	**Dimension**	
Normal module (mm)	2	
Normal pressure angle	20° 0’ 0”	
Helix angle	0° 0’ 0”	
Transverse module (mm)	2	
Transverse pressure angle	20° 0’ 0”	
	Small gear	Large gear
Number of teeth	16	35
Normal tooth profile shift coefficient	0	0.06307
Center distance (mm)	51.125	
Pitch circle diameter (mm)	32	70
Contacting pitch circle diameter (mm)	32.07843	70.17157
Addendum (mm)	1.99885	2.125
Dedendum- (mm)	2.5	2.37385
Tooth height (mm)	4.49885	4.49885
Clearance (mm)	0.5	0.5
Base circle diameter (mm)	30.07016	65.77848
Tip diameter (mm)	35.99771	74.25
Root diameter (mm)	27	65.25229
Start of contact diameter (mm)	30.09285	67.65436
Lead (mm)	0	0
Transverse contact ratio	1.57692	

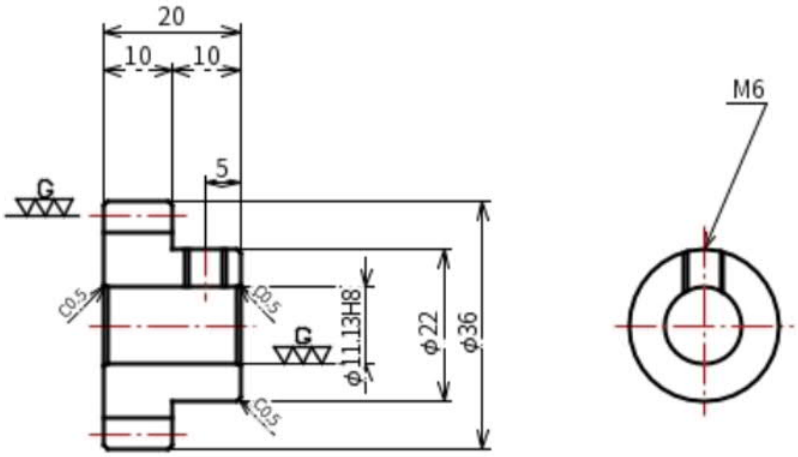

Figure 5.2: Pinion Drawing (G- Gear grinding, C- Chamfer, M6- 6mm pitch metric thread)

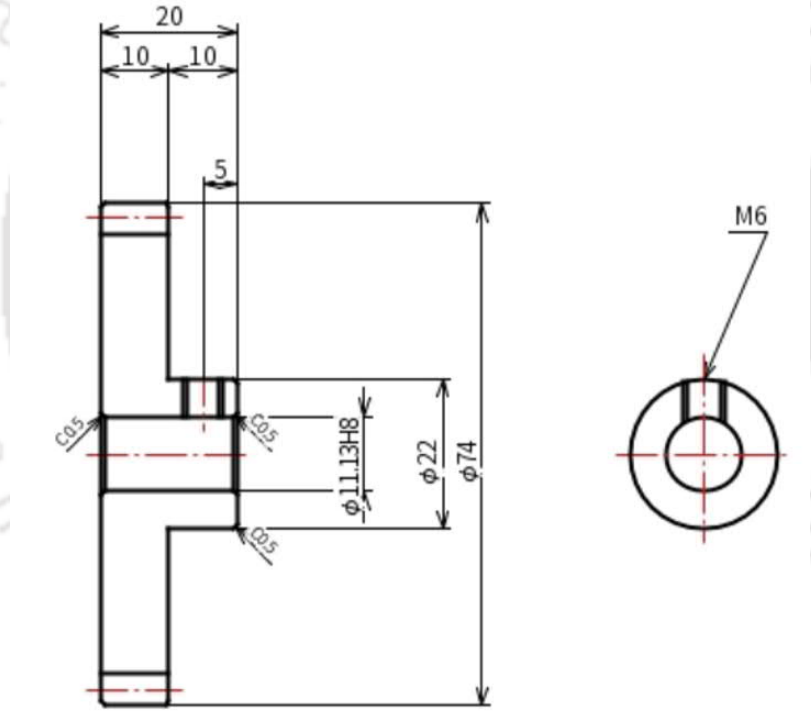

Figure 5.3: Gear drawing (G- Gear grinding, C- Chamfer, M6- 6 mm pitch metric thread)

5.3 Geared Rotor Experimental Rig

The geared rotor experimental rig components described in the previous section was assembled together. For driving the geared rotor, the input shaft was connected with 0.75 kW (1 HP) induction motor using a

spiral cut flexible coupling. The gear mesh was loaded during experiment by a magnetic torquer with 0.11 N-m maximum torque capacity and was coupled to the other end of the output shaft using a spiral cut flexible coupling to make sure that the gears are always loaded without slipping during the torque transfer.

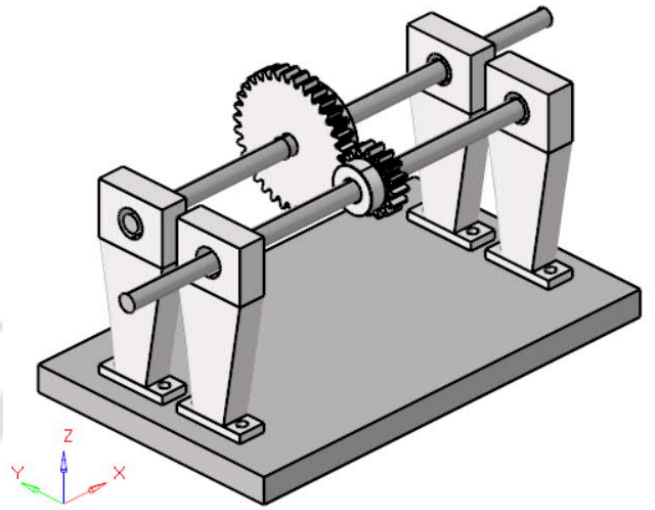

Figure 5.4: A CAD model of geared rotor experimental rig

The horizontal and vertical shaft displacements at gears were captured using proximity probes, which were firmly mounted on the base plate. The eddy current type proximity probes had sensitivity of 7870 mv/mm. The displacement probe placement, motor and magnetic torquer of the experimental setup are depicted in Fig. 5.6. The gear set which was fixed to the experimental kit, as shown in Fig. 5.5, had a gear ratio of 2.18 with the driven shaft is mounted with the bigger gear. When viewed from the hub of gears, the torque transfer took place through left flank of the gear. The smaller gear was fabricated with 5 μ m average profile crown and 0.2 μm average lead crown. The bigger gear wheel was manufactured with 2.2 μ m average profile crown and 4.5 μm average lead crown. The gear and pinion tooth microgeometry is read from inspection reports generated by gear manufacturer for this purpose.

Figure 5.5: Gear set used in the experimental rig

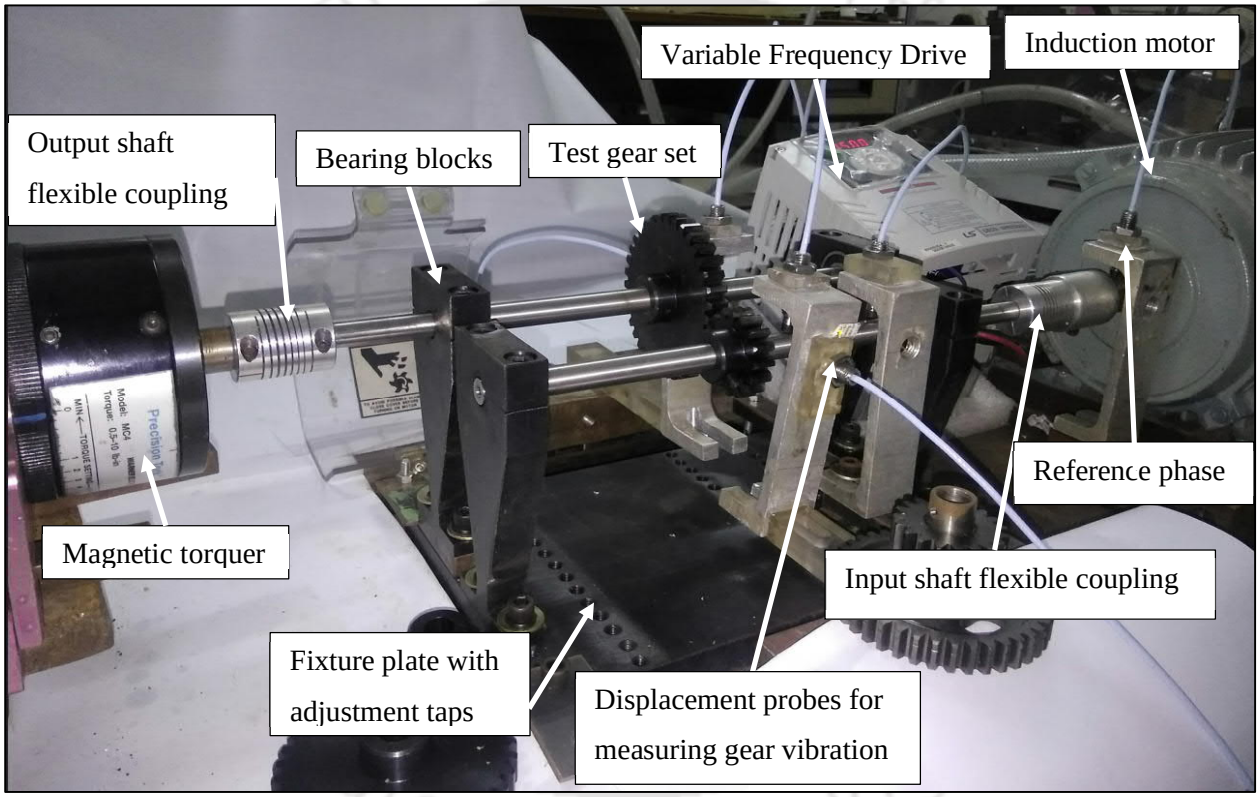

Figure 5.6: Experimental rig and probe positioning at Acoustics and Vibration lab of IIT Guwahati

5.4 Experimental Measurement

The power was given to the motor through a variable frequency drive as shown in Fig 5.6 to adjust the input shaft speed. The magnetic torquer was set to max capacity 0.1 Nm resisting torque with the adjustment key provided with it. The experimental probes were connected to oscilloscope to adjust the sensor with a screw

to maintain a specified gap between the probe and the shaft for getting the right measurement. Each probe was connected to an eight-channel data-acquisition system to digitize the signal further processing.

A variable frequency drive (VFD) VFD-M power source was used as a regulator to control the speed of motor as per requirement of the shaft spin speed. The motor was set to run at 970 rpm (16.15 Hz) for taking measurements. The geared rotor experimental rig was set to rotate few minutes to attain steady state condition before taking the measurement. The dSPACE DAQ system was utilized to store the measurement signal at a sampling frequency of 5,000 samples per second. A reference signal was utilized for acquiring displacement signals of the shaft for complete multiple shaft rotational cycles, i.e., for $\omega t = 2\pi n$, where n is the number of complete cycles during post processing of acquired signals. Using complete cycles of signals avoids leakage error (Singh and Tiwari, 2015) and that gives consistent estimates while using the identification algorithm. The horizontal and vertical measurements taken on time scale on both input and output shafts at the pinion and the gear were shown in Fig. 5.7. These signals were combined for each shaft to plot their orbits as shown in Fig. 5.8.

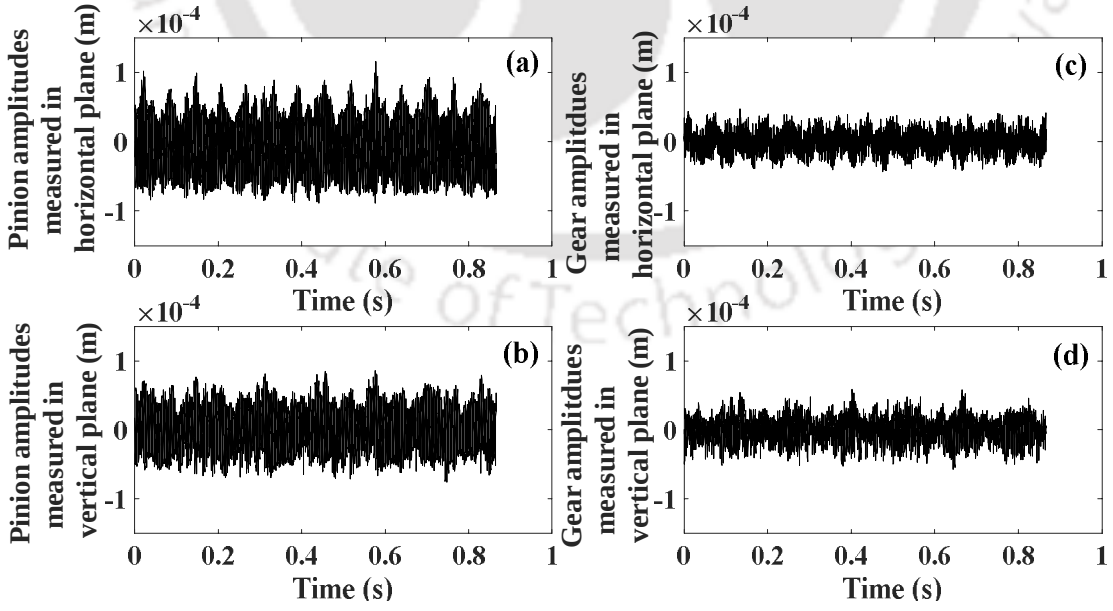

Figure 5.7: Measured time signal on the input and output shafts from the experimental rig

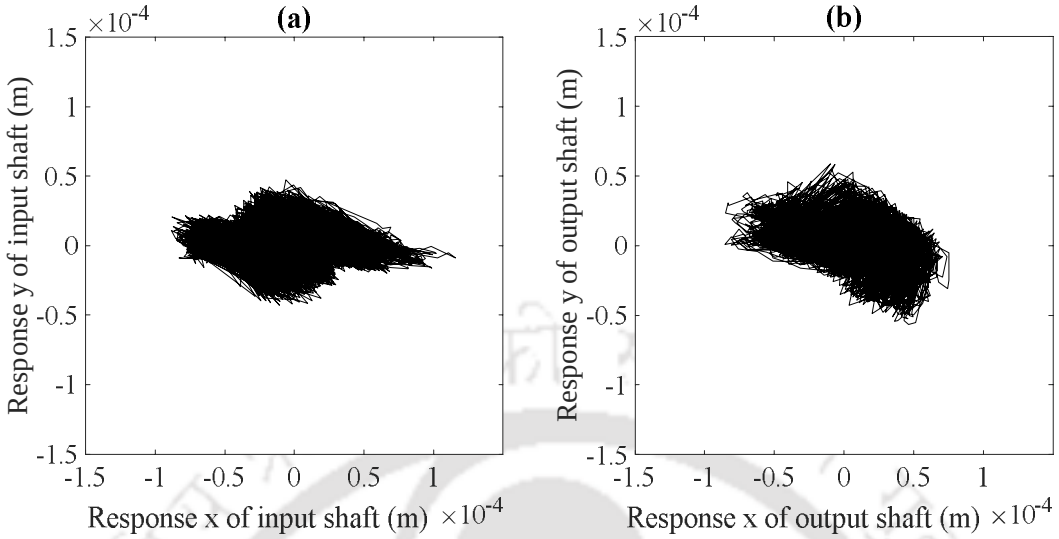

Figure 5.8: (a) Orbit response plot of the input shaft from experimental rig; (b) Orbit response plot of the output shaft from experimental rig.

5.5 Full Spectrum Response Analyses from the Experimental Rig

Gear meshing frequency of 258.4 Hz is calculated from the number of teeth in pinion (16) multiplied with its rotational frequency (16.15 Hz). When the plots of orbits are analyzed, it is found that they are different for both input and output shafts. Also, many cycles are manifested in the orbit plot specifies presence of several frequencies. Phase compensation of the measured signal is done by subtracting the phase of input and output shafts with the reference phases on the input and output shafts (output shaft phase is adjusted with the help of gear ratio) with the help of measured reference signal at the input shaft. Phase compensation helps to avoid leakage error by synchronizing the measurements related to different harmonics present in the system by having common reference for all the frequency components (Tiwari, 2017).

One block of measured time domain responses is chosen for transforming them into frequency domain. The phase compensated full-spectrum plot of experimental rig responses is shown in Fig. 5.9, which shows predominant peaks at five gear mesh forward and backward whirl frequencies. These harmonics are at 258.4, 516.8, 775.2, 1033.6, and 1292 Hz.

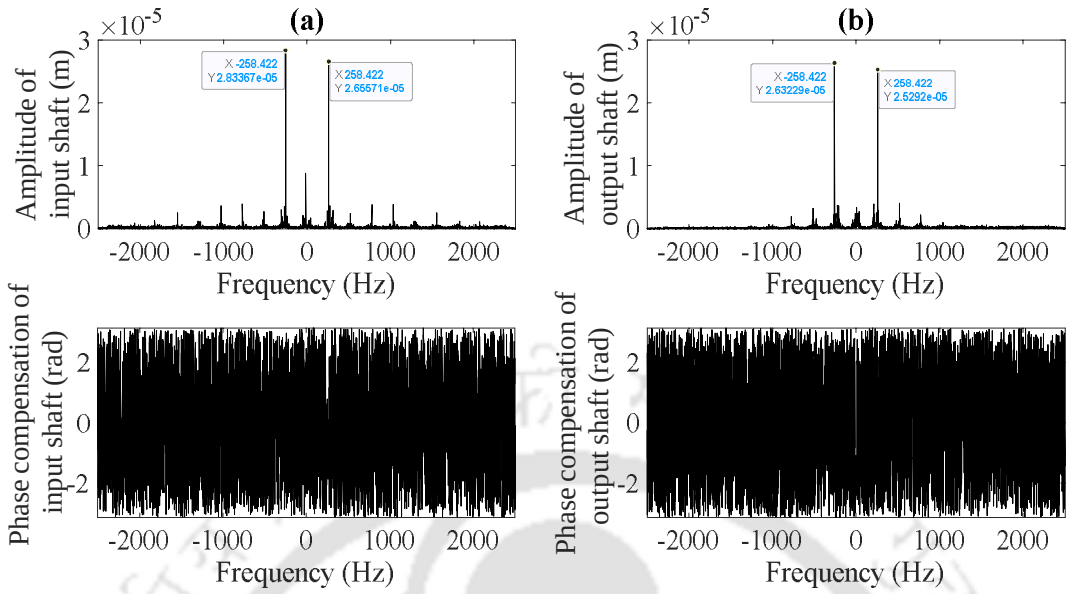

Figure 5.9: (a) Full spectrum responses of the input shaft from the experimental rig; (b) Full spectrum responses of the output shaft from the experimental rig

The asymmetric amplitudes of the forward and backward whirls of all five harmonics, which excites simultaneously at all harmonics are seen in the full spectrum. The asymmetric full spectrum amplitudes prove the asymmetric static TE hypothesis proposed in this research with the help of system model in Chapter 2 and with the numerical simulation in Chapter 4. As there is relatively small TE of the fourth and fifth harmonics in the present gear, relatively smaller amplitude peaks are reflected in the respective frequencies in the full spectrum. Also, there is relative difference in the peak amplitudes in the forward and backward whirls, which demonstrates asymmetricity in TE. Peak amplitudes at the driver and driven gear rotational frequencies are also seen at 16.15 Hz and 7.38 Hz, respectively.

5.6 Identification of Gear Mesh Dynamic TE Parameters using Experimental Rig Full Spectrum Responses

After getting full spectrum responses (both magnitude and phase) of test measured signal, the identification of the experimental rig gear mesh dynamic TE parameters is attempted in this section. Phase compensated

full spectrum responses from experimental rig of all the five harmonics of gear meshing frequencies along with responses at the gear and pinion shaft rotational frequency, as shown in Fig. 5.9 (the real and imaginary components at all the peaks are shown in full spectrum plots separately for input and output shafts are given in Fig. A2.1 and Fig. A2.2 in Appendix A), are used in the identification algorithm.

Using the numerically tested identification algorithm as discussed in Chapter 4, which has three steps in multiple parameter estimation procedure. The schematic of the three-step identification algorithm is shown in Fig. 5.10. As part of the first step using Eqn. 4.3, the static responses at zero frequency of the full spectrum are taken as response coefficients. On feeding the known physical parameters of experimental rig to the system along with measured responses at zero frequency in the identification algorithm and on pseudo inverting Eqn. 4.3, it gives the least-squares fit estimates of the gear mesh stiffness and mean transmission error parameters. These estimates are presented in Table 5.2.

In the second step, these two estimates are substituted in Eqn. 4.9 along with other physical parameters of the system and the respective harmonic responses at the gear meshing frequency of the measured full spectrum responses. On pseudo inverting, it gives the least-squares fit estimates of the gear mesh damping, variable components of asymmetric STE components and the runouts. The same step is repeated for all five harmonics by choosing the value of i for the respective harmonic. The estimates of all five harmonics are presented in the end of Table 5.2. The asymmetry of variable static TE components in the x and y directions of each harmonic are also seen to be different in the experimental estimation.

Finally, in the third step, using the estimates of previous two steps and other physical parameters of experimental rig are substituted in Eqn. 4.15. Also, the gear and pinion shaft frequency responses from the experimental rig in the full spectrum form are used and on pseudo inverting this equation gives the least-squares fit estimates of the pinion and gear runouts and their initial phases. Table 5.2 shows the estimates of eleven gear mesh dynamic TE parameters of the geared rotor experimental rig.

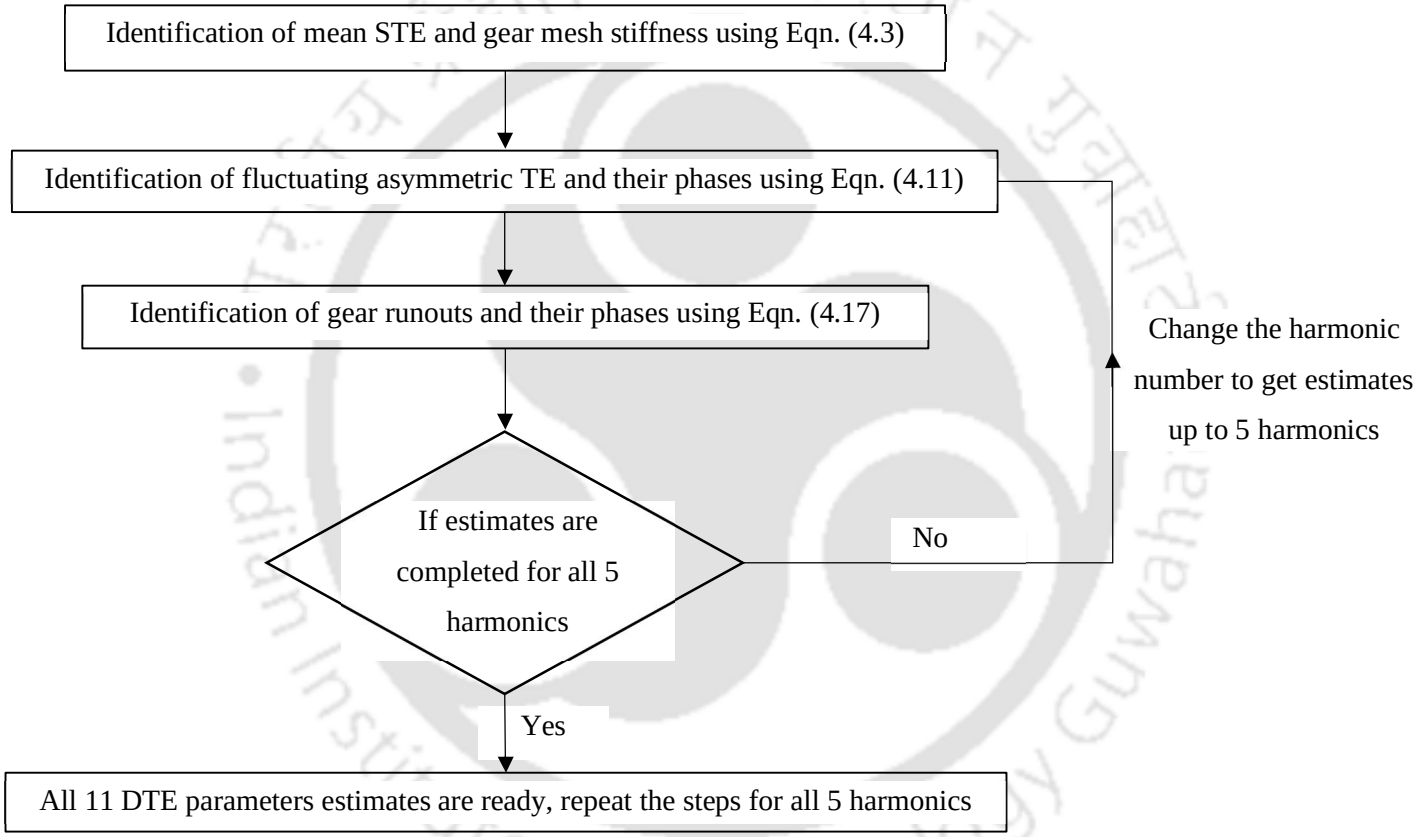

Figure 5.10: Identification algorithm for estimation of geared rotor parameters.

Table 5.2: Estimated experimental rig gear mesh DTE parameters

Parameter	**Units**	**Identified value**				
Gear mesh stiffness	N/m	23.6×10^{6}				
Mean transmission error	μm	0.23				
Gear mesh damping	Ns/m	2.445×10^{3}				
Pinion runout	μm	7.81				
Gear runout	μm	1.96				
Phase of pinion runout	rad	0.867				
Phase of gear runout	rad	2.69				
Variable TE harmonics		1^{st}	2^{nd}	3^{rd}	4^{th}	5^{th}
Variable TE in *x*-direction	μm	99.94	6.09	2.98	4.65	0.57
Variable TE in *y*-direction	μm	17.15	3.36	4.35	3.26	2.04
TE phase in *x*-direction	rad	0.49	0.65	0.97	2.33	1.47
TE phase in *y*-direction	rad	-0.40	-0.89	-1.78	-0.55	0.30

5.7 Validation of Geared Rotor System Model and the Identification Algorithm

This section is dedicated to the validation of geared rotor system model developed in Chapter 2 and for further validation of identification algorithm (IA) developed in Chapter 4. Using the full spectrum responses measured through the experimental rig the estimated dynamic TE parameters are obtained and presented in Table 5.2. These estimates are fed to the mathematical model for numerically generating the full spectrum responses at both input and output shafts. These numerically generated full spectrum responses are now compared with the measured full spectrum responses from the experimental rig for validating both the system model and the identification algorithm for correctness of estimates.

For this purpose, first the input shaft numerically generated full spectrum responses generated with the dynamic TE parameters estimated through experimental rig is compared with the measured full spectrum responses from experimental rig as shown in Fig. 5.11 in time domain and Fig. 5.12 in frequency domain. The comparison shows perfect matching of the gear, pinion and gear mesh frequencies up to five harmonics in Fig. 5.12. Also, we can observe the perfect match of amplitudes at the pinion and gear shaft frequencies, and at higher harmonics of the gear mesh frequencies of the input shaft in Fig. 5.12. Here we can also observe the asymmetry in amplitude in both forward and backward whirls at the same harmonic due to the asymmetric TE, which is present in the system model and same is manifested in measured response from experimental rig.

Also, an attempt is also made to compare the full spectrum response plots on the output shaft in Fig. 5.13 in time domain and Fig. 5.14 in frequency domain. It can be seen that a perfect matching in frequencies of gear shaft, pinion shaft and gear mesh up to five harmonics. The time domain amplitudes of simulated responses are very small compared to original test measured response as shown in Fig. 5.13. The same is reflected in frequency domain plots where the first harmonic of gear meshing frequency amplitudes of simulation deviated with full spectrum amplitudes from experimental rig due to lack of torque control adjustment at the output shaft similar to input shaft while taking the

measurements where very low torque is applied just to avoid tooth separation using magnetic torquer. For more accurate correlation a torque control transmission dyno is recommended in the future work.

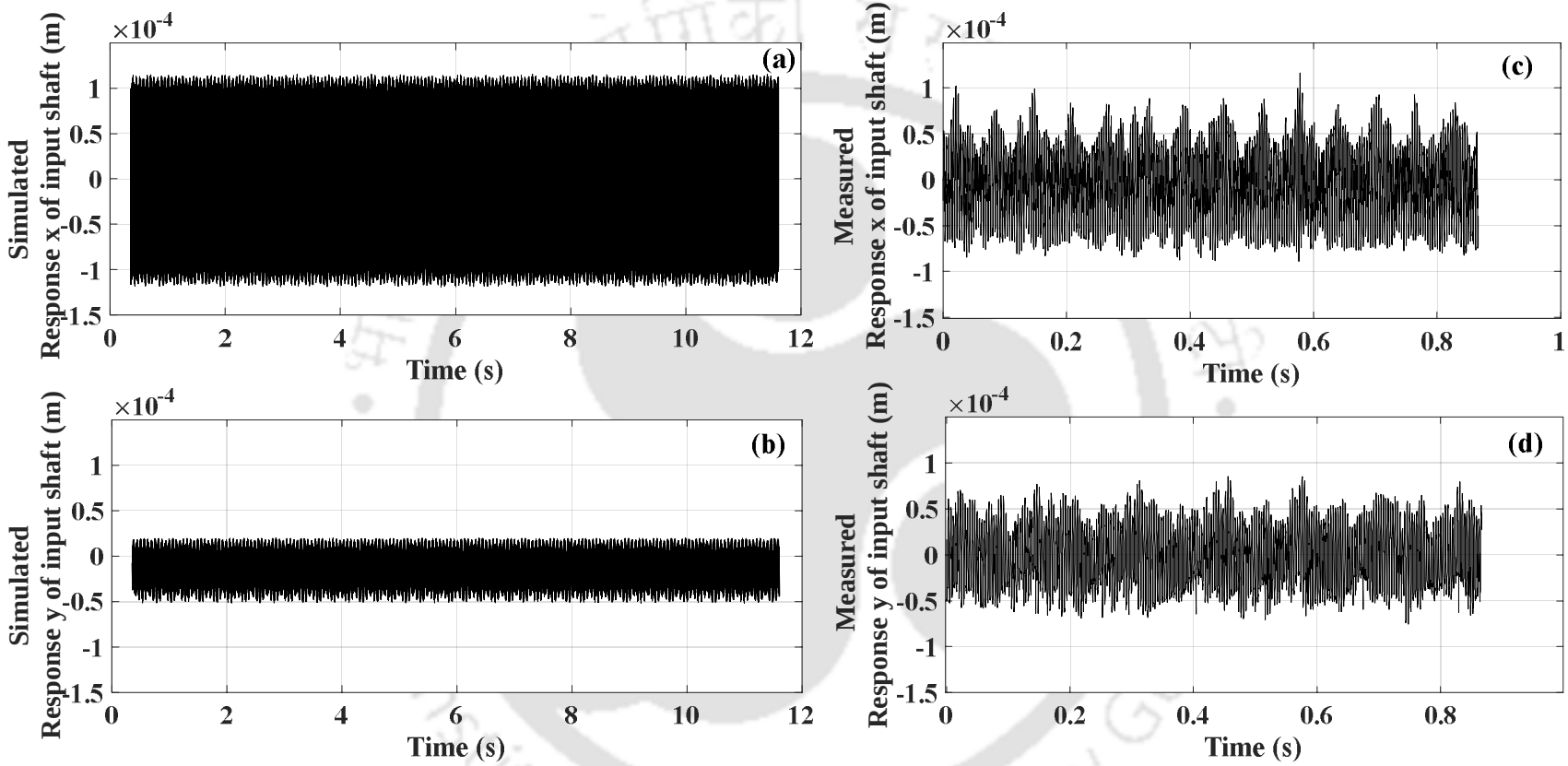

Figure 5.11: (a, b) Numerically generated time domain responses of the input shaft by feeding estimated dynamic TE parameters of the experimental rig (c, d) Time domain responses of the input shaft from the experimental rig

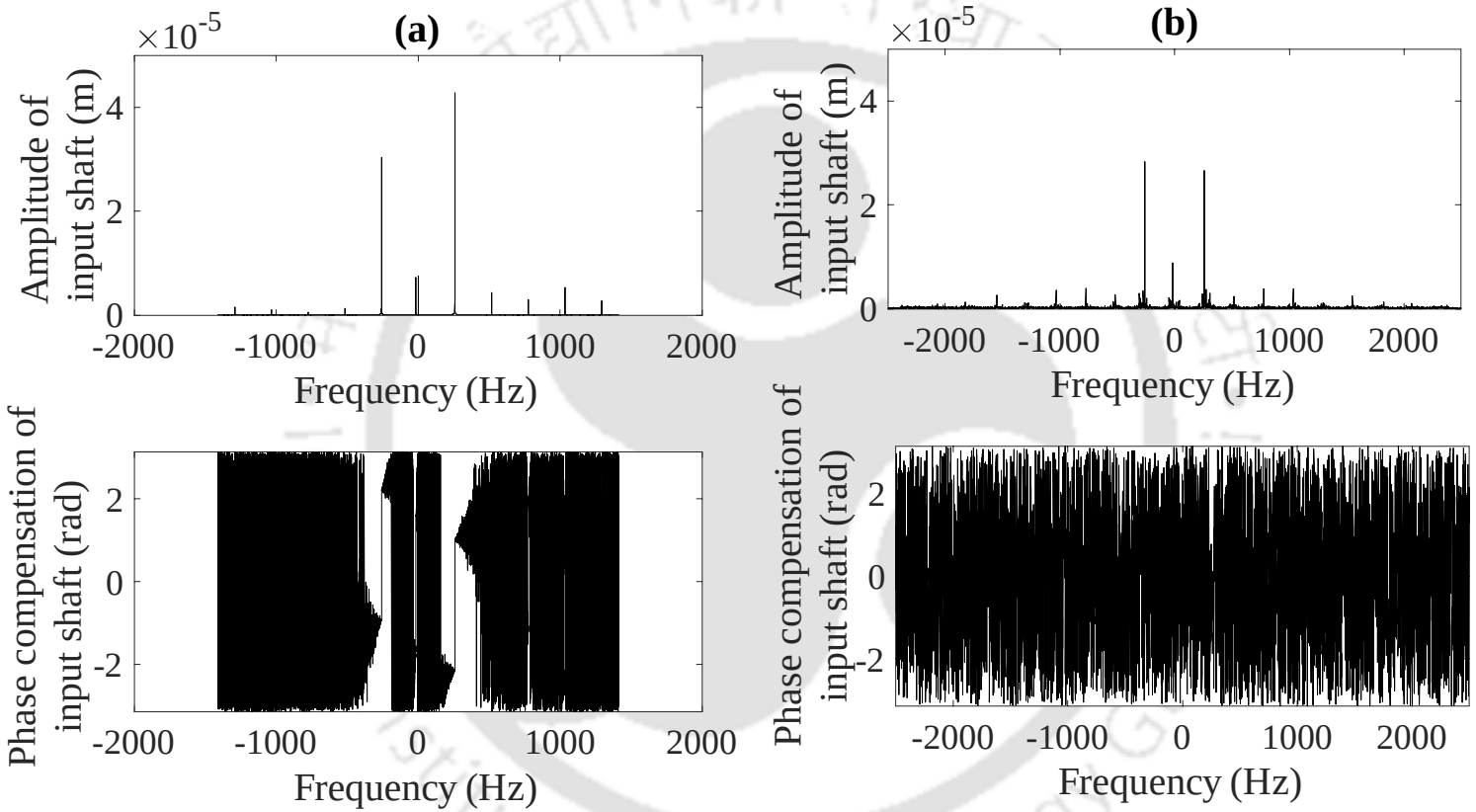

Figure 5.12: (a) Numerically generated full spectrum responses of the input shaft by feeding estimated dynamic TE parameters of the experimental rig (b) Full spectrum responses of the input shaft from the experimental rig

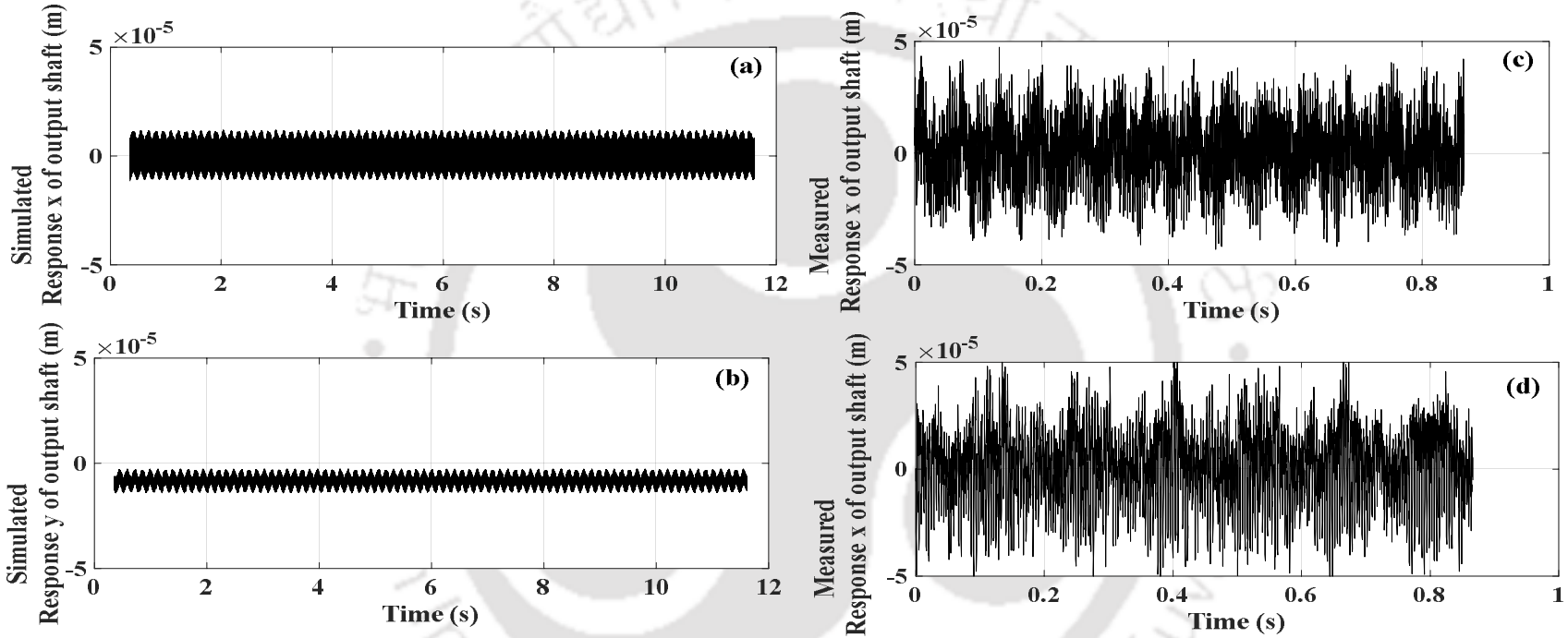

Figure 5.13: (a, b) Numerically generated time domain responses of the output shaft by feeding estimated dynamic TE parameters of the experimental rig (c, d) Time domain responses of the output shaft from the experimental rig

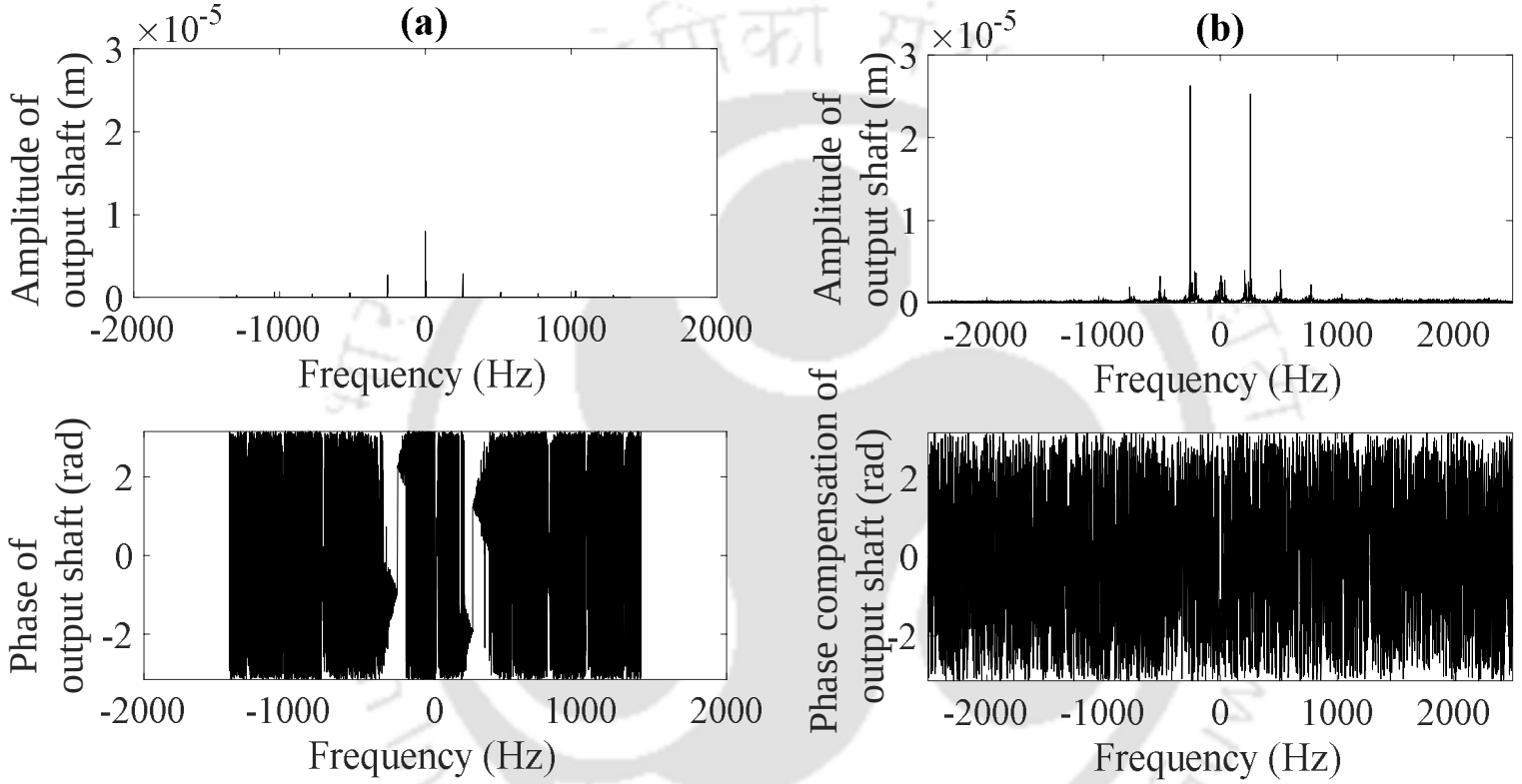

Figure 5.14: (a) Numerically generated full spectrum responses of output shaft by feeding estimated dynamic TE parameters of the experimental rig; (b) Measured full spectrum responses of output shaft from the experimental rig

5.7 Summary

The geared rotor experimental rig with experimental gear set is designed and developed in the Vibration and Acoustics Lab at IIT Guwahati. The experimental rig was used for measuring the geared rotor responses at the supporting shafts using displacement probes. The vibration responses were captured with right sampling duration to avoid leakage and aliasing effects. The test measured sampling data is chosen for frequency domain transformation to analyse the response in the full spectrum form. The full spectrum plots show asymmetric nature of amplitudes in the forward and backward whirls from test responses, which proves the asymmetric TE hypothesis of this research work. A three-step identification algorithm has been proposed in his thesis to identify the gear mesh dynamic TE parameters both using numerically simulated full spectrum responses (in Chapter 4) as well from test measured responses (in Chapter 5). The variation of asymmetry in the *x* and *y* direction are very low in some harmonics and little high in higher harmonics as seen from experimental estimation. Also, the geared rotor system model and the identification algorithm has been validated by comparing measured full spectrum responses (Bode plot) experimental rig with that of the numerically generated system model full spectrum responses (Bode plot) using experimentally identified parameters. The comparison looks well at input shaft in proving the proposed hypothesis of the asymmetric TE in geared rotor research. The deviation in measurements at output shaft in the first harmonic is due to lack of torque control arrangement in test at output shaft similar to input shaft. Also, the identification algorithm works well in getting estimates of the dynamic TE parameters of a geared rotor with lateral vibration measurements, which are otherwise very difficult to predict to visualise them.

CHAPTER 6

CONCLUSIONS AND RECOMMENDATIONS FOR FUTURE RESEARCH

6.1 Introduction

Geared rotor vibration problem is modelled using the system model approach based on the transverse vibration. The system model is excited with an asymmetric transmission error (TE) and other parameters are modelled as dynamic TE fault parameters (e.g., the asymmetric TE in two orthogonal planes at pitch point with their phases in two directions, gear mesh stiffness, gear mesh damping, and the gear and pinion runouts and their phases). Equations of motion are derived using Lagrangian dynamics based on energy expressions of the system. Numerically calculated responses of equations of motion are analysed using the orbit and full spectrum plots. Also, using the parametric variation of gear mesh parameters the dominant source of vibration is analysed in the geared rotor. The geared rotor system model developed is validated using responses from an experimental rig developed for this purpose. Then, the equations of motion are transformed in frequency domain to be used for development of identification algorithm. Using these transformations, a three-step identification algorithm is developed to estimate all the DTE parameters of gear mesh. Using numerical model, the identification algorithm is tested with different level of noise in numerically simulated responses. Geared rotor experimental rig parameters are identified with the same identification algorithm using measured responses. The identified parameters are validated by comparing numerically generated responses using these identified parameters and that with the measured responses from the experimental rig. Based on works presented in previous chapters, the conclusions are drawn out in the present chapter. Also, based on assumptions and limitations of the present research work, the scopes for future works are also summarised in this chapter.

6.2 Conclusions

The following are the main conclusions from the present research:

1. Deviation of a gear profile from its conjugate profile due to manufacturing variations has been quantified as asymmetric transmission error at the gear mesh in two mutually orthogonal directions.
2. For a practical gear drive the torque transfer can be aligned in oblique plane (i.e. the pressure angle), which transversely excite the geared rotor system in both horizontal and vertical directions as in the present formulation.
3. The TE has been modelled with the mean and variable components by considering required multiple numbers of harmonics in mathematical model in two mutually perpendicular directions at the gear mesh.
4. The phase of variable components of TE in both orthogonal directions at the gear mesh has been included to study its contribution to overall vibration spectrum.
5. Along with the asymmetric transmission error and its phase, which are modelled in mutually perpendicular directions at the gear mesh, which occur due to deviation of gear profile from its conjugate profile, the geared rotor excitation is affected by many other system level excitations, like the gear mesh stiffness, gear mesh damping, gear eccentricities, which has been considered as the dynamic transmission error in the present study.
6. All the geared rotor parameters (e.g., the asymmetric TE in two orthogonal planes at pitch point and phases in two directions, gear mesh stiffness, gear mesh damping, and the gear and pinion runouts and their phases), which contribute to the excitation of geared rotor has been modelled as the dynamic TE parameters.
7. The equations of motion of the gear drive with all the dynamic TE parameters (e.g., the asymmetric TE in two orthogonal planes at pitch point with their phases in two directions, gear mesh stiffness, gear mesh damping, and the gear and pinion runouts and their phases) has been derived using Lagrangian dynamics for the transverse vibration of a geared rotor.

8. The geared rotor system model response has been generated numerically using the derived equations of motion by considering dynamic TE excitations and the response are analysed using orbit plots to study its behaviour.
9. Time domain equations of motion has been transformed into frequency domain to obtain full-spectrum form to study the forward and backward whirl frequencies for the asymmetric TE.
10. The numerical response generated for the gear vibration problem has been studied in frequency domain by using full spectrum plots to investigate the forward and backward whirl behaviour. Parametric variation of gear mesh parameters has been performed to investigate dominant source of vibration.
11. It is observed from this study that the forward and backward whirl amplitudes are not same for the asymmetrical TE, which can be used to detect asymmetrical TE.
12. The geared rotor system model has been validated with the experimental setup developed for this purpose by comparing the test measured response with the numerical responses in both time domain and frequency domain using the full spectrum responses.
13. The linear differential equations of motion of the system have been transformed into frequency domain in the complex variable form for the transverse vibration analysis. This form helps in developing identification algorithm to accommodate responses in full spectrum form with the forward and backward whirl components.
14. A three-step identification algorithm has been developed using full spectrum responses to quantitatively identify the gear mesh dynamic TE fault parameters, including the asymmetric TE amplitudes and phases, gear mesh stiffness, gear mesh damping, gear runouts and their phases. The identification algorithm is found to estimate the considered dynamic TE fault parameters with 100 % accuracy when there is no noise introduced in the numerical simulation. When Gaussian noise is introduced, more data had to be fed to the algorithm from a greater number of speeds to get the better accuracy.
15. The system model and the identification algorithm has been validated by comparing the numerically simulated full spectrum responses using identified variables that with the test

measured full spectrum. It is observed that the comparison of plots looks well in terms of correlation with peak frequencies and amplitude at the input and output shafts

6.3 Major Contributions from Present Research

1. The conventional approach uses excitations due to the transmission error (TE) when the line of action (LOA) is aligned with the vertical direction, which ignores excitation in the horizontal direction. In this research work, the LOA of the gear mesh excitation is aligned in an oblique plane for a practical gear drive, which takes excitations in mutually perpendicular transverse directions.
2. A novel asymmetric transmission error excitation is considered to model the TE in two mutually perpendicular directions at the gear mesh to analyse the forward and backward whirl behaviour. This helped in detection of asymmetry in gear TE using the forward and backward whirl amplitudes.
3. The novelty of this research lies in considering several possible system level dynamic TE effects on the vibration spectrum. This research considered several system level excitations apart from the amplitudes of TE, namely the phases of TE, gear mesh stiffness, gear mesh damping, and gear eccentricities and its phases.
4. An experimental geared rotor experimental rig is designed and developed to demonstrate the effect of dynamic TE in the full spectrum response. The backward and forward whirls at different gear meshing harmonics are shown to be very effective in the detection of TE.
5. An identification algorithm is developed to quantitatively estimate the geared rotor DTE parameters, including the asymmetric TE components, mesh stiffness and damping and runouts.
6. An attempt is made to validate the identification algorithm by comparing numerical responses generated using test kit identified parameters with that of the test measured responses. The estimates of geared rotor DTE parameters by using linear dynamic model of the geared rotor system using test measured responses will surely give a new direction for solving the geared rotor real world problem with the experimental validation.

6.4 Limitations of the Present Research

1. The present research work assumes a linear relationship between response coefficients (*P* terms), displacement responses, and external forces. Hence, the deviation of the system from the linear range (e.g., the coupling between the torsional and lateral vibrations) may affect the accuracy of the methodology.
2. The geared rotor system is studied with the spur gear, which will not resist axial deformation on this shaft, this study is not applicable to other gears, like helical and bevel gears. Nevertheless, the fundamental concepts developed in this research work is applicable to all gears.
3. Flexibilities of bearings will influence geared rotor system response to some extent, which is not considered in this research. However, for geared rotor transferring low torques, the bearings will show more or less rigid behaviour.
4. Coupling between the torsion and lateral vibration is not considered in this research. However, for low torque applications and with torsionally stiff shafts the effect is negligibly small. For the high torque application, it needs to be considered.
5. The estimates of geared rotor parameters predicted in this research are limited to the modelling assumptions, like rigid bearings and torsionally rigid shafts. These estimates cannot be generalized to another geared rotor.
6. While estimating the TE (both magnitude and phase) tooth-to-tooth variation in TE is not considered, the TE is considered to be same for all teeth.

6.5 Recommendations for Future Research

1. Geared rotor response and identification can be tried and analysed with gear sets of varied micro geometry as the test kit is developed to handle gear sets of varied centre distances.
2. In this work, the gears are mounted at the centre of the shaft span, where system level effect, like the gyroscopic effect is negligible, this study can be extended to offset geared rotor systems.

3. This study can be extended by including dynamic effects due to gear mesh misalignments to study its effect on geared rotor responses. Even quantitative identification of the misalignment could be attempted along with TE.
4. Rigid bearings considered in this work, the effect of bearing flexibilities on the geared rotor responses can be tried. The bearing dynamic parameters could also be included in identification procedure to have better system model updating.
5. In the present study, the coupling between torsional vibration and lateral vibration is not considered, which is dominant in slender shafts. This study can be extended to have coupled torsional and transverse vibration, and effect of dynamic TE parameters on the dynamic behaviour.
6. The gear mesh stiffness is modelled as time-invariant in this work, this is true for gear with uniform web thickness and without having any gear web bank for weight savings. For the modern gear having gear web design based on weight optimization, in such cases modelling of gear mesh stiffness as time-varying is appropriate. This can be included in future study.
7. Other system level effects, like the gyroscopic effect, gear mesh misalignments, bearing stiffness and time varying mesh stiffness are not considered in this research to avoid complex equations of motion while modelling them using Lagrangian dynamics. This research can be extended with the finite element modelling to include them to study holistic behaviour of geared rotor system. The identification algorithm can be extended for getting estimates of geared rotor dynamic parameters of these system effects.
8. The geared rotor study can be extended by completely levitating the shafts on magnetic bearings (or with active control devices in addition to conventional bearings) to predict and control the TE behaviour by controlling current/voltage of magnetic bearings.
9. Similar to input shaft drive control, a torque control drive can be attached at the output shaft like transmission dyno to analyse the influence of torque variations at the output shaft on gear mesh dynamic parameters.
10. Change in amplitude due to asymmetric TE when compared with symmetric one along LOA can be analysed for all the harmonics.

References

- Bachschmid N, Pennacchi P and Vania, A, Diagnostic significance of orbit shape analysis and its application to improve machine fault detection. Journal of the Brazilian Society Mechanical Science and Engineering, 2 (2004) 200–208.
- Beghini M, Presicce F and Santus C, A method to define profile modification of spur gear and minimize the transmission error, AGMA Technical Paper, 04FTM3, October 2004.
- Benatar M, Handschuh M, Kahraman A, Talbot D, Static and dynamic transmission error measurements of helical gear pairs with various tooth modifications. Journal of Mechanical Design 141 (2019) 103301-1.
- Blankenship G W and Kahraman A, A gear dynamics experiments; Part I – Characterization of forced response. 7th ASME Power Transmission & Gearing Conference, San Diego, ASME Publication 88 (1996) 373–380.
- Cai Y, and Hayashi T, The optimum modification of tooth profile for a pair of spur gears to make its rotational vibration equal zero. In ASME International Power Transmission and Gearing Conference, 43 (1992) 453–460.
- Celikay A, Donmez A, Kahraman A, An experimental and theoretical study of subharmonic resonances of a spur gear pair, Journal of Sound and Vibration 515 (2021) 116421.
- Chaari F, Fakhfakh T and Haddar M, Analytical modelling of spur gear tooth crack and influence on gearmesh stiffness, European Journal of Mechanics – A Solids 28(3) (2009) 461-468.
- Challen B and Baranescu R Diesel Engine Reference Book. 2nd Edition, The Bath Press, Bath, 1999.
- Chen B, Huang K, Raghupathi S, Chandratreya I, Du Quang and Lipson H, Automated discovery of fundamental variables hidden in experimental data. Journal of Nature Computational Science 2 (2022) 433–442.
- Chen Z G, Shao Y M and LIM T C, Non-linear dynamic simulation of gear response under the idling condition, International Journal of Automotive Technology, 13(4) (2012) 541−552.
- Chen Z, Li C and Sanchez R V, Gearbox Fault Identification and Classification with Convolutional Neural Networks, Shock and Vibration 2015 (1) (2015) 1–18.
- Choi S T and Man S Y, Dynamic analysis of geared rotor-bearing systems by the transfer matrix method, Journal of Mechanical Design, Transactions of the ASME 123(4) (2001) 562-568.
- Darpe A K, Coupled vibrations of a rotor with slant crack, Journal of Sound and Vibration 305 (2007) 172–193.
- Edwards S, Lees A W, and Friswell M I, Fault diagnosis of rotating machinery, Shock and Vibration Digest 30 (1998) 4–13.

- Feng Z, Chen X and Liang M, Joint envelope and frequency order spectrum analysis based on iterative generalized demodulation for planetary gearbox fault diagnosis under nonstationary conditions. Mechanical Systems and Signal Processing, 76–77 (2016) 242-264.
- Flek J, Dub M, Kolár J, Lopot F and Petr K, Determination of Mesh Stiffness of Gear—Analytical Approach vs. FEM Analysis, Appl. Sci. 11 (2021) 4960.
- Fonseca D J, Shishoo S, Lim T, and Chen D, A genetic algorithm approach to minimize transmission error of automotive spur gear sets. Applied Artificial Intelligence 19 (2005) 153–179.
- Forsthoffer W E, *Forsthoffer's Best Practice Handbook for Rotating Machinery*. Elsevier. Butterworth-Heinemann, Oxford, United Kingdom, 2011.
- Friswell M I, Damage identification using inverse methods. Philosophical Transactions of the Royal Society A: Mathematical, Physical and Engineering Sciences, 365(1851) (2007) 393-410.
- Friswell M I, Penny J E, Garvey S D and Lees A W, Dynamics of Rotating Machines: Cambridge University Press. USA, 2010.
- Gai J, Zhong K, Du X, Yan K and Shen J, Detection of gear fault severity based on parameter-optimized deep belief network using sparrow search algorithm, Measurement 185 (2021) 110079.
- Genta G, Dynamics of rotating systems. Springer Science and Business Media, Politecnico di Torino, Italy, 2007.
- Goldman P and Muszynska A, Application of full-spectrum to rotating machinery diagnostics. Orbit, First Quarter (1999) 17–21.
- Guo H, Zhang J and Yu H, Dynamic modelling and parametric optimization of a full hybrid transmission, Proc IMechE Part K: J Multi-body Dynamics 233(1) (2019) 17–29.
- Harris C M, Handbook of Acoustical Measurements and Noise Control, 3rd edition, New York: McGraw-Hill Inc., 1991.
- Harris S L, Dynamic loads on the teeth of spur gears, Proceedings of the Institution of Mechanical Engineers, 172(1) (1958) 87–112.
- Hoang D T and Kang H J, A survey on Deep Learning based bearing fault diagnosis, Neurocomputing 335 (2019) 327–335.
- Hong L and Dhupia J S, A time domain approach to diagnose gearbox fault based on measured vibration signals, Journal of Sound and Vibration 333 (2014) 2164–2180.
- Houser D, 1988, Gear noise state of the art. CETIM Internoise 88, Avignon, 2 (1988) 601–606.
- Howard I, Jia S X and Wang J, The dynamic modeling of a spur gear in mesh including friction and a crack, Mechanical Systems and Signal Processing 15(5) (2001) 831–853.
- Huangfu Y, Chen K, Ma H, Li X, Han H and Zhao Z, Meshing and dynamic characteristics analysis of spalled gear systems: A theoretical and experimental study, Mechanical Systems and Signal Processing 139 (2020) 106640.

- Inalpolat M and Kahraman A, A dynamic model to predict modulation sidebands of a planetary gear set having manufacturing errors, Journal of Sound and Vibration 329 (2010) 371–393.
- Jardine A K S, Lin D, and Banjevic D, A review on machinery diagnostics and prognostics implementing condition-based maintenance, Mechanical Systems and Signal Processing 20 (2006) 1483–1510.
- Kahraman A and Blankenship G W, Effect of involute contact ratio on spur gear dynamics, ASME Journal of Mechanical Design, 121 (1999b) 112–118.
- Kahraman A and Blankenship G W, Effect of involute tip relief on dynamic response of spur gears, ASME Journal of Mechanical Design, 121 (1999a) 313– 315.
- Kahraman A and Singh R, Interactions between time-varying mesh stiffness and clearance non-linearities in a geared system. Journal of Sound and Vibration, 146(1):135–156, 1991.
- Kahraman A, Effect of axial vibrations on the dynamics of a helical gear pair, Journal of Vibration and Acoustics, 115 (1) (1993) 33-39.
- Kahraman A, Özgüven H N, Houser D R and Zakrajsek J, Dynamic analysis of geared rotors by finite elements. ASME Journal of Mechanical Design, 114 (1992) 507-514.
- Kayama F, The Dynamics of Parallel Axis Gears in an Automotive Transmission. PhD Thesis, University of Leeds, Leeds, 2005.
- Khan S, Tsutsumi S, Yairi T, Nakasuka S, Robustness of AI-based prognostic and systems health management, Annual Reviews in Control 51 (2021) 130–152.
- Kubur M, Kahraman A, Zini D M and Kienzle K, Dynamic Analysis of a Multi-Shaft Helical Gear Transmission by Finite Elements: Model and Experiment, ASME. J. Vib. Acoust. 126(3) (2004) 398–406.
- Lee A S, Ha J W and Choi D H, Coupled lateral and torsional vibration characteristics of a speed increasing geared rotor-bearing system, Journal of Sound and Vibration, 263 (2003) 725–742.
- Lee A S, Ha J W, Prediction of maximum unbalance responses of a gear-coupled two-shaft rotor-bearing system, Journal of Sound and Vibration, 283 (2005) 507–523.
- Lee C W and Joh C Y, Development of the use of directional frequency response functions for the diagnosis of anisotropy and asymmetry in rotating machinery: theory. Mechanical Systems and Signal Processing, 8(6) (1994) 665-678.
- Li C F, Zhou S H, Liu J and Wen B C, Coupled lateral-torsional-axial vibrations of a helical gear-rotor-bearing system. Acta Mechanica Sinica, 30(5) (2014) 746–761.
- Lu C, Wang Z and Zhou B, Intelligent fault diagnosis of rolling bearing using hierarchical convolutional network based health state classification, Adv. Eng. Informatics 32 (2017) 139–151.
- Lu C, Wang Z and Zhou B, Intelligent fault diagnosis of rolling bearing using hierarchical convolutional network based health state classification, Advanced Engineering Informatics 32 (2017) 139–151.

- Maliha R, Dogruer C U, Ozguven H N, Nonlinear dynamic modeling of gear-shaft-disk-bearing systems using finite elements and describing functions, Transactions on ASME, Journal of Mechanical Design126 (2004) 534–541.
- Mark W D, Isaacson A C and Wagner M E, Transmission-error frequency-domain-behavior of failing gears, Mechanical Systems and Signal Processing 115 (2019) 102–119.
- Mitchell J S, An Introduction to Machinery Analysis and Monitoring, Pann Well Books, Tulsa, Oklahoma, 1993.
- Mohamed A, Sassi S, and Paurobally M R, Model-based analysis of gears' dynamic behavior in the presence of multiple cracks, J. Shock Vib., 2018 (2018).
- Mohammed O D, Rantatalo M and Aidanpaa J, Improving mesh stiffness calculation of cracked gears for the purpose of vibration-based fault analysis, Engineering Failure Analysis. 34 (2013) 235-251.
- Morgan J, Dhulipudi M, Yakoub R and Lewis A, Gear Mesh Excitation Models for Assessing Gear Rattle and Gear Whine of Torque Transmission Systems with Planetary Gear Sets, SAE Technical Paper 2007-01-2245 (2007) doi:10.4271/2007-01- 2245.
- Munro R G, A review of the theory and measurement of gear transmission error. Proceedings of the First IMechE Conference on Gearbox Noise and Vibration, paper C404/032, (1990) 3–10.
- Özgüven H N and Houser D R, Mathematical models used in gear dynamics- A review, Journal of Sound and Vibration, 121(3) (1988) 383-411.
- Parker R G, Progress and problems in gear vibration and noise. Second International Conference on Damping Technologies, Army Research Lab Workshop 9302-AN-03, Stellenbosch, South Africa, April 2003, p. 13.
- Patel T H and Darpe A K, 2011, Application of full-spectrum analysis for rotor fault diagnosis. Proceedings of IUTAM Symposium on Emerging Trends in Rotor Dynamics (Editor: K Gupta), held in New Delhi. India, March 23-26, 2009. Springer, pp. 535–545.
- Paya B A, Esat I, and Badi M N M, Artificial neural network-based fault diagnostics of rotating machinery using wavelet transforms as a pre-processor, Mechanical Systems & Signal Processing 11 (5) (1997) 751–765.
- Qu L, Xie A X and Li X, 1993, Study and performance evaluation of some nonlinear diagnostic methods for large rotating machinery. Mechanism and Machine Theory 28(5) 699–713.
- Randall R B, Vibration-based Condition Monitoring: Industrial, Aerospace and Automotive Applications, John Wiley and Sons. Hoboken, New Jersey, United States, 2011.
- Rao B R and Ganti V, Gear whine noise path analysis and mitigation strategies for automotive transmissions, Presented at FISITA World Automotive Congress 2018, Chennai, India, F2018/F2018-NVB-024, 2-5 October 2018.

- Rao B R and Tiwari R, Optimum design of rolling element bearings using genetic algorithms, Mechanism and Machine Theory 42 (2007) 233-250.
- Rao J S Rotor dynamics. New Age International Limited Publishers, New Delhi, India, 1996.
- Rezaeianjouybari B and Shang Y, Deep learning for prognostics and health management: State of the art, challenges, and opportunities, Measurement 163 (2020) 107929.
- Roy D and Tiwari R, Experimental Identification of Internal and External Damping in a Rotor System with a Fatigue-Crack Using Full Spectrum. Exp Tech 44 (2020) 509–528.
- Samanta B, Artificial neural networks and genetic algorithms for gear fault detection, Mechanical System and Signal Processing 18 (2004) 1273–1282.
- Sarmah N and Tiwari R, Dynamic analysis and identification of multiple fault parameters in a cracked rotor system equipped with active magnetic bearings: a physical model based approach. Inverse Problems in Science and Engineering, Dec 14 (2019) 1-32.
- Sato T, Umezawa K and Ishikawa J, Effects of contact ratio and profile correction on gear rotational vibration. Bullettin of the JSME, 26 (1983) 2010–2016.
- Sawalhi N and Randall R B, Gear parameter identification in a wind turbine gearbox using vibration signals, Mechanical Systems and Signal Processing 42 (2014) 368–376.
- Sekhar A S, Crack identification in a rotor system: a model-based approach. Journal of Sound and Vibration, 270 (2004) 887-902.
- Shravankumar C and Tiwari R, 2013, Model-based crack identification using full-spectrum. ASME Gas Turbine India Conference. December 5–6, 2013, Bangalore, Karnataka, India (GTINDIA 2013-3756).
- Simon V, Optimal tooth modifications for spur and helical gears. Journal of Mechanism, Transmissions, and Automation in Design, 111 (1989) 611–615.
- Singh S and Tiwari R, Model-based fatigue crack identification in rotors integrated with active magnetic bearings, Journal of Vibration and Control 2017, 23(6) (2015) 980–1000.
- Singh S and Tiwari R, Model-based switching-crack identification in a Jeffcott rotor with an offset disk integrated with an active magnetic bearing. ASME, Journal of Dynamic Systems, Measurement and Control, 138(3) (2016) 031006.
- Song He, Li J, Muir M, Gautam GSJ, Rajeswara R. B., New Integrated Electromagnetic and NVH Analyses for Induction Traction Motors for Hybrid and Electric Vehicle Applications, WCX SAE World Congress Experience, 21 to 23rd April 2020, Detroit, USA.
- Southwick D, Using full-spectrum plots. Orbit, 14(4) (1993) 12–16.
- Southwick D, Using full-spectrum plots: Part 2. Orbit, 15(2) (1994) 1-10.
- Srinivas R S, Tiwari R and Kannababu Ch, Model based analysis and identification of multiple fault parameters in coupled rotor systems with offset discs in the presence of angular misalignment

and integrated with an active magnetic bearing, Journal of Sound and Vibration 450 (2019) 109-140.

- Tavakoli M, and Houser D, Optimum profile modifications for the minimization of static transmission errors of spur gears. Journal of Mechanism, Transmissions and Automation in Design, 108 (1986) 86–95.
- Temis Y, Kalinin D, and Kozharinov E, Simulation of Gear Systems with Dynamic Analysis, The 14th IFToMM World Congress, Taipei, Taiwan, October 2015.
- Tiwari R, Rotor Systems: Analysis and Identification: Boca Raton: 2017 CRC Press.
- Tuma J and Bilos J, Fluid instability of rotor systems with journal bearings. Engineering Mechanics, 14 (2007) 69–80.
- Velex P and Ajmi M, On the modelling of excitations in geared systems by transmission errors. Journal of Sound and Vibration, 290 (2006) 882-909.
- Wadkar S B and Kajale S R, Mode shapes, natural frequency and reliability of geared shaft with varying mesh stiffness, Journal of the Institution of Engineers. 92 (2011) 32-37.
- Walker H, Gear tooth deflections and profile modifications, Engineer, 170 (1040) 102–104.
- Wang J, Li R and Peng X, Survey of nonlinear vibration of gear transmission systems. Applied Mechanics Review, 56(2003) 309–329.
- Widodo A, and Yang B S, Support vector machine in machine condition monitoring and fault diagnosis, Mechanical Systems and Signal Processing 21 (2007) 2560–2574.
- Xingxin C, Xin Z, Gangming Wu, Research on online fault detection tool of substation equipment based on artificial intelligence, Journal of King Saud University – Science 34 (2022) 102149.
- Yechen Qin, Xiaolin Tang, Tong Jia, Ziwen Duan, Jieming Zhang, Yinong Li, Ling Zheng Noise and vibration suppression in hybrid electric vehicles: State of the art and challenges. Renewable and Sustainable Energy Reviews 124 (2020) 109782.
- Yu X, Li Z, He O, Yang Y, Du M and Peng Z, Gearbox fault diagnosis based on bearing dynamic force identification, Journal of Sound and Vibration 511 (2021) 116360.
- Zhang Q, Wang Jiu, Lyu S K, Study on Empirical Gear Profile Micro-modifications for Gear Transmission, Journal of the Korean Society of Manufacturing Process Engineers, 16 (2017) 54-62.
- Zhou S, Ren Z, Song G and Wen B, Dynamic characteristics analysis of the coupled lateral-torsional vibration with spur gear system. International Journal of Rotating Machinery 2015 (2015), Article ID 371408, 14 pages.

Publications from the Present Research

Journals accepted /communicated from the thesis

- Rao B R and Tiwari R, Detection of asymmetric transmission error in geared rotor system through transverse vibration analysis using full-spectrum, Propulsion and Power Research, Vol 9(3) (2020) 255-280.

- Rao B R and Tiwari R, Identification of the asymmetric transmission error and gear mesh dynamic parameters using full-spectrum responses in a geared rotor system, (Under review).

Papers presented in conferences

- Rao B R and Tiwari R, Analysis of geared rotor systems using full spectrum for low torque applications, Sixth National Symposium on Rotor Dynamics NSRD-2019, July 1-2, 2019, CSIR-National Aerospace Laboratories, Bangalore.

- Rao B R and Tiwari R, Identification of dominant source of vibration in geared rotors using full spectrum analysis, Proceedings of the XVI Vibration Engineering & Technology of Machinery Conference VETOMAC 2021, December 16 - 18, 2021, B.M.S. College of Engineering, Bengaluru.

Appendix A

A1. Real and imaginary amplitudes of simulation full spectrum plots given Fig. 4.2

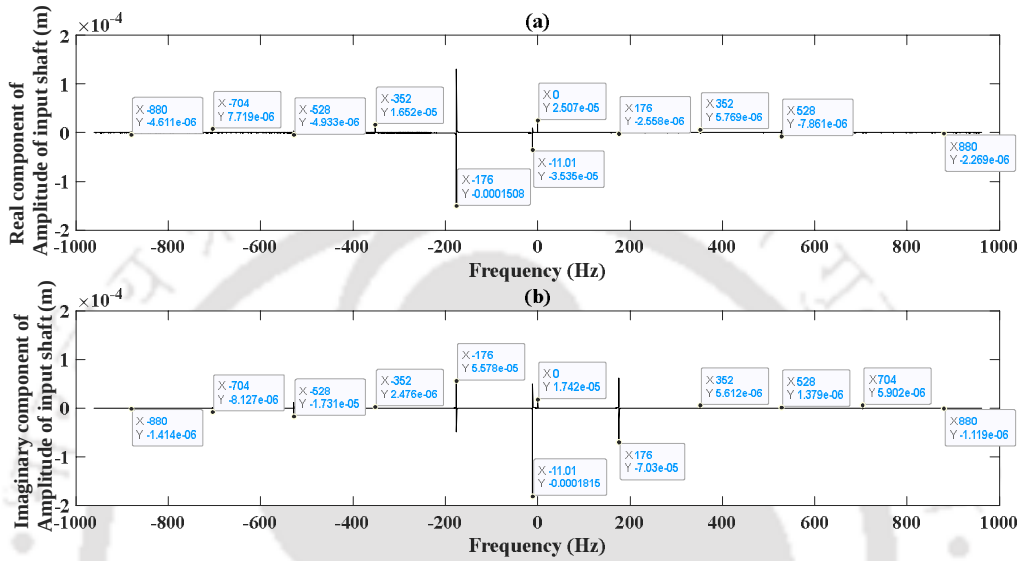

Fig. A1.1: (a)Real and (b)imaginary components of input shaft simulated full spectrum plot

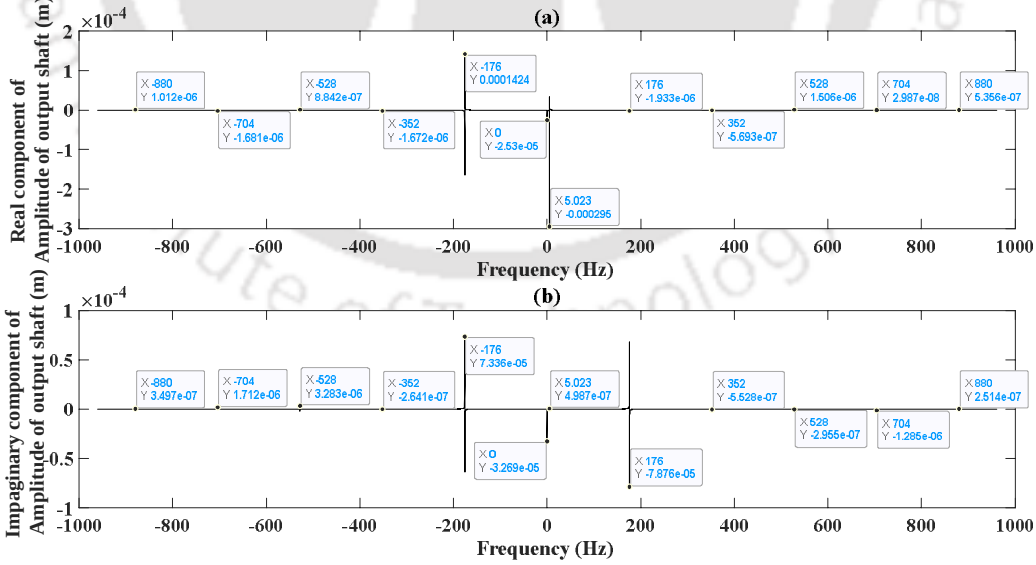

Fig. A1.2: (a)Real and (b)imaginary components of output shaft simulated full spectrum plot

A2. Real and imaginary amplitudes of simulation full spectrum plots given Fig. 5.9

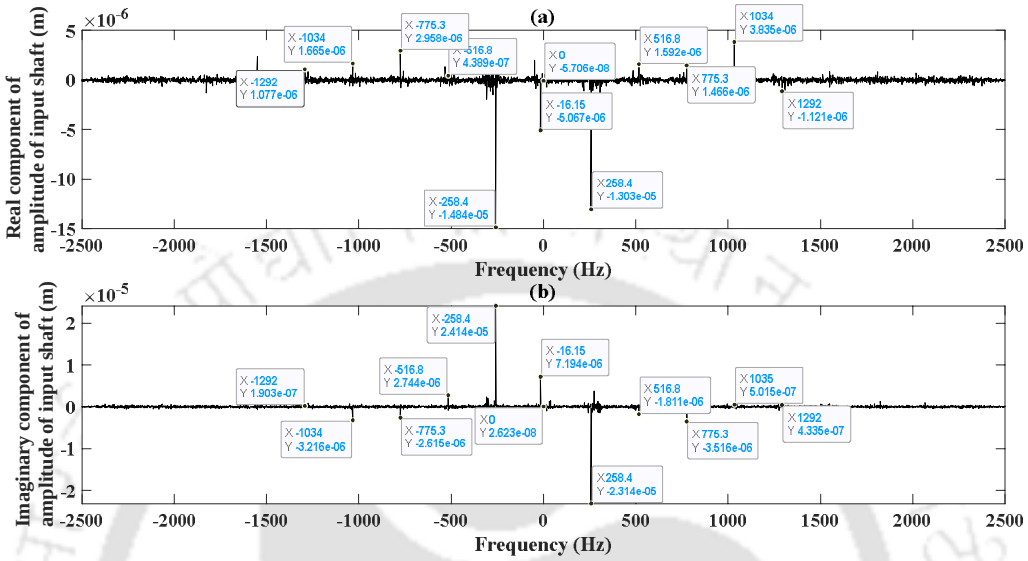

Fig. A2.1: (a)Real and (b)imaginary components of input shaft test measured full spectrum plot

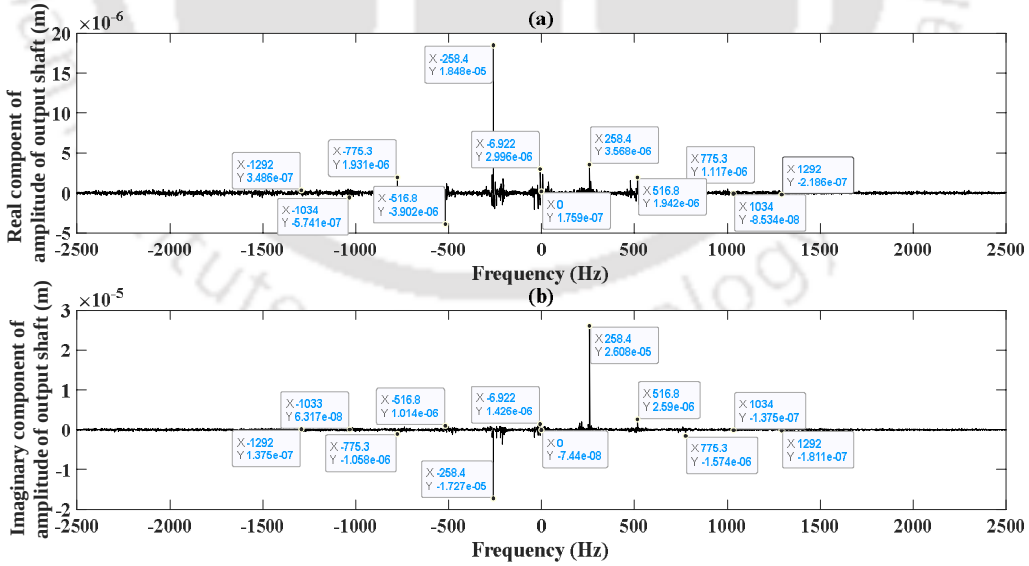

Fig. A2.2: (a)Real and (b)imaginary components of output shaft test measured full spectrum plot